

**THE STRUCTURAL ORGANIZATION AND SPECTRAL CHARACTERISTICS
OF VISUAL WORKING MEMORY IN THE MONKEY FRONTOPIRIETAL
NETWORK**

by

Bryan Conklin

A Dissertation Submitted to the Faculty of
The Charles E. Schmidt College of Science
in Partial Fulfillment of the Requirements for the Degree of
Doctor of Philosophy

Florida Atlantic University

Boca Raton, FL

December 2020

Copyright 2020 by Bryan Conklin

**THE STRUCTURAL ORGANIZATION AND SPECTRAL CHARACTERISTICS
OF VISUAL WORKING MEMORY IN THE MONKEY FRONTOPIRIETAL
NETWORK**

by

Bryan Conklin

This dissertation was prepared under the direction of the candidate's dissertation advisor, Dr. William Alexander, Center for Complex Systems and Brain Sciences, and has been approved by all members of the supervisory committee. It was submitted to the faculty of the Charles E. Schmidt College of Science and was accepted in partial fulfillment of the requirements for the degree of Doctor of Philosophy.

SUPERVISORY COMMITTEE:



William Alexander, Ph.D.
Dissertation Advisor



Randy D. Blakely (Nov 5, 2020 09:51 EST)

Randy D. Blakely, Ph.D.



Charles M. Gray, Ph.D.

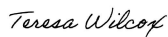


Earl K. Miller, Ph.D.



Gary W. Perry (Nov 6, 2020 15:04 EST)

Gary W. Perry, Ph.D.
Chair, Center for Complex Systems and
Brain Sciences



Teresa Wilcox, Ph.D.
Interim Dean, Charles E. Schmidt College
of Science



Robert W. Stackman Jr., Ph.D.
Dean, Graduate College

November 6, 2020

Date

ACKNOWLEDGEMENTS

I would like to thank Dr. Steven Bressler for taking a chance on an enthusiastic and naïve young man five years ago. It was Rhona who wisely suggested him to me. What followed was an unorthodox journey through the neuroscience landscape with long pit stops in the towns of Kandel and Fourier. Thanks to superb instruction from the likes of Drs. Robert Stackman Jr and Michael X Cohen, I learned the languages spoken there. I am grateful to current and past Centerites for their guidance during this time, especially Dr. Michael Mannino for the time he spent sharing insight into the nature of things here at the Center. I was lucky to receive high-quality mentorship from Dr. William Alexander when Dr. Bressler went on leave. His comments and direction helped me to finally write this all down in a manner that might make you think I know what I am talking about. As a result of thoughtful guidance from my committee members, Drs. Randy Blakely, Charles Gray and Earl Miller, you may be right. I am also indebted to Keyla Thamsten and Dr. Gary Perry for navigating the waters of bureaucracy to provide much-needed administrative support over the years. Last, and most importantly, I want to thank my loving family. My mom, and biggest fan, provided consistent childcare so I could focus on writing. My wife, Kathryn, has believed in and encouraged the pursuit of my passions. She selflessly managed our one-year-old daughter and her job to provide me with uninterrupted time to work. My happy, curious daughter, Gwynevere, provides sparks of joy and welcome periods of distraction throughout the day. It is these interactions and

relationships that have allowed me to succeed in this endeavor. Thank you all from the bottom of my heart.

ABSTRACT

Author: Bryan Conklin

Title: The Structural Organization and Spectral Characteristics of Visual Working Memory in the Monkey Frontoparietal Network

Institution: Florida Atlantic University

Dissertation Advisor: Dr. William Alexander

Degree: Doctor of Philosophy

Year: 2020

Working memory is a mental workspace which utilizes short and long-term memory to maintain and manipulate information. It is crucial in enabling cognitive control and is largely controlled by interactions within and between frontal and parietal cortices. Recent work has identified visual nonspatial, spatial, and visuospatial working memory spectral characteristics of the local field potential through simultaneous recordings from various areas across the monkey frontoparietal network. However, the reports are minimal in number, and there is no clear narrative tying together the heterogenous functionality of the characteristics. Here, a new spectral model of monkey visual working memory is proposed to address these shortcomings. It highlights functional roles for low, mid, and high frequency bands. Next, the organization of structural connectivity which gives rise to these spectral characteristics is investigated. A new binary association matrix representing connections in the frontoparietal network is

proposed. A graph theoretic analysis on the matrix found that a 3-node dynamical relaying M9 motif was a fundamental building block of the network. It is optimally structured for the synchrony found in the spectral model. The network was also found to have a small-world architecture, which confers the integration and specialization of function required by visual working memory. Afterwards, three hypotheses generated by the spectral model are tested on non-spatial data. The low and mid band hypotheses were supported by evidence, while the high band hypothesized activity was not observed. This adds credibility to the roles identified in the model for the low and mid band and identifies a need for further investigation of the high band role. Finally, opportunities to expand the spectral model, analyze the M9 motif, and further test the model are explored. In the future, the spectral model could evolve to apply its predictions to humans in the pursuit of treatments for neurological disorders.

DEDICATION

I dedicate this dissertation to my beautiful daughter, Gwynevere Page Conklin.

You motivate and inspire me. Stay curious my girl.

**THE STRUCTURAL ORGANIZATION AND SPECTRAL CHARACTERISTICS
OF VISUAL WORKING MEMORY IN THE MONKEY FRONTOPIRIETAL
NETWORK**

LIST OF TABLES	xiii
LIST OF FIGURES	xiv
LIST OF EQUATIONS	xvi
1 INTRODUCTION	1
1.1 Working Memory Models	2
1.2 Large-scale Networks Supporting Cognition	6
1.3 Data Acquisition	7
1.4 Time-Frequency Analysis	8
1.5 Working Memory Nonhuman Primate Tasks	9
1.6 Task-dependent Oscillations	12
1.7 Methods	13
1.7.1 Task Assignment	13
1.7.2 Frequency Bands	14
1.7.3 Limitations	16

1.8	Frequency Band Activity in Spatial vs Non-spatial Working Memory	17
1.8.1	Low Frequency Band.....	17
1.8.2	Mid Frequency Band.....	18
1.8.3	High Frequency Band	21
1.9	Frequency Band Activity in Visuospatial Working Memory	24
1.9.1	Low Frequency Band.....	24
1.9.2	Mid Frequency Band.....	25
1.9.3	High Frequency Band	26
1.10	Conclusion.....	29
2	ORGANIZATION OF AREAL CONNECTIVITY IN THE MONKEY	
	FRONTOPARIETAL NETWORK	35
2.1	Introduction	35
2.2	Results	38
2.2.1	The Frontoparietal Connectome	38
2.2.2	Graph Theoretic Analysis	41
2.2.3	Motifs.....	44
2.2.4	Small world.....	46
2.3	Discussion	47
2.4	Methods.....	52
2.4.1	Parcellation Scheme.....	52

2.4.2	Connections.....	53
2.4.3	Graph Visualizations.....	56
2.4.4	Graph Measures	56
2.4.5	Degree Distribution.....	56
2.4.6	Null Models	58
2.4.7	Motifs.....	59
2.4.8	Small world.....	60
3	SPECTRAL CHARACTERISTICS OF NON-SPATIAL VISUAL WORKING MEMORY IN THE MACAQUE FRONTOPARIETAL NETWORK.....	63
3.1	Introduction	63
3.2	Methods.....	65
3.2.1	Recording.....	65
3.2.2	Task.....	68
3.2.3	Trial rejection.....	69
3.2.4	Time-frequency Decomposition Using Complex Morlet Wavelets	70
3.2.5	Baseline Normalization.....	73
3.2.6	Window Selection for T-test.....	75
3.2.7	One-way t-tests	78
3.3	Results	78
3.4	Conclusion.....	83

4	FUTURE DIRECTIONS AND OPPORTUNITIES IN MONKEY FRONTOPARIETAL NETWORK RESEARCH ON VISUAL WORKING MEMORY	86
4.1	The Spectral Model of Visual Working Memory in the Monkey	88
4.2	The M9 Dynamical Relay Motif	89
4.3	Spatial vs Non-spatial Visual Working Memory Spectral Characteristics	90
4.4	Non-spatial Visual Working Memory Task Performance.....	92
4.4.1	Time Domain Task Performance Preliminary Analysis	93
4.5	Spectral Model of Monkey Visual Working Memory	98
4.6	Conclusion.....	99
5	APPENDIX A.....	101
5.1	Supplementary Discussion for Chapter 2.....	101
5.1.1	Areal Specialization	102
5.1.2	Connectivity	103
5.1.3	Motifs.....	104
5.1.4	Small World.....	104
5.2	Supplementary Figures for Chapter 2	105
6	APPENDIX B.....	112
7	REFERENCES	117

LIST OF TABLES

Table 1.1. Reported frequency band outliers.	16
Table 1.2. Summary of all spatial and non-spatial visual working memory studies on nonhuman primates	22
Table 1.3. Summary of all visuospatial studies on nonhuman primates	28
Table 5.1. Association matrix for the frontoparietal network	107
Table 5.2. Permutation test results by motif class.....	110
Table 5.3. Permutation test results by area.....	111

LIST OF FIGURES

Figure 1.1. Models of working memory.	3
Figure 1.2 “What” vs “Where” theory of functional specialization in nonhuman primate working memory.....	6
Figure 1.3. Venn diagram of the topics covered in this review.	13
Figure 1.4. Spectral Model of Visual Working Memory in the Monkey.....	32
Figure 2.1. Lateral, orbital, and medial views of macaque cortex.	39
Figure 2.2. Binary, directed adjacency matrix describing the connectivity of the frontoparietal monkey network.....	40
Figure 2.3. A graph representation of the frontoparietal network generated from the adjacency matrix.	41
Figure 2.4. Complementary cumulative distribution function (cCDF) of the in-degree distribution (A & C) and out-degree distribution (B & D) for the FPN plotted on a logarithmic scale.	42
Figure 2.5. Comparison of the structural motif frequency spectrum for the empirical FPN with random and lattice benchmark networks.	46
Figure 3.1. Recorded areas & experimental design	66
Figure 3.2. Example of LFP signals across all recording channels from a single trial....	67
Figure 3.3. Temporal and spectral resolutions for each complex Morlet wavelet.....	71
Figure 3.4. Set of 35 complex Morlet wavelets ranging in frequency from 4 to 100 Hz in 35 logarithmically spaced steps	72

Figure 3.5. Example trial prior to convolution.....	73
Figure 3.6. Monkey A Average Spectrograms Across All 23 Days & Across Correct & Incorrect Responses	77
Figure 3.7. Monkey B Average Spectrograms Across All 24 Days & Across Correct & Incorrect Responses	77
Figure 3.8. Monkey A time-frequency spectrograms showing dB baseline-normalized LFP power with rectangular windows of interest highlighted for each hypothesis generated by the visual working memory spectral model	81
Figure 3.9. Monkey B time-frequency spectrograms showing dB baseline-normalized LFP power with rectangular windows of interest highlighted for each hypothesis generated by the visual working memory spectral model	82
Figure 4.1. Event-related potentials (ERPs) for correct (blue solid) and incorrect (red dashed) trials across all recording days and channels.....	96
Figure 4.2. ERPs for correct (blue) and incorrect (red) trials from Monkey B	97
Figure 5.1. The degree distributions for the frontoparietal network.....	105
Figure 5.2. Pareto chart of the total degree for each node in the frontoparietal network.	105

LIST OF EQUATIONS

Equation 2.1 Power-law fit.....	57
Equation 2.2 Nonlinear least squares fit.....	58
Equation 2.3. Characteristic path length of a graph	60
Equation 2.4. Clustering coefficient ratio.....	60
Equation 2.5. Clustering coefficient of entire network	61
Equation 2.6. Normalized clustering coefficient	61
Equation 2.7. Normalized characteristic path length.....	61
Equation 2.8. Humphries' index of small-worldness	61
Equation 2.9. Telesford's alternative index of small-worldness	62
Equation 3.1. Complex Morlet wavelet.....	71
Equation 3.2. Time-frequency decibel baseline normalization	74

1 INTRODUCTION

A properly functioning memory is a key component of a healthy, productive life. One can simply examine the lives of those individuals who have suffered damage to their memory systems, such as Patient C (Clive Wearing) or Patient H.M. (Henry G. Molaison), to see this is true (Squire, 2009; B. A. Wilson et al., 1995).

There are multiple memory systems which work together to enable healthy memory functioning: long-term memory, sensory memory, short-term memory, and working memory (Baddeley et al., 2015). Long-term memory is a system which stores information for long periods of time, including both explicit and implicit material. Explicit long-term memory is understood as remembering things like facts, events, and places. Implicit long-term memory involves learning skills or priming (Squire, 1992). Sensory memory is synonymous with perception. It is mediated through the five senses and is fleetingly brief. It allows movies, which are images shown in rapid succession, to appear as one continuous stream. Short-term memory is a system which stores material temporarily over brief delays. Information may be retrieved from long-term memory, combined with sensory input, and loaded into the short-term system for task completion. However, it is important to note that tasks which require short-term memory involve only storage and retrieval of information, such as a repeating back sequences of digits (Jacobs, 1887). When task-relevant information needs to be processed in some manner, such as in the N -back task, working memory is employed. The N -back task requires participants to decide whether a viewed stimulus matches one presented N items prior, where N is

typically 1-4 (Conway et al., 2005). Working memory is understood as a mental workspace which draws on both short and long-term memory in its maintenance and manipulation of information. It is crucial in enabling cognitive control and serves as a proxy for general intelligence (Baddeley, 2012; Engle & Kane, 2003). Accordingly, much focus has been devoted to understanding working memory through cognitive modeling.

1.1 Working Memory Models

Researchers model cognitive processes to develop a theory of their origination and function. The working memory process is challenging to model because it is likely comprised of multiple operations which interact with other kinds of memory systems simultaneously (Baddeley, 2012). The modal model was the first proposed model of working memory (Figure 1.1a) (Atkinson & Shiffrin, 1968). Input flows through three main stages after entering via the senses: a sensory register, a short-term store, and a long-term store. The sensory register holds a fleeting memory trace processed by the senses. Next, information flows to the short-term store, which is agnostic to the original communication medium. Finally, the information transfers between long and short-term stores until a decision is made.

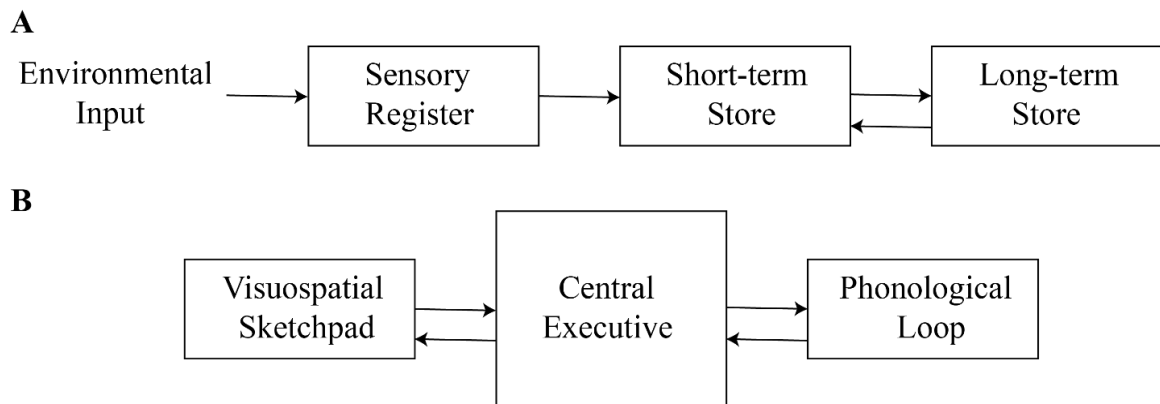


Figure 1.1. Models of working memory.

A. Modal model (Atkinson & Shiffrin, 1968). Input travels from the environment through the senses into the sensory register where it is temporarily stored until attentional mechanisms enable transfer into the short-term store. Input deemed sufficiently important is then transferred to the long-term store. The short-term and long-term stores can interact as much as necessary. Working memory uses information in the short-term store along with input from the long-term store to complete tasks. **B.** Multicomponent model (Baddeley & Hitch, 1974). The short-term store from the modal model of WM was broken up into 3 independent sub-systems: the visuospatial sketchpad, phonological loop, and central executive. The visuospatial sketchpad encodes information in WM using vision and space. The phonological loop is a mechanism for acoustically encoding information in WM. It relies on verbal rehearsal. The central executive is a system that functions as a command-and-control center which coordinates the interactions between the visuospatial sketchpad, phonological loop, and long-term memory.

The modal model began to fall apart when it could not account for individuals with memory deficits. According to the model, patients with short-term memory impairments should have a severely impaired long-term system since the long-term store receives its input directly from the short-term store. However, that is not true. Patients with severe short-term memory deficits exhibit no signs of long-term deficits (Shallice & Warrington, 1970). This paved the way for the widely-used multicomponent model (Baddeley & Hitch, 1974) of working memory (Figure 1.1b).

The multicomponent model breaks the short-term store of the modal model into three separate interacting systems: the visuospatial sketchpad, phonological loop, and the central executive. This permits patient-specific deficits within a single sub-system that do not impair the others, thereby addressing the shortcoming posed by the modal model. The multicomponent model has since been updated to include more parameters, but its overall structure has remained intact (Baddeley, 2012). The visuospatial sketchpad is used to process mental imagery comprising both visual and spatial properties. The sketchpad is thought to act as a temporary storage buffer of visuospatial information, but not necessarily the generation or maintenance of it (Pearson et al., 1999). It can be further decomposed into two separate subsystems: a passive store and an active device for repeating visuospatial information (Bruyer & Scailquin, 1998). The phonological loop,

when not utilized in service of a cognitive task, is simply a model of verbal short-term memory. It uses a temporary store of information as well as a verbal rehearsal process. It turns out the average capacity an individual can recall is around seven digits, plus or minus two (G. Miller, 1956). However, this is an example of simple passive reporting and does not involve more complex cognitive activities. The remembered information is not processed for learning, comprehension or reasoning, an indication of working memory (Baddeley et al., 2015). Thus, only verbal short-term memory is engaged. When the phonological loop is put to some cognitive use, like remembering the order of the digits (Jaeggi et al., 2010), then it becomes a function of working memory. From an evolutionary perspective, the phonological loop is thought to assist in language acquisition (Baddeley et al., 1988). It is also used in verbal self-instruction to control behavior. This was seen in developing children who would verbally cue themselves before performing a requested action (Luria, 1962). The central executive system directs working memory and is responsible for focusing and shifting attention (Engle & Kane, 2003; Robbins et al., 1996), controlling, and monitoring behavior, and dividing attention between two or more tasks (Logie et al., 2004). The supervisory attention system is at the heart of the central executive, permitting a flexible control of action (Norman & Shallice, 1986). These executive functions fall within the cognitive neuroscience domain of cognitive control (Braver, 2012). It is thought that the PFC is the seat of cognitive control and perhaps by extension, the central executive (E. K. Miller, 2000; E. K. Miller & Cohen, 2001).

Extending beyond these cognitive models to establish biological models of working memory involves a search for neural mechanisms. One such model builds upon

the idea that the central executive originates in the PFC. It posits the central executive of the nonhuman primate is an emergent property of domain-specific processors concurrently activated in the PFC and connected with domain-relevant long-term storage in sensory posterior regions and motor pathways (Goldman-Rakic, 1996a). This provides a framework for the central executive to function in a biological system through its prefrontal and parietal interactions. In constructing these more biologically realistic models, researchers focus on whether the memories themselves are stored in single locations (Tonegawa et al., 2015) of the brain or are hierarchical and distributed (Fuster, 1995). A more thorough review of this topic is covered by D'Esposito, (2007). In brief, the prefrontal and parietal cortical regions are identified as areas vital to facilitating models of working memory which link posterior sensory regions to higher-order association cortices in the active maintenance of sensory percepts (Figure 1.2). They can integrate perceptual representations through connections with unimodal association cortex. Ultimately, working memory is likely an emergent property of the functional interactions observed in networks involving the prefrontal and parietal cortices and other parts of the brain, such as the hippocampus. This review will focus on the prefrontal and parietal cortical contributions to working memory, both separately and combined as a large-scale network.

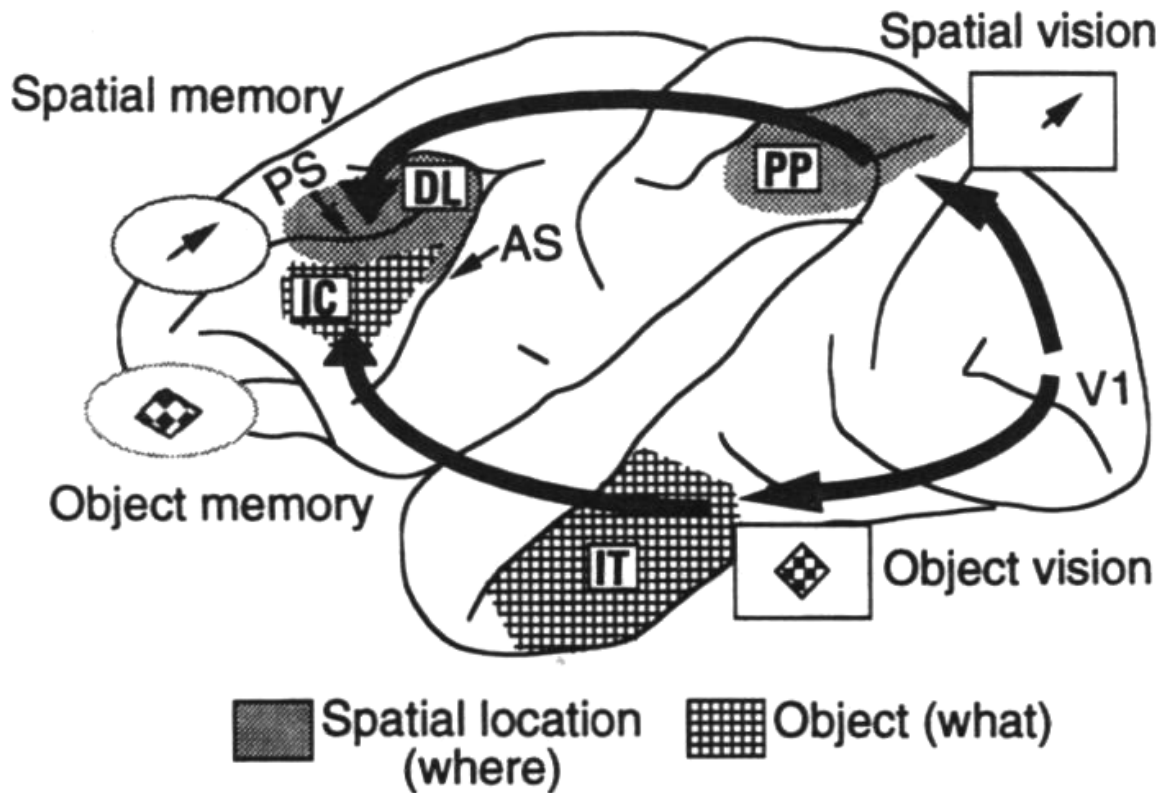


Figure 1.2 “What” vs “Where” theory of functional specialization in nonhuman primate working memory. The visual system (V1) passes information to both the posterior parietal (PP) cortex, which is concerned with spatial perception, and the inferior temporal (IT) cortex, which is associated with object recognition. These regions are connected to the dorsolateral (DL) and inferior convexity (IC) prefrontal cortices where representations of spatial location and object identity have been observed during working memory (Goldman-Rakic, 1995, 1996a, 1996b). This theory extends the original “what” and “where” pathways for non-spatial object identity projecting from occipital to inferior temporal cortex and object spatial information projecting from occipital to parietal cortex, respectively (Mishkin & Ungerleider, 1982). PS: principal sulcus; AS: arcuate sulcus. Originally published in: F. A. W. Wilson, Scaldidhe, & Goldman-Rakic (1993), “Dissociation of object and spatial processing domains in primate prefrontal cortex”, *Science*, 260(5116). Reproduced with permission from The American Association for the Advancement of Science.

1.2 Large-scale Networks Supporting Cognition

It was traditionally thought that the seat of different types of cognition could be localized to specific static regions of the brain (Downing & Kanwisher, 2001; Kanwisher et al., 1997). The most extreme version of this doctrine can be found in phrenology, whose proponents thought that the shape of the skull dictated mental capacities (Parker Jones et al., 2018). However, recent work has shown that cognition is supported by distributed large-scale brain networks that include the prefrontal cortex (Buschman &

Miller, 2007b; Saalman et al., 2007; Salazar et al., 2012; X.-J. Wang, 2010; Womelsdorf et al., 2007). Non-human primates have a well-developed prefrontal cortex and are evolutionarily closest to humans in comparison to other commonly used experimental animals such as rodents (Goldman-Rakic, 2011). Thus, they are the preferred model for animal studies on cognition, largely facilitated through invasive electrode recording during experimental tasks.

1.3 Data Acquisition

With technological advances over the years, it has become feasible to obtain large-scale simultaneous recordings from electrodes inserted into distributed regions of the brain, comprising many gigabytes or terabytes of data (Dotson et al., 2015, 2017; Hong & Lieber, 2019; Steinmetz et al., 2018). The very latest technology combines optogenetic stimulation with electrode recording to provide both spatial and temporal dynamics of neural activity. However, there are tradeoffs made between preserving areas for optical stimulation and damaging tissue with penetrating electrodes. Further details can be explored elsewhere (Galvan et al., 2017; Kleinbart et al., 2018; Yazdan-Shahmorad et al., 2016). This review will focus on studies which acquired data from large-scale distributed depth electrodes as this technology is more mature and widely used.

The amount of data provided by distributed depth electrode recording is substantial. Thus, it can be challenging to analyze without appropriate methods. Time-frequency (Mike X Cohen, 2014) and graph theoretic (Zalesky et al., 2016) analyses are well-suited for characterizing large-scale neural networks using large datasets. Correlations between spike trains recorded concurrently from distributed regions of the brain are also used to

examine information flow in networks (Campo et al., 2015). Best practices have been identified for the application and interpretation of these methods (Pesaran et al., 2018).

Signals must be sampled at regular intervals to apply spectral analysis, with frequencies of interest less than half of the sampling rate according to the Nyquist theorem (Mike X Cohen, 2014). Currently, the most effective method of sampling cognitive neural activity from electrodes is to obtain invasive electrophysiological recordings distributed throughout the brain of behaving non-human primates (Dotson et al., 2015, 2017). This technique provides large coverage of the brain with high spatial and temporal resolution adequate to capture cortical and subcortical dynamic coordination (Buzsáki, 2010; Tognoli & Kelso, 2014). It has resulted in the discovery of spectral characteristics of the frontoparietal network supporting a range of cognitive functions including attention (Fiebelkorn et al., 2018, 2019), categorization (Antzoulatos & Miller, 2016), decision making (Helfrich & Knight, 2016; Siegel et al., 2015) and the topic of this review, working memory (André M. Bastos et al., 2018; Buschman & Miller, 2007b; Compte et al., 2003; Lara & Wallis, 2014; Lundqvist et al., 2016; Pesaran et al., 2002; Salazar et al., 2012; Siegel et al., 2009).

1.4 Time-Frequency Analysis

Spectral characteristics of populations of neurons can be obtained by analyzing a continuous neural signal over time. The process of extracting frequency-specific information from temporal windows in the signal is known as time-frequency analysis. It is used to interpret signals that are non-stationary, which means they change over time (Mike X Cohen, 2014). Neuroscientists are primarily interested in changes in neural activity over time in relation to salient events such as stimulus processing, motor

planning or speech production. Thus, they have made use of the method to discover rhythmic patterns associated with a variety of perceptual, cognitive and motor functions (Buzsáki & Draguhn, 2004). However, it is important to keep in mind that methodological differences, such as the choice of time-frequency decomposition method or frequency band definition can impact results (X.-J. Wang, 2010). Typically, data used in the analysis is acquired from the electroencephalogram (EEG), magnetoencephalography (MEG), or electrodes in the brain. This review will explore the results of time-frequency analysis using the last, and most invasive, approach which provides two continuous signals: the neuronal firing rate (Compte et al., 2003) and the local field potential (LFP) (Pesaran et al., 2002).

1.5 Working Memory Nonhuman Primate Tasks

Traditionally, tests of working memory in the nonhuman primate are some variant of a delayed-response task. In the delayed-response task (Hunter, 1913), an animal is shown a stimulus, followed by a variable delay after which an action occurs that is informed by the previously observed stimulus. After the delay, the animal is not provided with any cues that would inform their response. Thus, they must use representational memory of what was presented during the stimulus to enable a correct response. This is different from tasks where the animal is shown something that immediately elicits a response using associational memory. The response here is driven by external stimuli in contrast to the inner model the animal uses in the delayed-response task (Goldman-Rakic, 2011).

The prefrontal cortex has been shown to be vital for correct performance of delayed-response tasks in non-human primates (Jacobsen & Nissen, 1936). Specifically,

the dorsolateral cortex is involved in tasks that require the integration of separate spatial and temporal elements of cognition. This describes most delayed-response or matching tasks used in cognitive studies. The ventral prefrontal cortex (vPFC) is involved in behavioral inhibition, which is used in delayed alternation tasks. These tasks require the non-human primate to alternate between two actions during each trial, resulting in an action opposite to that which was cued (Fuster, 2015). Lesions of the vPFC have been shown to induce deficits in the performance of visual delayed matching-to-sample tasks where the non-human primates have to match the object observed during stimulus, regardless of location, usually by saccade (Mishkin & Manning, 1978; R. Passingham, 1975). Conversely, lesions of the dorsal prefrontal cortex (dPFC) have been shown to impair spatial delayed-response tasks (Goldman & Rosvold, 1970; Mishkin & Manning, 1978; R. E. Passingham, 1985). These and other findings have motivated the hypothesis that the prefrontal cortex is responsible for coordinating the sustained activation of posterior cortical networks to support the visual and spatial short-term memory necessary for correct performance of delayed match-to-sample and response tasks, respectively (Fuster, 2015).

Early studies attempted to understand the role of non-human primate prefrontal cells in short-term memory using spike train analysis on the delay period in these tasks. It is thought that changes during this period may be related to the retention of information encoded during the cue period (Fuster, 1973; Fuster & Alexander, 1971; Kubota et al., 1974). Researchers used this approach to pursue a memory topography of the PFC. Areas 8, 9 and 46 were found to contain direction-specific memory cells (Funahashi et al., 1989, 1990, 1991). Moreover, cells were discovered dorsal to the principal sulcus that appeared

to respond preferentially during the delay period of spatial delayed-response tasks, while cells discovered ventral to the principal sulcus responded preferentially during the delay of non-spatial delayed-response tasks (Fuster et al., 1982; Goldman-Rakic, 1995; F. A. W. Wilson et al., 1993). This motivated a theory of prefrontal functional specialization (Goldman-Rakic, 1995, 1996a, 1996b) where spatial memory occurred in the dorsolateral portion and more ventral areas were responsible for non-spatial memory such as shape and color (Figure 1.2). The theory was an extension to the “what” and “where” visual pathways for non-spatial object identity projecting from occipital to inferior temporal cortex and object spatial information projecting from occipital to parietal cortex, respectively (Mishkin & Ungerleider, 1982). Transcranial magnetic stimulation has been used in support of this theory, establishing a separation between spatial and non-spatial deficits in dorsal and ventral lateral cortex, respectively (Mottaghy, 2002). However, other work in the human and non-human primate was not able to segregate identity and location in the lateral PFC based on spike-train analysis (N. G. Müller & Knight, 2006; Notger G. Müller et al., 2002; Rao et al., 1997).

A different interpretation of the spatial delayed-response tasks used to establish the theory is that the cells were not preferentially responding to cue-related information. Instead, their activity reflects a preparation for the ensuing motor action. Thus, a prospective motor working memory is proposed to function alongside a non-spatial visual working memory in the prefrontal cortex which acts in concert with the spatial information provided by the parietal cortex (Sasaki et al., 2020) to guide successful performance in delayed-response tasks (Fuster, 2000; Quintana & Fuster, 1992, 1999).

1.6 Task-dependent Oscillations

The preceding interpretation leads to the consideration of multiple networks activating concurrently during working memory. Some examples of networks purportedly active during the delay period include those that represent the rules of the task, the pending behavioral response, and reward expectation. These are enabled via interaction with long-term memory and are widely distributed throughout the brain (Fuster, 2015). Thus, it is reasonable to assume that working memory networks are embedded within larger cognitive networks which encode general aspects of the delay task.

A brain rhythm observed during spectral analysis can be understood as a signature of one of the concurrently active networks during working memory whose elements fire in synchrony and periodically (Fuster, 2015). This hypothesis helps explain the heterogeneity of spiking activity observed during different delay tasks such as the visual match-to-sample and spatial response (Shafi et al., 2007). The different patterns of spikes reflect participation in different co-occurring networks. In the context of delay tasks, the multitude of networks occurring over time enable the initial sensory percept to result in a subsequent motor action thereby establishing the perception-action cycle (Ardestani et al., 2016; Fuster, 2000).

The entirety of frequency-specific signatures of oscillatory networks observed during delay tasks can be interpreted as a “spectral fingerprint” of the underlying neural computation necessary to complete the task (Siegel et al., 2012). These fingerprints are useful for comparing the cognitive processes that are assumed to support experimental tasks. In this review, the spectral fingerprints of delayed-response, matching and more complex visuospatial tasks acquired by invasive, distributed electrophysiological

recordings will be identified to establish commonalities and differences between large-scale frontoparietal visual spatial, non-spatial, and visuospatial working memory in the nonhuman primate (Figure 1.3). The local dynamics within frontal and parietal regions will be explored as well as the long-range interactions between them.

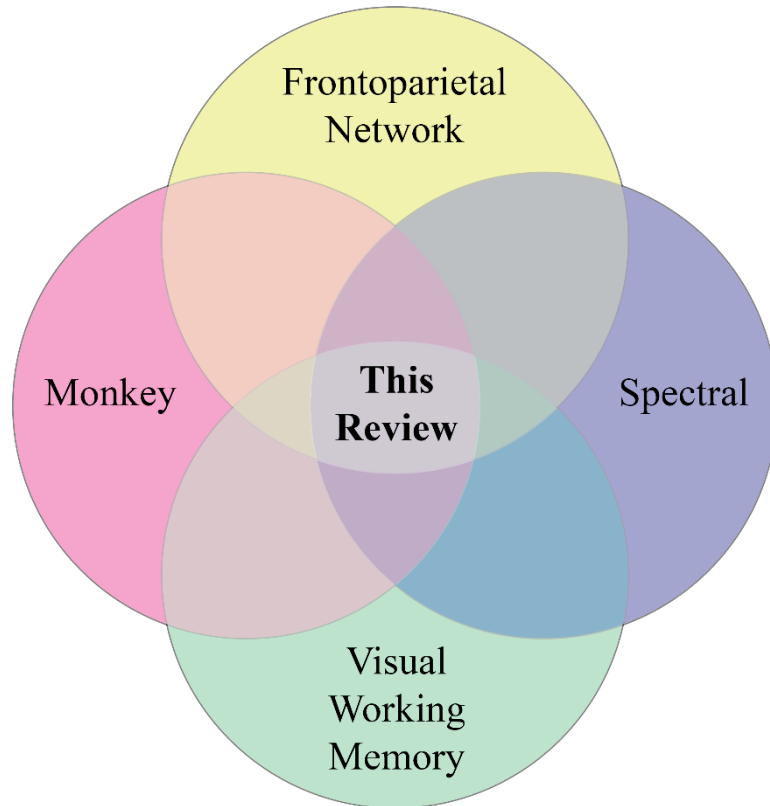


Figure 1.3. Venn diagram of the topics covered in this review. The spectral characteristics reported in the monkey frontoparietal network during visual non-spatial, spatial, and visuospatial working memory tasks will be synthesized and explored.

1.7 Methods

1.7.1 Task Assignment

Experimental tasks were categorized according to whether visual non-spatial, spatial, or visuospatial working memory was utilized. Experiments where the monkey simply had to process the color or identity of an object over a delay period, irrespective of where it appeared during stimulus, were assigned as a visual non-spatial working

memory task. Tasks in which the monkey was required to process a spatial property, regardless of the object conveying it, over a delay period were categorized as relying on visual spatial working memory. Delayed-saccade tasks where the monkey had to saccade to a position identified during stimulus have traditionally been considered tests of spatial working memory. However, they may instead be facilitated by prospective motor working memory whereby the monkey stores the motor plan of where to move his or her eyes over a delay period (Fuster, 2015). For the purposes of this study, these tasks, which were identified as a test of spatial working memory originally, remained categorized as visual spatial working memory tasks. Finally, tasks that required the monkey to process both an identification property of an object and its place in space over a delay period were categorized as visuospatial working memory. One exception was a single study that pooled together visual non-spatial and spatial working memory tasks, as previously defined. This necessitated a visuospatial task assignment (André M. Bastos et al., 2018).

1.7.2 Frequency Bands

Low, mid, and high range frequency bands appear to support spatial, non-spatial and visuospatial working memory (Table 1.2 and Table 1.3). However, the ranges differ between visuospatial and spatial/non-spatial tasks. For the spatial and non-spatial tasks, the low frequency band is comprised of components under 15hz, typically in the 1-10Hz range consisting of delta (1-4Hz), theta (4-8Hz) and alpha (8-12Hz). The middle frequency band generally comprises components between 12-35Hz. Traditionally, this range is referred to as beta. The high frequency band is any component above 35Hz, also known as gamma. These are canonical bands which require empirical validation.

For the visuospatial tasks, the low frequency band is again mostly comprised of components under 20Hz (Table 1.3). The mid band ranges from 15-50Hz. There is a slight overlap based on the reported band boundaries, with the majority of the components falling within a single category (Table 1.1). The high frequency band is comprised of components greater than 50Hz. It is interesting that the empirical reports of high band visuospatial activity are 15 Hz higher than the spatial/non-spatial empirical reports.

Not all reported bands fit neatly into these categories (Table 1.1). When the beginning or ending frequency of a reported band in a study spanned two categories, the median component determined the category for the result. The median is a good proxy for how most components are categorized. For example, the 8-25Hz range (Dotson et al., 2014) starts within the range established by the spatial/non-spatial tasks for the low frequency band, but ends in the mid. Its median component is 16.5, which is in the mid band. This qualifies the 8-25hz band as belonging to the mid-band category. Indeed, most of its components (12-25Hz) fall in the 12-35Hz spatial/non-spatial mid-band range. Three additional reported ranges, 5-20Hz (Compte et al., 2003), 10-30Hz (Jacob et al., 2018) and 25-90Hz (Pesaran et al., 2002), spanned the spatial/non-spatial bands and were categorized as low, mid, and high, respectively. Only two reported ranges spanned the visuospatial categories, 4-22Hz (André M. Bastos et al., 2018) and 8-50Hz (Kornblith et al., 2016), which were categorized as low and mid, respectively.

	Range (Hz)		Median	Category
	Start	End		
Spatial vs Non-spatial	5	20	12.5	low
	8	25	16.5	mid
	10	30	20	mid

	25	90	57.5	high
Visuospatial	4	22	13	low
	8	50	29	mid

Table 1.1. Reported frequency band outliers.

The median of each range was used to categorize them into appropriate spatial/non-spatial or visuospatial frequency bands. Spatial/non-spatial outlier reported ranges: 5-20Hz (Compte et al., 2003), 8-25Hz (Dotson et al., 2014), 10-30Hz (Jacob et al., 2018), and 25-90Hz (Pesaran et al., 2002). Visuospatial outlier reported ranges: 4-22Hz (André M. Bastos et al., 2018) and 8-50Hz (Kornblith et al., 2016).

1.7.3 Limitations

The preference in most investigations of working memory is to focus on examining just a single area of the brain. This is likely partly due to the relatively easier surgery and subsequent recording from a single area versus multiple. Many studies target the PFC to characterize its spiking activity or oscillations, ignoring the rest of the brain and its potential role (Barbosa et al., 2020; Funahashi, 2006; Lundqvist et al., 2016; Markowitz et al., 2015; X. L. Qi & Constantinidis, 2012). Others do record from multiple regions that can function together as a working memory network, but only analyze the activity within areas, not between (Katsuki & Constantinidis, 2013; X.-L. Qi, 2010; Quintana & Fuster, 1999). Until there is technology that is able to provide all neural activity from the entire brain during a task, studies will likely fail to report the specific contribution of all brain areas necessary for the successful completion of the experimental task.

Furthermore, there are several different parcellation schemes used by various groups. Parcellation boundaries between areas differ based on whether they were derived using cytoarchitecture or functional considerations (D. Pandya et al., 2015). Many studies in this review relied on functionally established boundaries using techniques like microstimulation. Accordingly, some areas may take up more cortical real estate than others, like lateral prefrontal cortex (lpFC) (Antzoulatos & Miller, 2016). The areas may

have latent specialization which can only be uncovered if split into dorsal and ventral components, such as areas 46d and 46v (Michael Petrides & Pandya, 2007), respectively. Researchers should specify which atlas, or parcellation scheme, they are using. It would be ideal if all labs could agree on a preferred atlas for experimentation.

The low number of studies finding high frequency activity in strictly spatial and non-spatial working memory tasks makes it difficult to draw any meaningful conclusions. This could mean high frequency activity does not influence working memory processes in these tasks.

There were only two studies which focused on frontal cortex and found low frequency activity during a visuospatial task (André M. Bastos et al., 2018; Lara & Wallis, 2014). Furthermore, only one study explored parietal and frontoparietal directed connectivity in visuospatial tasks (Kornblith et al., 2016). More studies utilizing visuospatial tasks must be conducted before meaningful conclusions can be made about the support provided by different frequency bands.

1.8 Frequency Band Activity in Spatial vs Non-spatial Working Memory

As previously noted, three frequency bands can be observed supporting spatial and non-spatial visual working memory tasks: a low (1-15Hz), mid (12-35Hz), and high (35Hz+) band (see Methods and Table 1.2).

1.8.1 Low Frequency Band

Within frontal and parietal cortices, low frequency spiking power was suppressed during the delay period via inhibitory interneurons (Compte et al., 2003; Joelving et al., 2007). Conversely, low frequency LFP power increased within frontal and parietal

cortices during the memory delay of non-spatial tasks (Jacob et al., 2018). Thus, the low frequency network appears to be differentially activated during the delay period in separate frontal and parietal regions according to whether the nonhuman primate is completing a spatial or non-spatial task.

Whereas there was a difference in the power of separate regions between spatial and non-spatial tasks, there is a consistent connectivity found across tasks between frontal and parietal regions. Specifically, directed functional connectivity in the low frequency band from frontal area PMd/F2 to parietal PRR/MIP was observed during the retrieval of spatial goals in response to a “go” cue, after the delay period but before a movement response. This suggests a top-down retrieval of goal information from spatial working memory (Martínez-Vázquez & Gail, 2018). Directed feed-back connectivity was also found in the low frequency band from prefrontal cortex (pFC) to VIP during the memory delay of a non-spatial task. Upon further investigation, a phase-dependent code between pFC spikes from sample-encoding neurons and the LFP in VIP during the delay was found to differentiate between task-relevant and distracting stimuli (Jacob et al., 2018). In both cases, a top-down control signal was transmitted from frontal to parietal cortices during and after delay periods to enable successful completion of both spatial and non-spatial working memory tasks in the low frequency band. Thus, this may be the preferred channel for top-down communication in support of these tasks.

1.8.2 Mid Frequency Band

LFP power and synchrony in the mid frequency band of separate frontal and parietal regions increased during the epoch of a spatial task when a category was encoded, part sample and part delay (Antzoulatos & Miller, 2016). This stands in contrast

to non-spatial tasks where mid frequency power in separate frontal and parietal regions was observed to decrease during the delay period (Jacob et al., 2018; Lundqvist et al., 2018). Additionally, a 32Hz mid frequency component was found to optimally encode objects at different phases of its cycle during the memory delay of a non-spatial task (Siegel et al., 2009). Therefore, like the low frequency network, the mid frequency network also appears to be differentially activated in separate frontal and parietal cortices depending on whether a spatial or non-spatial task is being performed. In the non-spatial task specifically, it may be used to encode objects at different phases.

The mid frequency band's involvement across frontal and parietal regions is more heterogeneous in its support of spatial and non-spatial tasks. Directed functional connectivity in the mid band from parietal PRR/MIP to frontal PMd/F2 was observed when the monkey was holding a state during the delay period of a spatial task, independent of working memory content. This points to a potential role in withholding movement (Martínez-Vázquez & Gail, 2018). In another spatial task, synchrony between frontal 8A/FEF and parietal AIP was observed during category encoding. After further inspection, it was discovered that spiking neurons in frontal 8A/FEF synchronized to parietal AIP's mid band LFP suggesting a directed influence from frontal to parietal cortices during spatial categorization (Antzoulatos & Miller, 2016). Thus, the mid band has been shown to exhibit both top-down and bottom-up neural activity across different frontoparietal pairs in support of spatial working memory tasks.

The mid frequency band has been observed serving a range of functional roles supporting non-spatial working memory tasks. Undirected connectivity in the mid band between frontal FEF/lpFC and parietal LIP around the time of saccade was stronger in a

top-down visual search non-spatial task when compared with a bottom-up salient pop-out task. The top-down visual search task likely required more working memory resources (Buschman & Miller, 2007b). A later study also found undirected synchrony during the delay period in the mid band between frontoparietal pairs including frontal areas 6DR, 8Ad, 8B, dPFC and vPFC and parietal areas PEC, PE, PG, MIP and LIP which encoded the identity of the object presented as stimulus. The synchrony patterns were discovered to be regulated by activity arising in the posterior parietal areas, suggesting a feed-forward encoding mechanism (Salazar et al., 2012). Additionally, the LFP relative phase of the mid band exhibited simultaneously in-phase and anti-phase correlations between the same frontoparietal pairs during the delay period suggesting that the integration and segregation of the large-scale frontoparietal network is dynamically regulated (Dotson et al., 2014). Finally, in a numerosity non-spatial task, directed connectivity from parietal VIP to frontal pFC increased in the mid band during cue and distractor presentations suggesting a feed-forward processing of the most recently viewed numerical input (Jacob et al., 2018).

Based on the results above, the mid band has a clear role in supporting non-spatial working memory through frontoparietal synchrony occurring at different times throughout the trials. Further, it appears processing travels in a feed-forward mid-band channel from parietal to frontal cortical areas. This stands in contrast to the dual feed-forward and feed-back mid-band processing observed in spatial tasks. The mid band may function across the frontoparietal network in a bidirectional capacity in support of spatial working memory and unidirectional in support of non-spatial working memory.

1.8.3 High Frequency Band

In frontal cortex, high frequency bursting activity was observed in the LFP of the lpFC at the end of the delay period of a non-spatial task as the monkey prepared to use a working memory object to compare against test objects. When the working memory object was no longer needed after the trial ended the bursting decreased (Lundqvist et al., 2018). In parietal LIP, high frequency LFP power increased during the memory delay of a spatial task and was able to decode direction and timing of the planned movement (Pesaran et al., 2002). Perhaps bursting is a unique feature of non-spatial frontal working memory activity. More studies are needed to test this hypothesis. Regardless, results from these studies suggest activity in the high frequency band within frontal and parietal regions increases during the delay period of both spatial and non-spatial tasks.

Stronger high frequency synchrony was observed in the LFP between parietal LIP and frontal FEF/lpFC during the delay and around the time of saccade in a bottom-up non-spatial task when compared with a top-down visual search task. The synchrony was likely unrelated to working memory processes as the bottom-up task tested salience and did not require the monkey to remember anything (Buschman & Miller, 2007b). Thus, the high frequency power observed within frontal and parietal regions may support spatial and non-spatial working memory processes, but the synchrony observed between non-spatial frontoparietal pairs may not.

Table 1.2. Summary of all spatial and non-spatial visual working memory studies on nonhuman primates

The first two rows summarize spectral characteristics reported as power and synchrony found within frontal and parietal regions for the type of working memory labeled in each column. The third row summarizes spectral characteristics reported as synchrony and directed connectivity measures between frontal and parietal regions for the type of working memory labeled in each column. Low band results are in purple, mid band is in blue and high band is in green.

	Spatial	Non-spatial
Frontal	<ul style="list-style-type: none"> □ Across areas FEF/46, spiking power in low band (5-20Hz) was suppressed during delay, along with elevated firing. <ul style="list-style-type: none"> ○ Power suppression facilitated through inhibitory interneurons (Compte et al., 2003) □ In 8A/FEF and 8A/FEF<->45/46, increased LFP power and synchrony in the mid band (15-32Hz) band occurred during category encoding (sample & delay) and was associated with category selectivity (Antzoulatos & Miller, 2016) 	<ul style="list-style-type: none"> □ In vlpFC, Spike-LFP synchrony during delay in low 3Hz & mid 32Hz (Siegel et al., 2009) □ First of two objects optimally encoded at earlier 32Hz phase (Siegel et al., 2009) <ul style="list-style-type: none"> ○ Different objects encoded at different phases □ In IPFC, LFP high band (50-120Hz) power bursts increased, and mid band (20-35Hz) decreased at end of delay, when monkey anticipated a need to use WM object to compare against test objects. When WM object no longer needed post-trial, high band power decreased and mid band increased (Lundqvist et al., 2018) □ Mid band may regulate high band and information content of WM, clearing it out post-trial by suppressing high band □ In lpFC, increased LFP power during delays in low band (2-8Hz), while mid band (10-30Hz) decreased (Jacob & Daniel, 2018)
Parietal	<ul style="list-style-type: none"> □ In 7a (PG/PFG), spiking power suppressed in low band (5-10Hz) during delay, increased mid band (15-20Hz) during fixation (Joelving et al., 2007) □ In LIP, LFP high band (25-90Hz) power increased during delay <ul style="list-style-type: none"> ○ Decode direction & timing of planned movement from LFP (Pesaran et al., 2002) □ In AIP, increased LFP synchrony in low band (2-4Hz) and increased LFP power and synchrony in mid band (15-32Hz) during category encoding (sample & delay) related to category selectivity (Antzoulatos & Miller, 2016) 	<ul style="list-style-type: none"> □ In VIP, increased LFP power found during memory delays in low band (2-8Hz), while mid band (10-30Hz) decreased (Jacob & Daniel, 2018)
Frontoparietal	<ul style="list-style-type: none"> □ Directed FC in mid band (12-32Hz) from PRR (MIP) to PMd (F2) while holding current state during delay, independent of WM content <ul style="list-style-type: none"> ○ Indicates role in states where animal withholds movement (Martínez-Vázquez & Gail, 2018) □ Directed FC in low band (1-10Hz) from PMd (F2) to PRR (MIP) during retrieval of spatial goals in response to “go” cue, after delay, prior to movement response <ul style="list-style-type: none"> ○ Suggests top-down retrieval of goal information from spatial WM in 1-10Hz low band (Martínez-Vázquez & Gail, 2018) 	<ul style="list-style-type: none"> □ Stronger LFP coherence between LIP and FEF/lpFC in high band (35-55Hz) during bottom-up pop-out task in memory delay and around time of saccade (before and after) vs top-down visual search task, which req’d more WM. <ul style="list-style-type: none"> ○ Mid band (22-34Hz) coherence stronger in top-down visual search task vs bottom-up pop-out task around time of saccade ○ Suggests different frequency bands differentially support the tasks and may be responsible for top-down (frontal neurons show selectivity before parietal) and bottom-up (parietal neurons show selectivity before frontal) processes (Buschman & Miller, 2007b)

	<ul style="list-style-type: none"> □ In AIP<->8A/FEF, increased LFP synchrony in mid band (15-32Hz) band during category encoding (sample & delay) associated with category selectivity <ul style="list-style-type: none"> ○ 8A/FEF spiking neurons synchronized to AIP mid band at same time, suggesting unidirectional PFC influence on PPC(Antzoulatos & Miller, 2016) 	<ul style="list-style-type: none"> □ Directed FC feed-back signaling from pFC to VIP increased in low band (2-8Hz) during memory delays, while feed-forward signaling from VIP to pFC increased in mid band (10-30Hz) during cue/distractor <ul style="list-style-type: none"> ○ Suggests feedforward of most recently viewed numerical input and feedback differentiated between multiple memorized inputs (Jacob & Daniel, 2018) □ Phase dependent low band (4-8Hz) code between pFC spikes from sample-encoding neurons and LFP in VIP during memory delay separates between task-relevant and distracting stimuli (Jacob & Daniel, 2018) □ Mid band (12-22Hz) coherence during delay between frontoparietal pairs including frontal areas 6DR, 8Ad, 8B, dPFC and vPFC and parietal areas PEC, PE, PG, MIP and LIP found to encode object identity <ul style="list-style-type: none"> ○ Also synchrony patterns governed by activity arising first in the posterior parietal areas (Salazar et al., 2012) □ LFP relative phase in mid band (8-25Hz) exhibits simultaneous in-phase and anti-phase correlations within and between regions of frontoparietal network comprised of frontal areas 6DR, 8Ad, 8B, dPFC and vPFC and parietal areas PEC, PE, PG, MIP and LIP during delay period. <ul style="list-style-type: none"> ○ Suggests task-dependent integration and segregation of large-scale frontoparietal network is dynamically regulated (Dotson et al., 2014)
--	--	---

1.9 Frequency Band Activity in Visuospatial Working Memory

Some studies used experimental tasks that incorporated aspects of both spatial and non-spatial working memory. These tasks were considered to test visuospatial working memory function. With contributions from both types of visual working memory, it was expected that the low, mid, and high band signatures explored earlier would appear in varying degrees in the visuospatial results.

Accordingly, a low (1-20Hz), mid (15-50Hz), and high (50Hz+) frequency band emerged again in support of visuospatial working memory tasks (Table 1.3). However, their ranges are different from the spatial/non-spatial bands (see Methods).

1.9.1 Low Frequency Band

There were only reports of low frequency activity in visuospatial tasks in the frontal cortex. In frontal PMd, 8a, 8B, SMA/ACC, dlPFC and vlPFC, peaks in the low frequency band of the LFP from 200ms before and 500ms after stimulus, during the delay, of three pooled spatial and non-spatial tasks were observed in deep laminar layers 5 and 6. It was thought that this deep low band regulates the high band to maintain the contents of working memory (André M. Bastos et al., 2018). In a separate study, increased low frequency LFP power in frontal vlPFC upon cue presentation and during the early delay period of a visuospatial task was observed at electrodes with spatially selective neurons relative to non-spatial electrodes (Lara & Wallis, 2014).

The low frequency network was identified earlier as being stronger in the LFP during the delay of non-spatial tasks while the spiking power was weaker for spatial tasks in the frontal cortex. However, the visuospatial results explored above also provide a role for the low frequency network in the LFP during the delay period of the spatial

component of the task. Further, it appears the network may originate from layers 5 and 6 of the frontal cortex. Taken together, this suggests that the low frequency network in the LFP supports both spatial and non-spatial tasks, likely originating in the deep layers of frontal cortex.

1.9.2 Mid Frequency Band

The mid frequency band was observed within and across frontal and parietal regions during two separate visuospatial studies. In frontal FEF and lpFC, bursting in the mid band increased during the early and mid-delay period and decreased during the cue and late delay of a visuospatial task (Lundqvist et al., 2016). During the cue period of a different visuospatial task in frontal FEF and lpFC and parietal LIP, LFP power in the mid band decreased with contralateral visuospatial stimulus load (Kornblith et al., 2016). During the delay period in the same areas, LFP power in the mid band increased with contralateral visuospatial load. Also during the delay period, LFP power in the mid band in vlpFC increased in both 1 and 2-item trials. Within frontal lpFC, synchrony in the mid band decreased during the delay period with contralateral load. Finally, long-range synchrony in the mid band between frontal FEF and parietal LIP and frontal lpFC and parietal LIP during the cue period increased with contralateral load.

Whereas the mid band network was observed primarily during the delay period of spatial and nonspatial tasks, power within frontal and parietal areas in the LFP in the mid band appears to be differentially modulated throughout the trial in support of visuospatial working memory, based on the results above. Synchrony within frontal and across frontal and parietal areas in the mid-band LFP also modulates according to the epoch of the trial in support of visuospatial working memory.

1.9.3 High Frequency Band

High frequency activity has been observed within frontal and parietal cortices while nonhuman primates perform visuospatial working memory tasks. In frontal FEF and lpFC, high frequency bursting in the LFP increased during the cue period and throughout a visuospatial trial, especially at the end of the delay period as the monkey anticipated decoding working memory content. It was thought that this high frequency activity may gate working memory content by activating or suppressing spiking in encoding and decoding neurons (Lundqvist et al., 2016). Another study which pooled spatial and nonspatial tasks found high frequency power peaks in frontal PMd, 8a, 8B, SMA/ACC, dlPFC and vlPFC during the cue and delay periods in layers 1-3 (André M. Bastos et al., 2018). Furthermore, most of the delay period activity was found in the high frequency band in layers 1-3. The researchers suggested that this superficial high frequency band encoded stimulus information during the delay. As stated earlier, the deep low band may regulate this superficial high band. In frontal lpFC and FEF and parietal LIP, high frequency power in the LFP increased during cue presentation with contralateral visuospatial stimulus load (Kornblith et al., 2016). Recall, the mid band power in the same areas decreased during this epoch. This led the researchers to propose that the mid frequency activity observed during the delay may contribute to top-down processing and higher frequency activity observed during the cue may promote bottom-up sensory processing.

As reported in the spatial and non-spatial tasks, the high frequency network observed in frontal and parietal LFP power supports visuospatial working memory as well. Most studies above observed the high frequency power during the cue or delay periods of the

task, likely originating in superficial laminar layers of the frontal cortex. It would be helpful if future studies analyzed the direction of information transfer to discover whether a primarily top-down or bottom-up role emerges for the network.

Table 1.3. Summary of all visuospatial studies on nonhuman primates

The first two rows summarize spectral characteristics reported as power and synchrony found within frontal and parietal regions at different points throughout the visuospatial working memory trials. The third row summarizes the synchrony reported by a study between frontal and parietal regions during a visuospatial working memory task. Low band results are in purple, mid band is in blue and high band is in green.

	Visuospatial
Frontal	<ul style="list-style-type: none"> □ In FEF (8Ad & 8Av) and IPFC (46d/v, 9/46d/v, 45), LFP high band (45-100Hz) burst rate increased during cue period and throughout trial, esp at end of delay in anticipation of decoding WM content (Lundqvist et al., 2016) □ LFP mid band (20-35Hz) burst rate increased during delay period, esp early and mid and decreased during cue and late delay <ul style="list-style-type: none"> ○ High band bursts may gate/protect WM content by activating/suppressing spiking in encoding/decoding neurons (Lundqvist et al., 2016) □ In frontal PMd, 8a, 8B, SMA/ACC, dIPFC and vIPFC, LFP high band (50-250Hz) power peaks found in power from -200 – 500ms post stimulus (during delay) in superficial layers 1-3 and low band (4-22Hz) peaks in deep layers (5-6) (André M. Bastos et al., 2018) <ul style="list-style-type: none"> ○ Delay period activity largely in superficial layers (André M. Bastos et al., 2018) <ul style="list-style-type: none"> □ Superficial high band encoded stimulus information during delay (André M. Bastos et al., 2018) ○ Deep low band phase modulates superficial high band <ul style="list-style-type: none"> □ Suggests deep may regulate superficial high band to maintain contents of WM (André M. Bastos et al., 2018) □ In IPFC and FEF, during stimulus presentation, LFP power in high band (50-100Hz) increased and mid band (8-50Hz) decreased with contralateral visuospatial stimulus load (Kornblith et al., 2016) □ In IPFC and FEF, during delay period, LFP power in mid band (15-50Hz) increased with contralateral visuospatial stimulus load (Kornblith et al., 2016) □ Within IPFC, during delay period, synchrony in mid band (15-50Hz) decreased with contralateral visuospatial stimulus load (Kornblith et al., 2016) □ In vlpFC, during delay period, LFP mid band (20-35Hz) power increased in 1 and 2-items trials. <ul style="list-style-type: none"> ○ Also, on stimulus presentation and at beginning of delay period, increased low band (2-7Hz) power at electrodes with spatially selective neurons relative to nonspatial channels ○ Suggests a mechanism whereby PFC may maintain color information in posterior sensory cortex (Lara & Wallis, 2014)
Parietal	<ul style="list-style-type: none"> □ In LIP, during stimulus presentation, LFP power in high band (50-100Hz) increased and mid band (8-50Hz) decreased with contralateral visuospatial stimulus load (Kornblith et al., 2016) □ In LIP, during delay, LFP power in mid band (15-50Hz) increased with contralateral visuospatial stimulus load (Kornblith et al., 2016)
Frontoparietal	<ul style="list-style-type: none"> □ In FEF<->LIP and IPFC<->LIP, during stimulus presentation, synchrony in mid band (16-30Hz) increased with contralateral visuospatial stimulus load (Kornblith et al., 2016) <ul style="list-style-type: none"> ○ Support the view that mid band oscillations may contribute to top-down processing and high band oscillations (observed during cue presentation) to bottom-up sensory processing (Kornblith et al., 2016)

1.10 Conclusion

Generally, low, mid, and high frequency bands of activity support spatial, non-spatial and visuospatial working memory in a similar manner (Table 1.2 and Table 1.3). The low frequency network within frontal and parietal regions emerges in the LFP power in support of both spatial and non-spatial tasks. The frontal components appear to originate in the deep layers of cortex (André M. Bastos et al., 2018). It also serves as a channel for frontal cortex to send signals to parietal to complete either non-spatial or spatial tasks.

The low frequency network's role may be to sustain attention and target selected stimuli. Studies have shown low frequency components serve as the basis for the environmental sampling which constitutes visual attention (Fiebelkorn et al., 2018; Helfrich et al., 2018). Furthermore, the low frequency band enables stimulus selection during the cue period either by signal enhancement or suppression of competing stimuli (Foster & Awh, 2019). A sustained internal attention to the targeted stimulus is essential for the completion of both spatial and non-spatial working memory tasks.

Mid band activity was observed in a variety of roles in support of spatial, non-spatial and visuospatial working memory. Within frontal and parietal regions, the LFP power was differentially modulated between spatial and non-spatial tasks during the delay period. However, in a visuospatial task, it was modulated throughout the entire trial. Additionally, the mid band serves as a channel for feedforward parieto-frontal activity supporting non-spatial working memory, while it supports spatial working memory through both feedforward and feedback processes between frontal and parietal cortices. Finally, like the power, LFP synchrony within frontal and across frontal and

parietal regions modulates through the entire trial in support of visuospatial working memory.

The mid band network may act as a filter, protecting working memory content from degradation from competing stimuli over time (Engel & Fries, 2010). Spatial category maintenance (Antzoulatos & Miller, 2016) and non-spatial object encoding (Salazar et al., 2012) provide ways in which the mid band maintains working memory content over time in order to complete a task. It is critical that the monkey can maintain a spatial, non-spatial or visuospatial working memory representation for successful task performance. The mid band may fulfill this role in a task-dependent manner utilizing synchrony, feedback, and feedforward processing as necessary in order to protect and filter relevant working memory content.

The high frequency band within frontal and parietal regions supported spatial, non-spatial and visuospatial working memory tasks in a largely similar fashion. However, evidence is lacking for a role for the high frequency band in linking frontal and parietal regions in support of these tasks. The high frequency network emerged during the delay of spatial, non-spatial and visuospatial tasks in the LFP power. Additionally, it was observed during the cue period of a visuospatial task and arises from the superficial layers of frontal cortex.

The high frequency band may be responsible for transferring working memory information within the frontal and parietal areas (André M. Bastos et al., 2015). It was observed in the coherence of a bottom-up task where parietal neurons exhibited rule-selectivity prior to frontal neurons (Buschman & Miller, 2007b). It also emerged in the LFP power of electrodes with bottom-up task-relevant information about stimulus

location (Kornblith et al., 2016). Transferring working memory content using the high band within the PFC, visual sensory and association areas is essential for the completion of any visual non-spatial, spatial, or visuospatial working memory task.

In summary, each band has a distinct role which can be illustrated with a spectral model of monkey visual working memory (Figure 1.4). The low band sustains broad attention by selecting relevant content through long-range communication between frontal and parietal cortices. Furthermore, the low frequency network manifests in the power locally within frontal and parietal regions. The mid band protects and categorizes content in working memory through additional long-range frontoparietal interactions. Its network is also expressed in the power within frontal and parietal regions. The high band transfers working memory content within local regions for subsequent action. Thus, the bands act in a distributed, coordinated, and concurrent manner with specialized functions.

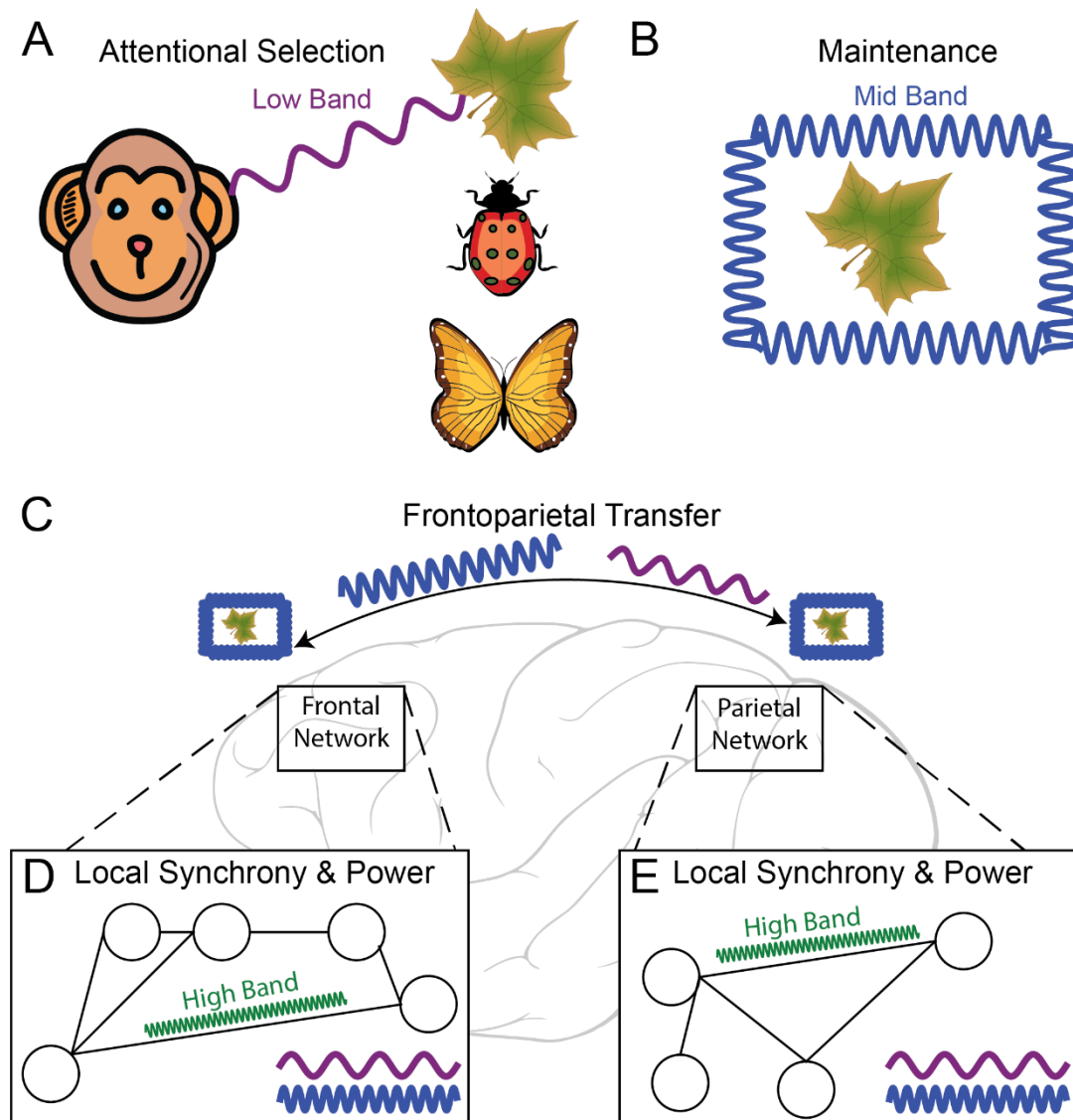


Figure 1.4. Spectral Model of Visual Working Memory in the Monkey.

A. Attentional selection. The monkey initiates a working memory task by selecting among competing stimuli using the low frequency band (purple). **B.** Maintenance of working memory content. The stimulus is maintained over a delay, protected from noise and distracting stimuli by the mid frequency band (blue). **C.** Frontoparietal transfer of working memory information. The low and mid bands enable long-range communication between frontal and parietal regions in support of the task. **D & E.** Local synchrony and power in frontal and parietal regions, respectively. Within each region (rectangles), the circles represent nodes and the lines connecting them represent edges in a hypothetical network. The high frequency band (green) enables transfer of the working memory content between local brain areas (circles). Differential power in low and mid bands within frontal and parietal regions also support the task. These bands function and interact in this manner throughout the trial in support of visual non-spatial, spatial, and visuospatial working memory.

The spectral model supports the idea that the central executive emerges as a result of simultaneous processors in the frontal and parietal regions (Goldman-Rakic, 1996a). It

serves as a mechanistic model, defining how each frontal and parietal domain-specific processor functions. It extends the theory by explaining how the regions could transfer information over such long distances and for what purpose. Specifically, information theory has established that effective information transfer over long distances is achieved at greater fidelity with lower frequencies. Joining these two areas to enable both the selection and protection of visual stimulus information is crucial for visuospatial working memory performance. The model also poses more questions concerning the nature of the interaction between the bands. How do they coordinate to ensure temporally effective activation? Does one band emerge as controller over another? How do these bands malfunction in pathologies? All these questions remain to be explored through further experimentation.

To expand upon the question concerning temporal coordination, it is likely the bands act in concert with one another, facilitating the complex interactions necessary to complete a task. It has already been proposed that the mid band regulates the high band, utilizing it to load in the information content of working memory and clearing it out when finished (Lundqvist et al., 2018). Correspondingly, the low band may enable the original content selection, which is subsequently transferred via the high band, under the direction of the mid band. With such dependence between bands, any perturbation during the trial could either have deleterious consequences or serve to enhance performance, subject to the timing and nature of the disruption. In fact, it is well-established that timely low frequency stimulation improves visual working memory performance in humans (Hsueh et al., 2016; Polanía et al., 2012; Reinhart & Nguyen, 2019; Reis et al., 2016). Efforts to

better understand the coordination amongst these bands would yield a more complete mechanistic understanding of visuospatial working memory.

In conclusion, the low, mid, and high bands dynamically organize in support of spatial, non-spatial and visuospatial working memory tasks. A new spectral model detailing their respective roles was proposed. Opportunities for future exploration include the temporal coordination between bands and how their malfunction contributes to pathologies. Establishing a detailed understanding of the spectral components underlying visuospatial working memory is important in proposing treatments for memory disorders and shedding light on related aspects of cognition.

2 ORGANIZATION OF AREAL CONNECTIVITY IN THE MONKEY FRONTOPARIETAL NETWORK

2.1 Introduction

The mammalian brain engages cortical neural networks during behavior (Bressler & Menon, 2010; Buzsáki & Draguhn, 2004). The networks are composed of brain areas, or nodes, connected via axonal projections, or edges (Newman, 2018; Sporns et al., 2004). This structural organization of the network permits a set of functional interactions observed in neural signals recorded during behavior (Z. Wang et al., 2015).

A prominent functional interaction observed in neural signals is that of synchronous activity (Varela et al., 2001). Recent studies have explored the structure-function relationship as it relates to synchrony through theoretical computational modeling. Vicente, Gollo, Mirasso, Fischer, & Pipa (2008) established that an apex node reciprocally connected to two unconnected nodes could foster zero-lag synchrony via dynamical relaying between the two unconnected nodes despite axonal conduction delays. This provided a topological mechanism for previously published findings from multicellular electrophysiological recordings which found distributed synchronous discharge in different structures of the cortex, hippocampus and thalamus (Contreras et al., 1996; Traub et al., 1996). Gollo, Mirasso, Sporns, & Breakspear (2014) extended this line of work by showing that a just a single resonance pair, two reciprocally connected nodes, could foster zero-lag synchrony in 3-node motifs. Further, they showed that the dynamical relay M9 motif, which has two resonance pairs, was optimally structured to

provide both zero and non-zero phase lag synchrony. Finally, they found that the synchrony initiated locally with a resonance pair could propagate through the entire network, thereby impacting global network dynamics. These studies provide candidate topological mechanisms for the neural synchrony that has been reported to support cognitive functioning.

It is thought that an impaired structure-function relationship results in, or contributes to, various cognitive impairments. This phenomenon has been explored in aging, schizophrenia and autism (Anderson et al., 2011; Ben Bashat et al., 2007; Fornito et al., 2012; Nakagawa et al., 2013; Persson et al., 2006). A better understanding of the connectivity patterns that arise in mammals without mental health disorders can allow for comparison with the patterns which characterize impairments observed in disorders within the context of connectomics (Polanía et al., 2012; Reinhart & Nguyen, 2019).

Cognitive processing can occur through neural interactions both within and between regions of the cortex, forming large-scale cortical networks (Bressler & Menon, 2010; Mesulam, 1990; Mishkin & Ungerleider, 1982). The frontoparietal network (FPN) is one such large-scale network comprised of sub-networks characterized by functional oscillatory dynamics that support aspects of cognition such as attention, cognitive control and working memory in both humans and non-human primates (Corbetta, 1998; Fiebelkorn & Kastner, 2019; Lundqvist et al., 2016; Marek & Dosenbach, 2018; Salazar et al., 2012; Zanto & Gazzaley, 2013). These dynamics exhibit unique spectral power and near-zero (König et al., 1995; Singer, 1999; Singer & Gray, 1995) and non-zero (Andre M. Bastos et al., 2015) phase-lag synchrony properties (Antzoulatos & Miller, 2016; Fries et al., 1997, 2008; Jacob et al., 2018; Kornblith et al., 2016; Salazar et al., 2012).

However, it is not understood how the unique structure of the FPN enables these properties to occur in the patterns required to support cognitive processing. The topological properties of this network remain to be elucidated.

Here the anatomical connections of the FPN are identified based on collated tract-tracing studies and examine the ways in which the topology acts as a reliable, integrative substrate while contributing to the reported neuronal dynamics which support varied cognitive functions. A new association matrix is proposed that uses a more finely detailed parcellation scheme than previous studies (Markov et al., 2014) with enough nodes for future analyses which require a high level of resolution (Cavada & Goldman-Rakic, 1989). A graph theoretic topological analysis (Albert & Barabási, 2002; Newman, 2018) was conducted to discover connectivity patterns in the 399 connections that make up the FPN and how they support cognitive functioning. The FPN is shown to be made up of relatively homogeneous connectivity between areas with an apparent lack of hub nodes controlling information flow. Further, the FPN utilizes a structural motif known for optimally promoting near-zero and non-zero neural synchrony (Gollo et al., 2014). Finally, the FPN is discovered to be a small-world network, conferring both functional specialization and topological integration. Therefore, the FPN leverages a distributed connectivity architecture useful for critical information processing. It is optimally structured to support various aspects of cognition through neural synchrony and integration into coherent streams which support overall behavior.

2.2 Results

2.2.1 The Frontoparietal Connectome

To identify the structural connectivity of the FPN, axonal projections between and within the frontal and parietal regions of the monkey were collated using the results of tract-tracing studies on non-human primates (Methods and Table 5.1) according to the parcellation scheme established by Petrides & Pandya (2007) (Figure 2.1).

These connections were assembled into a binary, directed adjacency matrix comprised of 30 nodes, 17 frontal and 13 parietal (Figure 2.2).

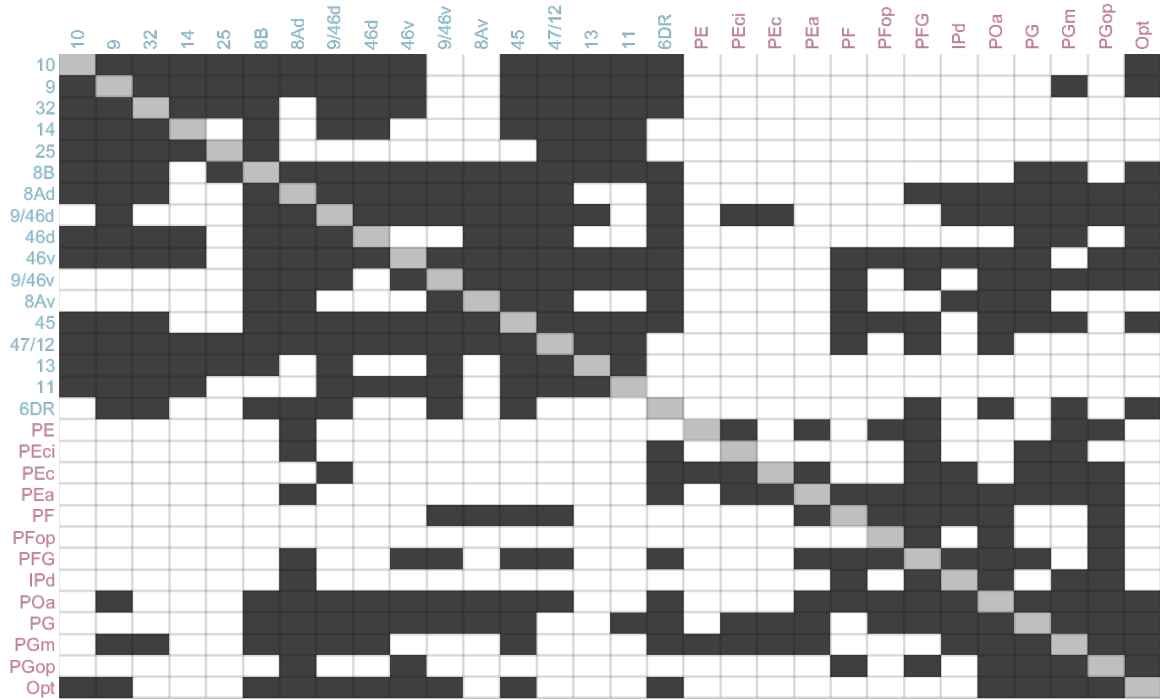


Figure 2.2. Binary, directed adjacency matrix describing the connectivity of the frontoparietal monkey network.

The rows of the matrix represent source nodes, and the columns represent projection target nodes. All nodes represent architectonic areas from the Petrides & Pandya (2007) parcellation scheme. Connections are indicated with a black square. White squares represent connections that were not reported in the collated studies. Grey squares on the diagonal represent within-area connections and are not considered in the graph analysis. The 17 frontal areas are in blue, while the 13 parietal areas are in pink.

The adjacency matrix can be used to visualize network topology as a graph to better understand connectivity patterns (Figure 2.3). Here, nodes are sized according to their total degree, with bigger nodes representing areas with a greater number of incoming and outgoing connections than smaller nodes. Apart from a few parietal areas and one frontal, most of the areas in the FPN are of a similar size, representing similar total connectivity. The strength of connections does not factor into this calculation because the adjacency matrix is binary.

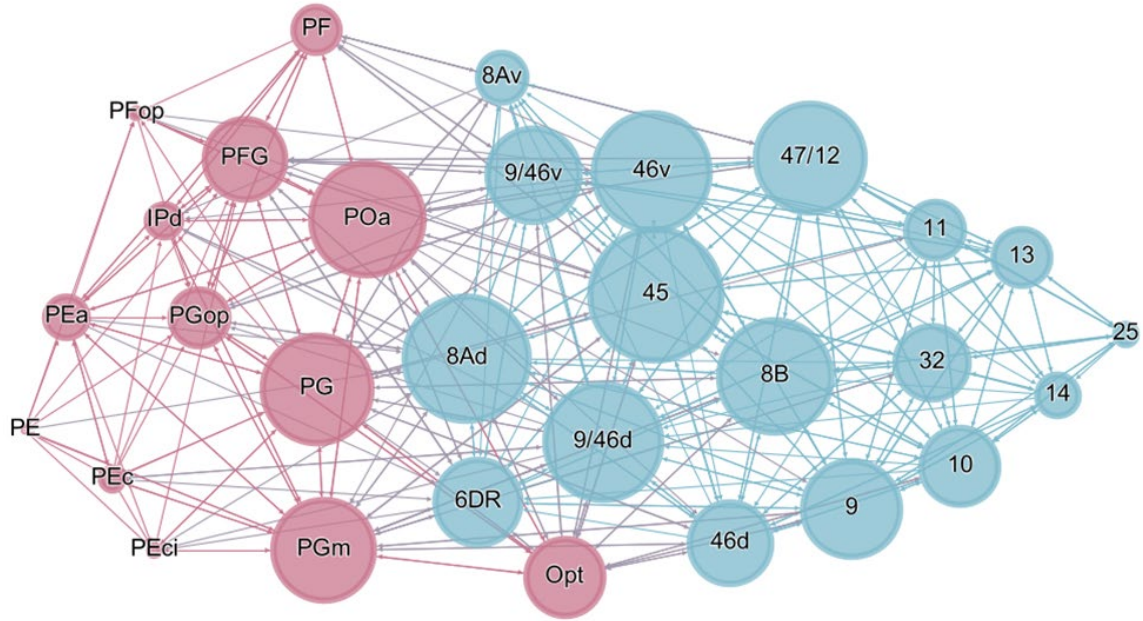


Figure 2.3. A graph representation of the frontoparietal network generated from the adjacency matrix. Frontal nodes are colored in blue and parietal in pink. The 399 directed edges between nodes represent projections between sources and targets. Node size is determined by total degrees, which is the sum of in-degree and out-degree connectivity. Bigger nodes represent a greater total degree than smaller nodes. The spatial distribution of the nodes is a function of the ForceAtlas layout in Gephi, a network visualization and analysis open-source software tool (Methods). The layout controls clustering and dispersion of nodes via attraction and repulsion strength parameter values (Cherven, 2015). Most nodes are of a similar size, representing relatively homogeneous connectivity.

2.2.2 Graph Theoretic Analysis

Degree distributions convey information about how connectivity is allocated across the network (Zalesky et al., 2016). The FPN's in and out degree distributions can be characterized as either single-scale, scale-free or broad-scale. Single-scale distributions are highly unlikely to contain hubs, while scale-free and broad-scale distributions have a high likelihood of hub nodes (Barabási & Albert, 1999).

The topology of some brain networks (Eguíluz et al., 2005; van den Heuvel et al., 2008; Varshney et al., 2011) present with hub nodes which serve to coordinate the majority of information transfer in the network (Newman, 2018). These scale-free degree distributions are fit by a power law (Barabási & Albert, 1999) with no node exhibiting

connectivity typical of other nodes. However, other studies have reported networks of the brain which do not follow power laws (Humphries et al., 2006; Modha & Singh, 2010; Sporns & Zwi, 2004).

Both tails of the degree distributions of the FPN were tested according to the Clauset, Shalizi, & Newman (2009) recipe to determine whether they were fit by a power law (Methods) (Clauset et al., 2009). The following parameter values were calculated for the in-degree distribution fit: $a = 3.375$, $x_{min} = 12$ and $L = -62.197$ and for the out-degree distribution fit: $a = 3.2521$, $x_{min} = 10$ and $L = -70.3376$.

The degree distributions were visualized by plotting their complementary cumulative distribution functions (cCDF) on logarithmic axes (Zalesky et al., 2016) with their estimated power-law fits (Clauset et al., 2009) (Figures 2.4a & b). The cCDF conveys the probability of finding a node with degree larger than some random value, x . Scale-free networks will approximate a straight line in these plots (Amaral et al., 2000).

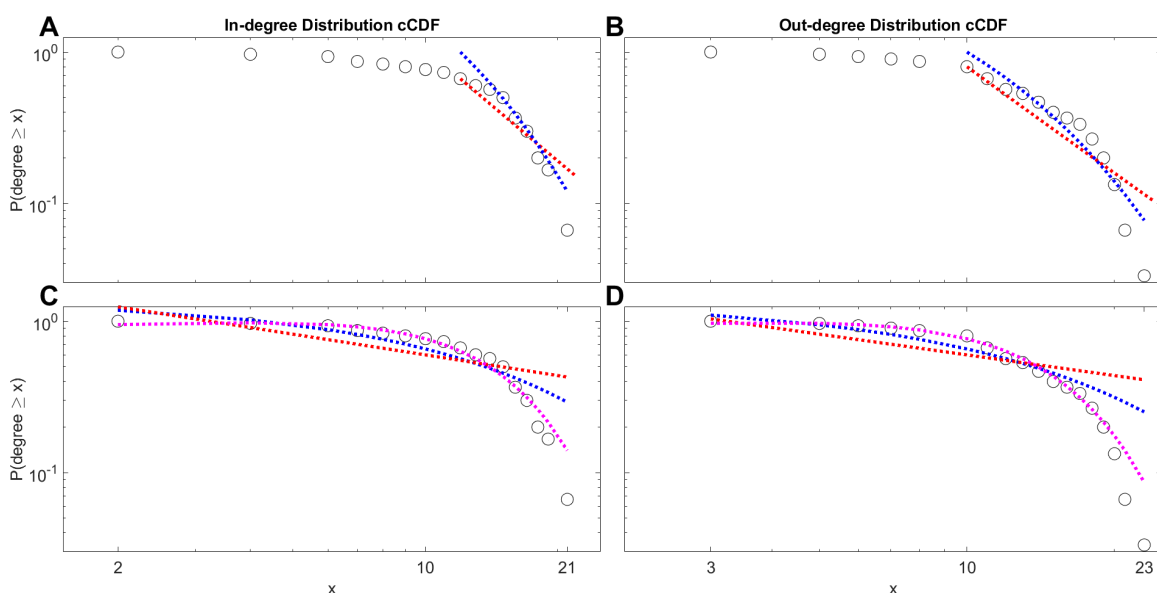


Figure 2.4. Complementary cumulative distribution function (cCDF) of the in-degree distribution (A & C) and out-degree distribution (B & D) for the FPN plotted on a logarithmic scale.

Tail fits calculated according to the recipe proposed by Clauset et al., (2009) are shown in **A** & **B** and fits over the entire distribution are shown in **C** & **D**. Black circles represent the empirical distribution, the red dotted line represents a power-law fit, blue dotted line represents an exponential fit and the purple dotted line represents a Gaussian fit (**C** & **D** only). **A**. The tail fit begins from a lower bound estimate of $x=12$ (x_{\min}). However, it is not likely that the in-degree distribution follows a power law ($D = 0.2097$, $p = 0.0158$)(Clauset et al., 2009). Rather, a log-likelihood ratio shows an exponential distribution is a better fit to the tail of the distribution ($R = -3.386$, $p = 0.00071$)(Alstott et al., 2014). **B**. The tail fit begins from a lower bound estimate of $x=10$ (x_{\min}). The goodness-of-fit test does not rule out the possibility that the out-degree data may have been drawn from a power-law distribution ($D = 0.1446$, $p = 0.1728$)(Clauset et al., 2009). However, a log-likelihood ratio shows that an exponential fit may be just as good, or bad ($R = -1.676$, $p = 0.094$)(Alstott et al., 2014). **C**. A Gaussian model ($\text{adj } R^2 = 0.9740$), fits the in-degree empirical data better than an exponential ($\text{adj } R^2 = 0.8293$) or power law ($\text{adj } R^2 = 0.5660$). **D**. A Gaussian model ($\text{adj } R^2 = 0.9909$), fits the out-degree empirical data better than an exponential ($\text{adj } R^2 = 0.8981$) or power law ($\text{adj } R^2 = 0.06988$).

Next, the Kolmogorov-Smirnov statistic was used to test the goodness-of-fit between the empirical data and that drawn from a power-law distribution (Clauset et al., 2009). The in-degree data is not likely to have been drawn from a power-law distribution ($D = 0.2097$, $p = 0.0158$). However, a power-law distribution cannot be ruled out for the out-degree data ($D = 0.1446$, $p = 0.1728$). The data needs to be compared with other distributions to determine whether they match the data as well, or better.

Finally, different distributions were tested to see whether they were better fits to the tail of each distribution (Alstott et al., 2014). The log-likelihood ratio was calculated between the two candidate distributions. It was positive if the data was more likely in the first distribution and negative if more likely in the second distribution. Using this ratio, the exponential distribution was found to fit the tail of the in-degree data significantly better than a power-law distribution ($R = -3.386$, $p = 0.00071$). However, this does not mean the exponential distribution is an objectively good fit for the data. The ratio showed no significant difference between a power-law fit of the tail of the in-degree data and the following distributions: log-normal ($R = -1.6299$, $p = 0.103$), log-normal positive ($R = -4.40$, $p = 0.1031$) and truncated power-law ($R = 3.693$, $p = 0.082$). Despite the support for a power-law fit of the tail of the out-degree distribution based on the goodness-of-fit test

in the previous step, the ratio showed the following distributions were no better or worse: exponential ($R = -1.676, p = 0.094$), log-normal ($R = -0.978, p = 0.328$), log-normal positive ($R = -1.798, p = 0.328$) and truncated power-law ($R = -1.918, p = 0.083$). It may be that all these distributions describe the data equally poorly.

Due to the poor fits to the candidate distributions using the tail-fitting recipe proposed by Clauset, Shalizi, & Newman (2009), the entire empirical in-degree (Figure 2.4c) and out-degree (Figure 2.4d) distribution data was also fit to power, exponential and gaussian models (Methods). These distributions qualify as potential fits based on their success in real-world connection distribution data (Amaral et al., 2000; Humphries et al., 2006). The in-degree data was most consistent with a Gaussian distribution (adj $R^2 = 0.9740$), in contrast to the exponential (adj $R^2 = 0.8293$) and power law (adj $R^2 = 0.5660$) distributions. The out-degree data was also most consistent with a Gaussian distribution (adj $R^2 = 0.9909$), in contrast to the exponential (adj $R^2 = 0.8981$) and power law (adj $R^2 = 0.6988$) distributions.

2.2.3 Motifs

Most studies analyze subgraphs of the larger monkey FPN due to technological limitations (Antzoulatos & Miller, 2016; Jacob & Daniel, 2018; Kornblith et al., 2016; Salazar et al., 2012). Some subgraphs may carry more importance in establishing the topological organization of the larger FPN than others. These subgraphs are known as structural motifs that serve as essential building blocks for the larger system (Milo, 2002; Sporns & Kötter, 2004). They enable a variety of transient connection dynamics known as functional motifs (Zalesky et al., 2016). Motifs of size 3 ($M=3$) are typically studied (Sporns & Kötter, 2004). They are the most computationally tractable. The studies of the

monkey FPN usually have at least 3 recording sites spanning the network. Additionally, the modeling work detailing the structure-function relationship through neural synchrony was based on size 3 motifs (Gollo et al., 2014; Vicente et al., 2008). Accordingly, the FPN was analyzed to determine which structural motifs of size 3 were overrepresented in comparison with benchmark null networks. Any overrepresented motifs serve as the anatomical building block(s) of the network and give rise to specific functional interactions which can be observed in the literature. Further, regional areas that participate in these essential structural motifs can be important recording targets in electrophysiological studies that aim to describe cognitive behavior supported by the FPN.

To discover the anatomical building blocks used to create the FPN, structural motifs comprised of 3 areas or nodes were analyzed to determine which occurred with a significantly greater frequency than would be expected by chance. There are 13 possible motif classes of size three (Sporns & Kötter, 2004).

As reported in other studies of cortical connectivity (Harriger et al., 2012; Honey et al., 2007; Sporns & Kötter, 2004), motif class ID 9 (M9) was found to be significantly overrepresented ($p = 0$, $z = 12.0322$ random networks, $p = 0.0489$, $z = 1.6121$ lattice networks) (Table 5.2) in the empirical FPN (Figure 2.5). It forms an open triangle where two nodes are bidirectionally connected to a third apical node but are not connected to each other. The M9 motif is known as the dynamical relaying motif due to the unique functional capabilities it provides (Gollo et al., 2011; Vicente et al., 2008). The M13 motif also appeared to be overrepresented, but not to a statistically significant extent ($p = 0$, $z = 19.1224$ random networks, $p = 0.0538$, $z = 1.6108$ lattice networks) (Table 5.2).

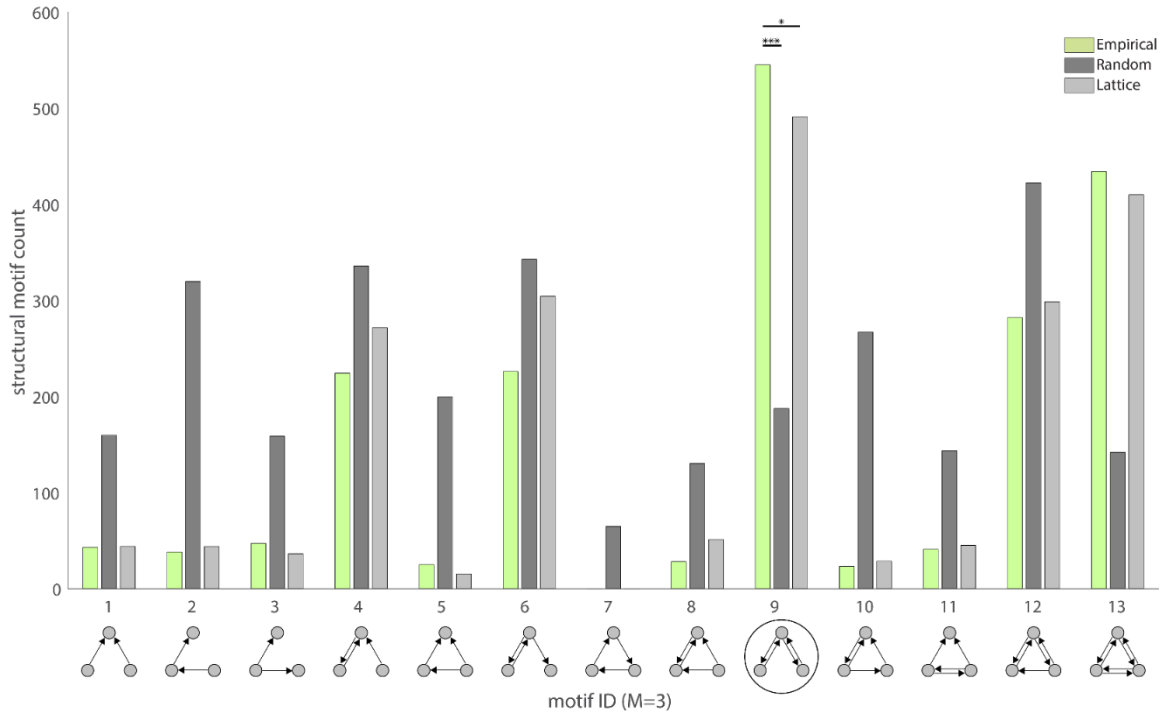


Figure 2.5. Comparison of the structural motif frequency spectrum for the empirical FPN with random and lattice benchmark networks. Motif class ID 9 was overrepresented in comparison to 100,000 random benchmark networks ($p = 0$, $z = 12.032$) and lattice networks ($p = 0.049$, $z = 1.612$). This dynamical relaying motif serves as a fundamental anatomical building block of the network, conferring a repertoire of functional dynamics such as neural synchrony that can be used to support various aspects of cognition. Empirical structural motifs counts are in green. Motif counts for random networks are in dark grey and the counts for lattice networks are in light grey.

2.2.4 Small world

Networks demonstrating topology simultaneously consistent with a small characteristic path length and a high degree of clustering are called “small-world” networks (Watts & Strogatz, 1998). These networks cluster nodes into modules thereby minimizing wiring costs and efficiently integrating the topology. The result is an optimal information processing paradigm marked by fast transmission speeds and successful integration. There have been reports of many networks in neuroscience qualifying as small-world, such as the neural network of *C. elegans*, the brain-stem reticular formation and the mouse connectome (Humphries et al., 2006; Rubinov et al., 2015).

Two indicators of “small-worldness” were calculated for the FPN using 100,000 null networks. First, Humphries’ index, σ (Methods), was estimated as 1.1429. A value greater than 1 is considered an indication that the network is small-world. Second, Telesford’s alternative index, ω , was estimated as 0.0297. A value close to 0, specifically one that falls within the range of $-0.5 \leq \omega \leq 0.5$, is considered an indication that the network is small-world. Negative values indicate a graph with more lattice-like characteristics and positive values indicate more random characteristics. Both metrics provide strong support for classifying the FPN as a small-world network with Telesford’s index showing a very slight skew towards random characteristics.

2.3 Discussion

The tail of the in-degree distribution of the FPN does not appear to follow a power-law (Clauset et al., 2009), which can only occur in the presence of hub nodes. Additionally, because it is more likely to have been drawn from an exponential distribution, it is not considered heavy-tailed (Alstott et al., 2014; Asmussen, 2003). Heavy tailed distributions have many outliers. Exponential distributions are not likely to have outliers. Exponential decay in the tail of the degree distribution of neural networks has also been reported elsewhere (Amaral et al., 2000; Modha & Singh, 2010). It is important to keep in mind that this result only states the tail of the data is better fit by an exponential distribution than a power law. It does not imply that the exponential distribution is an objectively good fit.

The tail of the out-degree distribution of the FPN had moderate support for a power law fit. However, it was not significantly different from an exponential, log-normal, log-normal positive or truncated power-law fit either. These distributions may all be bad fits.

At minimum, the results support the view that neither degree distribution follows a power law.

The entire in and out degree distributions yielded strong results for both a Gaussian and exponential fit (Mathworks®, 2019). The Gaussian fit may be stronger because it uses an extra parameter.

Notably, with both procedures yielding either Gaussian or exponential fits for the data, it is highly likely both distributions have a single, characteristic scale (Amaral et al., 2000). Single-scale systems have a very low probability of large deviations from a characteristic modal value, resulting in a relatively homogenous distribution of connectivity across nodes (Zalesky et al., 2016).

Thus, the FPN is organized in such a way that the total number of incoming and outgoing connections to and from each of its nodes is relatively consistent across areas. There are only a small number of areas that greatly differ in the number of their total incoming and outgoing connections. Strategically, this could mean that information is diffused throughout the network, enabling concurrent or redundant processing. This creates a reliable substrate over which neural representations can be formed, maintained, and communicated (Moreno et al., 2004).

Conversely, scale-free networks with hub nodes contribute to a heterogenous connectivity profile. Simulations have shown that scale-free networks are more resilient against random node failures than single-scale networks (Albert et al., 2000; Albert & Barabási, 2002). This is because there are a much greater number of low-degree nodes in the scale-free networks leading to a greater likelihood that the random failures occur in

these nodes. Therefore, there is little to no impact on overall network functionality. A disease that successfully impairs cognitive function supported by the single-scale FPN may owe its effectiveness to a random attack strategy.

The simulations also show that scale-free networks are much more vulnerable to targeted attacks on their highly connected hub nodes than the single-scale networks. The hub nodes represent single points of failure in the network. It is possible that serious diseases have evolved to target hub nodes, resulting in important cell death. This behavior may be what enables rapid disease progression in some patients. In a single-scale topology, if disease or other form of neural insult negatively impacts a single area, other similarly connected areas can pick up the slack, salvaging the integrity of the network and thereby supporting appropriate function.

The M9 dynamical relaying motif was statistically overrepresented in the FPN, establishing its importance as an anatomical building block of the network. Previous studies have established that its structure is ideal for providing both zero-lag synchrony between its driven nodes and non-zero phase synchrony between its relay and either driven node (Gollo et al., 2014; Vicente et al., 2008).

The synchrony initiated by M9's resonance pair can extend to nodes upwards of four steps removed with very little synchrony decay (Gollo et al., 2014). Therefore, it may serve as the mechanism for zero and non-zero lag synchrony throughout the entire FPN. Crucially, this establishes the M9 motif as a proposed generative topology which likely gives rise to the synchrony previously reported in subgraphs of the FPN supporting attention (Fiebelkorn & Kastner, 2019), categorization (Antzoulatos & Miller, 2016),

working memory (Jacob et al., 2018; Salazar et al., 2012) and cognitive control (Stokes et al., 2017).

Finally, of the 3-node motifs with resonance pairs, the M9 class was observed to be the most robust to large conduction delays and delay mismatches (Gollo et al., 2014), which are a defining feature of the long-range cortical FPN.

Overall, the M9 motif is a maximally versatile building block for the FPN, conferring global near-zero and non-zero synchrony, enabling robust streams of communication and binding which support multiple aspects of cognition.

The FPN's small-world architecture provides an economic (Bassett & Bullmore, 2017) substrate for the brain to process information while minimizing wiring cost. Information can flow efficiently due to a low global path length and integrate in functionally specialized modules due to high clustering. This serves as an elegant solution to the problem of integrating function while allowing for concurrent specialization. The simultaneous specialization and integration of function has been observed empirically in studies of cognition in both humans and non-human primates (Fiebelkorn & Kastner, 2019; Watson & Chatterjee, 2012).

Notably, despite a relatively homogeneous degree distribution with no clear evidence of hub nodes, there was enough dispersed integration to qualify the network as small world. The Telesford index did identify slightly random characteristics for the network, which supports the degree distribution findings. Ultimately, this suggests that small-world networks do not need to have nodes with much larger degrees relative to the

rest of the network. If the nodes all have a sufficiently large relative number of connections, this provides the necessary integration to qualify as small-world.

Finally, small-world characteristics have been shown to better support oscillatory synchronization in contrast to random or lattice networks(Lago-Fernández et al., 2000; Masuda & Aihara, 2004). Thus, in addition to the synchrony advantage afforded by the over-represented M9 motif, the small-world qualification permits the FPN to optimally conduct neural synchrony in support of cognition.

In conclusion, the monkey FPN is uniquely anatomically constructed to support various important cognitive functions. Its fundamental building block is a dynamical relaying motif which confers the optimal 3-node connectivity profile for the synchrony necessary to support types of cognition like working memory and attention. Its small-world architecture provides the integration and specialization of function that complex cognitive tasks require. Finally, the degree of connectivity in the network is dispersed, establishing a reliable substrate for engaging in complex cognitive tasks.

Understanding the structural mechanism which gives rise to the functions a network is known to support provides a pathway to examine various neurological disorders. In diseases such as schizophrenia, Parkinson's disease or Alzheimer's disease, aspects of cognition that the FPN is known to support such as working memory and attention are impaired. Using the results of this study, scientists can examine the ways in which the organization of anatomical connectivity between areas in the FPN are different in pathological animal models or patients suffering from these disorders. Treatments could be devised that impact the pathological network in order to bring it closer to

exhibiting the properties that networks in healthy individuals show (Bassett & Sporns, 2017).

Additionally, engineers interested in exploring the mechanisms of cognition at a network level can use these results to explore their physical instantiation in machines. It would be interesting to see how the FPN may be realized in a neuromorphic circuit which emphasizes homogeneous connectivity in a small-world architecture using a dynamical relaying motif as its core building block (Schuman et al., 2017).

Finally, future empirical studies may want to use the FPN connectivity matrix presented here to identify subgraph regions of interest for recording during cognitive tasks. For instance, a research team interested in studying working memory neural dynamics may want to target areas that form the M9 motif so that the origination of any near-zero or non-zero phase lag synchrony contributing to working memory function is more likely to be identified.

The author hopes that in the future this level of graph theoretic analysis will be applied to other large-scale cortical networks supporting complex functions.

2.4 Methods

2.4.1 Parcellation Scheme

Non-human primate parcellation schemes are numerous and varied. Some of the ways they are derived include establishing boundaries based on cytoarchitecture, myeloarchitecture, or function (Bonin & Bailey, 1947; Brodmann, 1909; Economo & Koskinas, 1925; Felleman & Van Essen, 1991; Markov et al., 2014; D. N. Pandya & Yeterian, 1985; Vogt & Vogt, 1919; Walker, 1940). This study uses the parcellation

scheme identified in Petrides & Pandya (2007) (Figure 2.1). In this scheme, there are sixteen prefrontal areas: 10, 9, 32, 14, 25, 8B, 8Ad, 9/46d, 46d, 46v, 9/46v, 8Av, 45, 47/12, 13, 11, one frontal area 6DR and thirteen parietal areas: PE, PEci, PEc, PEa, PF, PFop, PFG, IPd, POa, PG, PGm, PGop, Opt. The prefrontal areas were delineated based on architectonic characteristics identified by Petrides & Pandya (1994) and the posterior parietal areas based on Pandya & Seltzer (1982). Area 6DR was included for its hypothesized involvement in the FPN (Salazar et al., 2012).

This scheme was chosen because it allows for a level of granularity sufficient for exploring possible functional implications (Goldman-Rakic, 2011; M. Petrides, 2005) and it provides enough areas (30) for a graph theoretic analysis (Bullmore & Sporns, 2009). For instance, analyses such as the Clauset, Shalizi, & Newman (2009) recipe for analyzing power-law distributed data require enough nodes to ensure the accuracy of the technique (Alstott et al., 2014). Each delineated area is considered a node. The connections between them are called edges.

2.4.2 Connections

Published tract-tracing studies were collated, and results were interpreted according to the Petrides & Pandya (2007) parcellation scheme. The studies utilized both retrograde and anterograde tracing techniques. Retrograde tracers injected into an area migrate back along axons to the neuronal somas they originate from (Lavail & Lavail, 1972). Anterograde tracers injected into an area are transported away from the soma to their site of termination (Cowan et al., 1972). The resulting labeled neurons or boutons can then be seen under a microscope allowing for statements to be made about direct axonal projections between areas.

If a tracer clearly had uptake into adjacent areas, its results were not considered in the analysis. Tracer injection sites were defined according to the author's interpretation of a mapping to the selected parcellation scheme. Many connections were present in multiple studies. However, others were only reported in a single study due to the small number of tract-tracing investigations on particular areas of cortex represented in the parcellation scheme (Table 5.1).

It is important to keep in mind that most studies involved Old World macaque monkeys (*Macaca fascicularis*, *Macaca mulatta*, or *Macaca nemestrina*) (Cawthon, 2005c, 2005b, 2006a), but a small number also involved New World monkeys such as squirrel monkeys (*Saimiri sciureus*) (Cawthon, 2006b) or owl monkeys (*Aotus trivirgatus*) (Cawthon, 2005a). Both kinds are of the infraorder Simiiformes. Furthermore, the connections were collated from both hemispheres, across sexes and age groups. The intention was to provide a broad overview of the connections comprising the non-human primate frontoparietal network irrespective of variables such as non-human primate species, sex, age, or hemisphere.

Existing resources for obtaining connectivity information on the FPN were analyzed for efficacy. First, the work presented in Markov et al. (2014) served as an excellent example of a comprehensive whole-brain network analysis and provided valuable connectivity information. However, there were not enough unique areas injected to be useful to examine the frontoparietal network, specifically.

Next, the Collation of Connectivity data for the Macaque (CoCoMac) database was considered for obtaining connectivity information (Bakker et al., 2012; Stephan et al., 2001). This database serves as a repository for macaque neural connections reported

in the tract-tracing literature. To deal with the problem of inconsistently named areas, boundary conflicts and differing resolutions from parcellation schemes chosen by researchers, CoCoMac uses a routine that attempts to automatically map connections between schemes. This gives CoCoMac the ability to make connection statements which apply to specific parcellation schemes. Unfortunately, the accuracy of these statements is questionable, making them unreliable for use in analysis. For instance, if a study using a parcellation scheme different from that proposed by Petrides & Pandya (2007) reports that area 46 projects to area LIP (lateral intraparietal sulcus), CoCoMac won't be able to make a reliable statement about whether the connection should be from 46d, 46v, 9/46d or 9/46v to area POa, the area which corresponds to LIP (Medalla & Barbas, 2006). Clearly, the original study in this example lacks the specificity necessary to report a connection which applies to the selected parcellation scheme. The only solution is to re-interpret the finding from the original study using the selected parcellation scheme. Accordingly, all tract-tracing studies were re-interpreted, as necessary.

Unfortunately, there is no universally accepted method for defining connection strength between areas, despite recent interesting approaches (Markov et al., 2014). The studies used in this analysis reported binary or qualitative descriptions of axonal connectivity. This results in the unfortunate situation where a dense connection between two areas is treated the same as a sparse connection. The binary directed matrix that results from this scenario, however, is still more informative than its undirected version, which is primarily used in fMRI studies with diffusion tensor imaging. The binary directed matrix reports a connection as either existing (with a 1) or not discovered (with a 0). It is important to note that the absence of a connection does not mean there is no

projection between the two areas. Rather, it means that a connection between the areas was not reported.

2.4.3 Graph Visualizations

The spacing of the nodes in Figure 2.3 is controlled by the ForceAtlas layout in Gephi, an open-source network visualization and analysis software tool (Bastian et al., 2009). Force-directed layouts, like that used in the ForceAtlas layout, quantify levels of spatial attraction and repulsion for the nodes based on some measure of pair-wise node distance like topological path length, the minimum number of edges between any two nodes (Zalesky et al., 2016). These layouts minimize edge crossings, enhance symmetry, keep edge lengths uniform, spatially distribute nodes in a uniform manner and correlate node position with their topological adjacency.

2.4.4 Graph Measures

All graph theoretic analyses were conducted using the publicly available Brain Connectivity Toolbox (Rubinov & Sporns, 2010).

2.4.5 Degree Distribution

To determine whether the FPN's degree distributions were scale-free or broad-scale, an analysis was conducted to test whether its in or out-degree distributions follow a power law. The recipe for evaluating the existence of power-law scaling proposed by Clauset, Shalizi, & Newman (2009) was followed using the publicly available MATLAB and Python (Alstott et al., 2014) scripts. The recipe is to first fit a power-law to the data above some lower bound, x_{min} , using maximum likelihood estimation, then test its goodness of fit and finally to compare the power law with alternative distributions using a likelihood ratio test. A lower bound is used because it is typical for empirical data to only

follow a power law for values above some level of x (Clauset et al., 2009). This results in a fit for the tail of the distribution.

First, the data is fit to a power-law using maximum likelihood estimation using the publicly available MATLAB function ‘plfit’.

The fitting procedure estimates parameter values for Equation 2.1:

$$P(\text{degree} = x) \sim x^{-a} \text{ for } x \geq x_{min}$$

Equation 2.1 Power-law fit

Where a is the maximum likelihood estimate of the scaling exponent, x_{min} is the estimated degree of the lower bound of power-law behavior and L is the log-likelihood (equation 3.5 in Clauset et al., 2009) of the data $x \geq x_{min}$ under the fitted power law.

Next, the goodness of fit between the empirical data and that drawn from a power-law distribution is tested using the Kolmogorov-Smirnov statistic in the publicly available MATLAB function ‘plpva’. There were 5,000 semiparametric repetitions of the fitting procedure. The statistic provides a p-value that allows a determination to be made about whether the power-law hypothesis can be ruled out. If $p \leq 0.1$, the power law can be ruled out

Finally, the power law fit is compared with alternative distributions using a log-likelihood ratio test enabled via the Powerlaw Python package (Alstott et al., 2014). The distributions’ tails are compared to see which is a better fit to the data. If the log-likelihood ratio is positive, the data was more likely in the first distribution. If it is negative, the data was more likely in the second distribution. The p-value indicating directional significance is also provided.

Additionally, the entire in and out-degree distribution data were fit to power, exponential and gaussian models using MATLAB's method of nonlinear least squares error minimization (Mathworks®, 2019), which minimizes the following:

$$S = \sum_{i=1}^n (y_i - \hat{y}_i)^2$$

Equation 2.2 Nonlinear least squares fit

Where n is the number of empirical data points, y_i is the probability of a node's degree being greater than or equal to a random degree (the cCDF), \hat{y}_i is the predicted probability value and S is the summed square of residuals.

2.4.6 Null Models

The FPN was rewired using two different algorithms to generate null distributions used in the motif and small world analyses. Each algorithm creates networks at either end of the topological spectrum: random and lattice based (Watts & Strogatz, 1998). The first algorithm functions by rewiring two random connections involving four nodes to a new connection scheme involving the same four nodes ensuring the connections in the new scheme do not already exist. If they do exist, the process is abandoned and begun anew with two different random connections. The algorithm proceeds in this fashion, maintaining the same network size, connection density and in and out-degree distributions as the original network, resulting in a random network (Maslov & Sneppen, 2002). It has been shown that completing the rewiring process at least 10 times the number of edges in the network is a long enough time to wait to ensure sufficient mixing (Milo et al., 2003). The FPN has 399 edges. So, there were 3,990 iterations used to generate each null network.

The second algorithm functions in much the same way as the first. After rewiring the two random connections and ensuring they are novel, it must also be confirmed that they

are now closer to the diagonal of the adjacency matrix than they were previously. This ensure connections only link nearby nodes. If this is not the case, the process is abandoned and begun anew with two different random connections. Just like the first algorithm, the network size, connection density and degree distributions are maintained. The result is a latticed network (Sporns & Zwi, 2004).

2.4.7 Motifs

All 13 classes of structural motifs of size three (Sporns & Kötter, 2004) were tested for overrepresentation in the empirical FPN. The number of instances of each motif class were counted in the FPN, yielding a motif spectrum. These empirical frequencies were compared to 100,000 random and lattice benchmark networks' motif spectra. P-values for each motif class were calculated as the fraction of times the frequency count of a benchmark network was higher than the count in the empirical FPN. If the p-value was less than 0.05 for both the random and lattice benchmark networks, the motif class was considered to be significantly overrepresented in the empirical FPN.

The amount of times each area participated across the 13 classes was quantified in the empirical FPN and compared to the frequency observed in the 100,000 random and lattice benchmark networks as well. P-values were calculated as the fraction of times the frequency count of each area's participation in motif classes exceeded that observed in the empirical FPN. If the p-value was less than 0.05 for both the random and lattice benchmark networks, the area was considered to be significantly overrepresented in the empirical FPN.

2.4.8 Small world

The small-world topology of a network can be quantified by comparing its observed characteristic path length, L , and clustering coefficient, C , with their distributions in null networks.

Average path length measures how efficiently information can be routed in a network. For any nodes i and j , the shortest path length, $l_{i,j}$, between them is defined as the total number of edges one must traverse in navigating from node i to node j along the quickest route in the binary directed graph of the network. This can be computed for each node in a network algorithmically (Dijkstra, 1959). Next, each node's shortest path length is averaged to quantify the average path length of the entire network, the characteristic or global path length:

$$L = \frac{1}{n} \sum_{i=1}^n l_{i,j}$$

Equation 2.3. Characteristic path length of a graph

The clustering coefficient measures a network's level of integration in terms of 3-node subgraphs. For any node i , its clustering coefficient is calculated using the following ratio:

$$C(i) = \frac{\text{Quantity of connected node pairs that are connected to } i}{\text{Quantity of node pairs that are connected to } i}$$

Equation 2.4. Clustering coefficient ratio

Next, each node's clustering coefficient is averaged to quantify the clustering of the entire network:

$$C = \frac{1}{n} \sum_{i=1}^n C(i)$$

Equation 2.5. Clustering coefficient of entire network

There are two metrics used to quantify the small-worldness of a network: Humphries' index of small-worldness, σ (Humphries et al., 2006) and Telesford's alternative index, ω (Telesford et al., 2011). The calculation of Humphries' index requires the characteristic path length and clustering coefficient be normalized to their average values in appropriately randomized null networks. The following normalized values are obtained:

$$\gamma = \frac{C}{C_{rand}}$$

Equation 2.6. Normalized clustering coefficient

Where C_{rand} is the average clustering coefficient calculated for an ensemble of appropriately randomized null networks.

$$\lambda = \frac{L}{L_{rand}}$$

Equation 2.7. Normalized characteristic path length

Where L_{rand} is the characteristic path length calculated for an ensemble of appropriately randomized null networks.

Next, the normalized values are divided, providing the following index:

$$\sigma = \frac{\gamma}{\lambda}$$

Equation 2.8. Humphries' index of small-worldness

From Equation 2.8, if $\lambda \sim 1$ (low path length) and $\gamma > 1$ (high clustering), then $\sigma >$

1. Values of $\sigma > 1$ are typically considered an indicator of a network's small-world organization.

The calculation of Telesford's alternative index stems from the idea that appropriately matched lattice networks are better suited to normalize the clustering coefficient metric than randomized networks. This is because a lattice network presents with maximal clustering, while a random network presents with minimum global path length. Hence, Telesford et al. (2011) propose the following index:

$$\omega = \frac{L_{rand}}{L} - \frac{C}{C_{latt}}$$

Equation 2.9. Telesford's alternative index of small-worldness

Where C_{latt} and L_{rand} are the average clustering coefficient and characteristic path length calculated for an ensemble of appropriately matched lattice and randomized null networks, respectively.

The index ranges between -1 and 1. A value close to 0 is typically considered an indicator of a network's small-world organization.

3 SPECTRAL CHARACTERISTICS OF NON-SPATIAL VISUAL WORKING MEMORY IN THE MACAQUE FRONTOPARIETAL NETWORK

3.1 Introduction

Working memory is thought to be largely controlled by interactions both within and between frontal and parietal cortices (Fuster & Alexander, 1971; Goldman-Rakic, 1995, 2011). Recent attempts have been made to characterize aspects of the spatial (Antzoulatos & Miller, 2016; Martínez-Vázquez & Gail, 2018; Pesaran et al., 2002), nonspatial (Dotson et al., 2014; Jacob et al., 2018; Lundqvist et al., 2018; Siegel et al., 2009), and visuospatial (André M. Bastos et al., 2018; Lara & Wallis, 2014; Lundqvist et al., 2016) spectral characteristics of the local field potential (LFP) through simultaneous recordings from various areas across the monkey frontoparietal network. However, the reports are minimal in number, and there is no clear narrative tying together the heterogenous functionality of the characteristics. A new effort at forming a spectral model of monkey visual working memory has been proposed to address these shortcomings, but it remains largely untested (Conklin Chapter 1). In this study, three hypotheses generated by the spectral model are tested on previously examined visual working memory data (Dotson et al., 2014; Salazar et al., 2012). LFP activity is analyzed from simultaneous recordings in frontal and parietal regions during a delayed-response oculomotor non-spatial visual working memory task.

According to studies that went into the creation of the spectral model of visual working memory, it is likely that low (1-15Hz), mid (12-35Hz) and high (35Hz+)

frequency band LFP activity will be observed both within and between frontal and parietal regions. First, frontal and parietal regions should show increased low-band LFP power during the delay period (Jacob et al., 2018), likely related to attentional selection (Fiebelkorn et al., 2018; Foster & Awh, 2019; Helfrich et al., 2018). Second, the mid-band LFP power within frontal and parietal regions should decrease during the delay period (Jacob et al., 2018; Lundqvist et al., 2018), potentially serving to protect and filter task-relevant working memory content, maintaining it over time (Conklin Chapter 1; Engel & Fries, 2010). It may also be used to encode objects at different phases (Siegel et al., 2009). Indeed, a previous analysis of this dataset found that objects were encoded in the mid-band across regions (Salazar et al., 2012). Moreover, the synchrony was regulated by activity arising first in posterior regions. This parieto-frontal directed connectivity role for the mid band network was supported in later work where it was observed during the presentation of stimuli (Jacob et al., 2018). Since the mid-band activity between frontoparietal areas has been sufficiently explored on this dataset (Dotson et al., 2014; Salazar et al., 2012), it will not be a focus here. Third, high frequency band LFP power bursts should be observed within frontal areas near the end of the delay period (Lundqvist et al., 2018), possibly enabling the transfer of working memory content necessary for completion of the task (André M. Bastos et al., 2015). High-band synchrony between frontal and parietal areas should also increase around the same time. However, this activity is likely unrelated to working memory processes and will not be investigated here (Buschman & Miller, 2007b).

Time-frequency decomposition was used to enable this analysis. The time-domain LFP signal during correct trials was transferred to the time-frequency domain through

complex Morlet wavelet convolution. The average frontal and parietal signals from each recording session were used to test each hypothesis using three directional single-sample t-tests with Bonferroni correction (Methods). Monkeys A and B showed increased low-band and decreased mid-band dB baseline normalized LFP power across frontal and parietal regions during the delay period. No power bursts were observed in the dB baseline normalized LFP power within frontal areas of either monkey. Thus, the visual working memory spectral model generated correct hypotheses for the low and mid bands, but not for the high band. The absence of high-band activity may be a result of the time frequency decomposition method and chosen parameters. It could also suggest a more nuanced role for the high band in the model. Additional analyses using different time-frequency decomposition methods could be beneficial. Furthermore, future studies are needed to test the generalizability of the model's predictions.

3.2 Methods

3.2.1 Recording

Two female rhesus macaques (Monkey A and Monkey B) were implanted with a post for head-restraint, scleral search coils to track saccades (Judge et al., 1980) and two recording chambers (Gray et al., 2007) over frontal and parietal regions (see more details in Dotson et al., 2014; Salazar et al., 2012) (Figure 3.1a & b). Specifically, recordings in the right hemisphere of Monkey A were obtained from frontal areas dPFC, vPFC, 8B, and 9L and parietal areas PEC, LIP, MIP, and PG. Recordings in the left hemisphere of Monkey B were obtained from frontal areas dPFC, 8B, 6DR, and 8Ad and parietal areas PG, LIP, PE, and PEC.

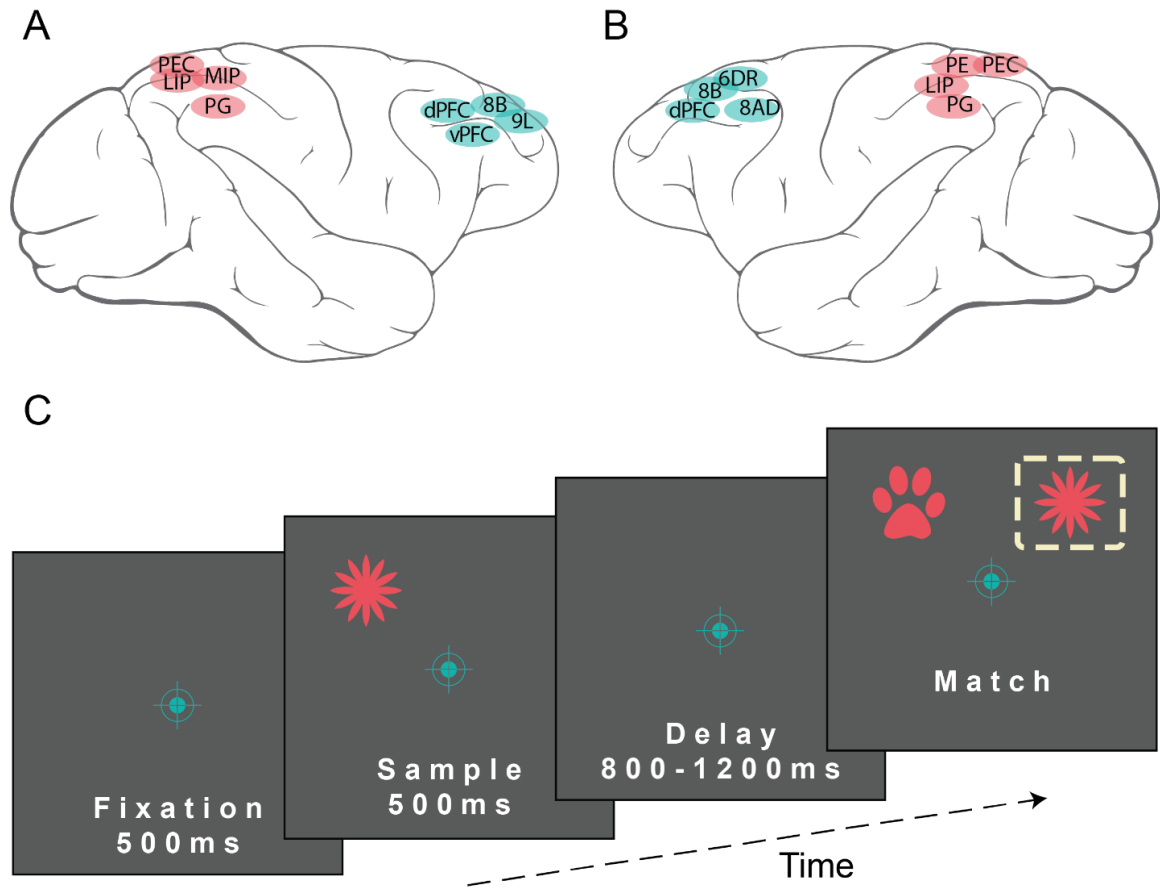


Figure 3.1. Recorded areas & experimental design

A. Recording locations in the right hemisphere of Monkey A: frontal areas dPFC, vPFC, 8B, 9L and parietal areas PEC, LIP, MIP, PG. **B.** Recording location in the left hemisphere of Monkey B: frontal areas dPFC, 8B, 6DR, 8Ad and parietal areas PG, LIP, PE, PEC. **C.** Experimental design. Each trial began with a 500ms fixation period followed by a 500ms sample period during which the monkey was presented with a stimulus. The sample period was followed by a variable delay period lasting 800-1,200ms. The trial ended during the match period, after the delay, when a distractor and correct object was presented. The monkey had to saccade to the object observed during the sample period if the identity rule was in-play (as shown) or to the location observed during the sample period if the location rule was in-play (not shown). Fixation had to be maintained throughout the trial until the monkey made a saccade during the match period.

Each recording session was obtained in a single day. Monkey A had recording sessions over 23 days. Monkey B had recording sessions over 24 days.

Broadband signals were simultaneously recorded from electrodes in both regions. The signals were amplified by 5k, filtered to 1k-10kHz and digitized to 30kHz. Laminar information was not obtained. However, the maximum recording depth reached around 10mm from the surface of the cortex.

Each electrode's broadband signal was down-sampled to 1kHz and low-pass filtered to remove frequency components above 250hz to obtain the local field potential (LFP) for further analysis. This study focuses solely on dynamics in the LFP (Figure 3.2).

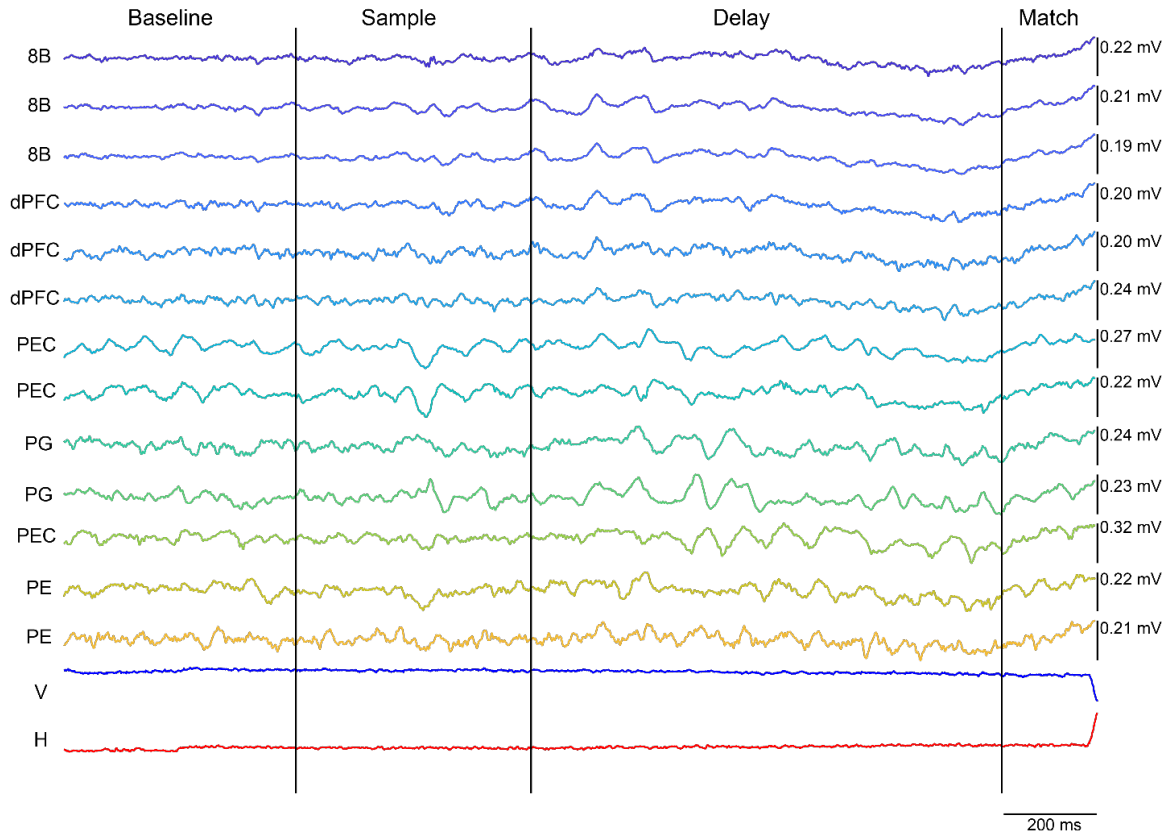


Figure 3.2. Example of LFP signals across all recording channels from a single trial. This is from a recording in Monkey B on day 17, trial 1,164. Three channels were in frontal area 8B, three in frontal dPFC, two in parietal PEC, PG, and PE and a single channel in parietal area PEC. The vertical and horizontal eye channels are shown from the beginning of fixation up until a saccade was made in the match period ~200ms in. The vertical scale of each trace is shown on the right. Trial epochs are labeled along the top axis.

After recording, each monkey was euthanized (pentobarbital, 100 mg/kg i.v.), and the brains were removed. A Nissl stain was used to identify electrode tracks marking the actual recording areas. The areas were classified according to the Paxinos et al. (1999) parcellation scheme.

3.2.2 Task

A more detailed description of the task and basic analysis methods is available in the original manuscript (Salazar et al., 2012). A delayed match-to-sample visual oculomotor task was used to test visual working memory (Figure 2.1c). The monkey needed to acquire fixation on a cross presented on the screen of a 19-inch monitor for 500ms to initiate the trial (baseline period). Afterwards, a stimulus was presented at one of three locations and remained on the screen for 500ms (cue period). One of three possible samples served as the stimulus at one of three possible locations at the vertices of an invisible triangle around the fixation cross. A variable delay of 800-1200ms followed the cue period during which the stimulus disappeared, and the monkey had to maintain fixation on the remaining cross (delay period). The delay was variable to control for expectation effects. Finally, following the variable delay, matching and distractor objects were presented at two locations on the screen (match period). If the identity rule was in play, the monkey had to saccade to the object which matched the identity of the object presented during the cue period, regardless of where that object was located during the match period. If the location rule was in play, the monkey had to saccade to the location where the original object was presented during the cue period, regardless of the identity of the object in that location during the match period. Correct responses triggered a juice reward for the monkey. Fixation was held throughout the trial until the match period necessitated a saccade response.

Rules were switched when the monkey achieved greater than 80% performance after 300 consecutive trials using a sliding window of 100 trials. The rule-switch occurred with no cue to the monkey. It had to recognize the novel context to restore the juice

reward. Rule switches generally happened once or twice in a recording session. The positions and identities of objects were chosen with equal probability in a pseudo random sequence. Object locations were rotated 180 degrees every other day and a different set of objects was chosen each day to reduce bias for object location and identity. MonkeyLogic (Asaad & Eskandar, 2008) and custom software were used to provide experimental control and visualizations. (more details can be found in Salazar et al., 2012).

The rules were established to permit an examination of visual working memory by way of the identity rule versus spatial working memory thought to facilitate the location rule. However, the nature of the location rule permitted the possibility that the monkey was simply storing a motor plan of the pending saccade over the delay period. This means that instead of experimentally observing the intended usage of spatial working memory, the monkey would have relied on a prospective motor working memory (Fuster, 2015). Hence, only the identity rule trials, which presume to be a reliable test of visual working memory, were used in the analyses for this study (Salazar et al., 2012).

3.2.3 Trial rejection

There were electrical artifacts in certain LFP signals that needed to be removed. They appeared as major transient or sustained fluctuations in the amplitude distributions of the signals. Trials with transient artifacts were identified by observing when the maximum amplitude of the LFP exceeded 12 standard deviations computed across all trials. Trials with sustained artifacts were identified by calculating the Kurtosis of the distribution of spectral power at each frequency across all trials. If the Kurtosis exceeded a threshold of eight, the trial with the largest power value was removed and Kurtosis was recalculated. This process continued until the residual distribution dropped below the

Kurtosis threshold or the rate of change of the Kurtosis evaluated over all previous iterations was not significantly different from zero, $p > .0001$. This method was applied to each frequency in the spectrum to remove trials with both narrow and broadband artifacts. Channels were removed from analysis when more than four percent of their associated trials exhibited artifacts (for further details see Salazar et al., 2012).

3.2.4 Time-frequency Decomposition Using Complex Morlet Wavelets

Time-frequency analysis was implemented by convolving the LFP signal with a set of complex Morlet wavelets, defined as complex sine waves tapered by a Gaussian. The frequencies of the wavelets ranged from 4 Hz to 100 Hz in 35 logarithmically spaced steps. The full-width at half-maximum (FWHM) ranged from 400 ms to 100 ms with increasing wavelet peak frequency. This resulted in a spectral FWHM range of 2 Hz to 8 Hz (Figure 3.3). The FWHM is a more informative and computationally efficient method of defining the width of the Gaussian window than the traditionally used number-of-cycles parameter (Michael X Cohen, 2018).

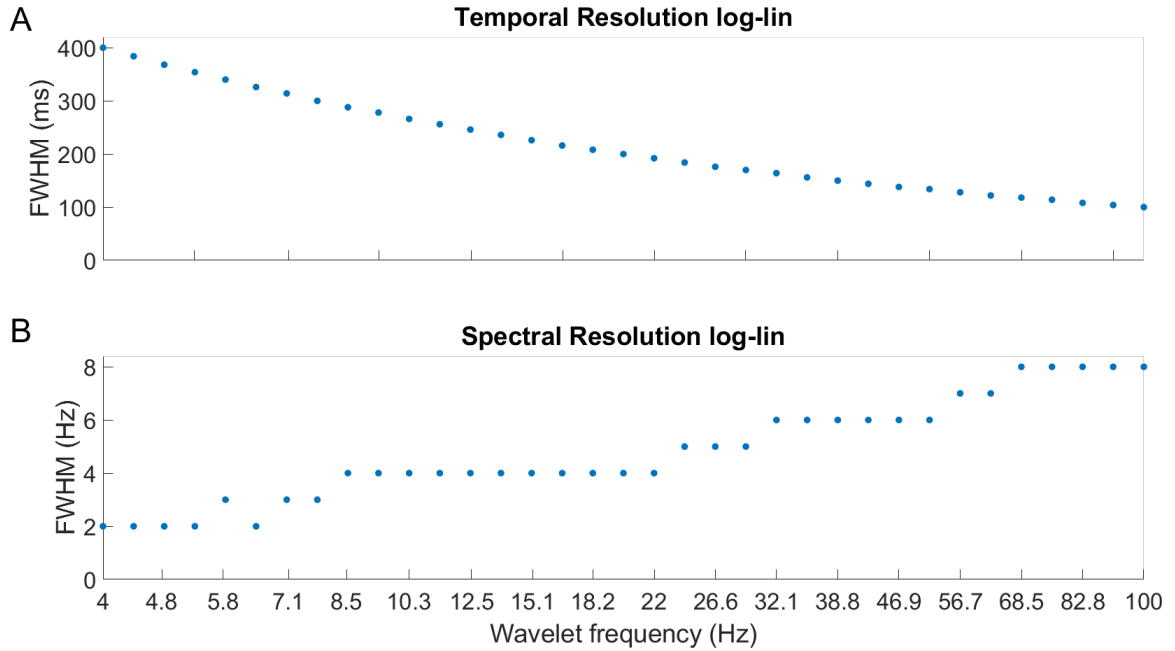


Figure 3.3. Temporal and spectral resolutions for each complex Morlet wavelet. The resolution is a function of the FWHM in ms for the temporal domain and Hz for the spectral. As the frequencies increase, the temporal resolution increases (400-100ms) (A), (B) while the spectral resolution decreases (2-8Hz) and vice-versa as the frequencies decrease. This illustrates the fundamental trade-off between temporal and spectral precision inherent in time-frequency analyses. It is not possible to have arbitrarily good precision in both. Instead, it is considered an advantage to smooth over some aspect of time and frequency to visualize non time-locked and non phase-locked neural activity averaged over individuals and/or trials

Complex Morlet wavelets are complex sine waves tapered by a Gaussian. They can be defined as the product of a complex sine wave and a Gaussian window:

$$\omega = e^{2i\pi ft} e^{\frac{-4 \ln(2)t^2}{h^2}}$$

Equation 3.1. Complex Morlet wavelet

where $e^{2i\pi ft}$ defines the complex sine wave and $e^{\frac{-4 \ln(2)t^2}{h^2}}$ defines the Gaussian window. Further, i , f , and t are the imaginary operator, frequency in Hz, and time in seconds, respectively. The parameter h is the FWHM in seconds (Michael X Cohen, 2018).

The family of wavelets created for this analysis is well-formed. They taper to zero on both ends in the time-domain and their representation in the frequency domain is Gaussian (Figure 3.4). These properties are necessary to avoid edge artifacts during convolution with the LFP signal (Mike X Cohen, 2014).

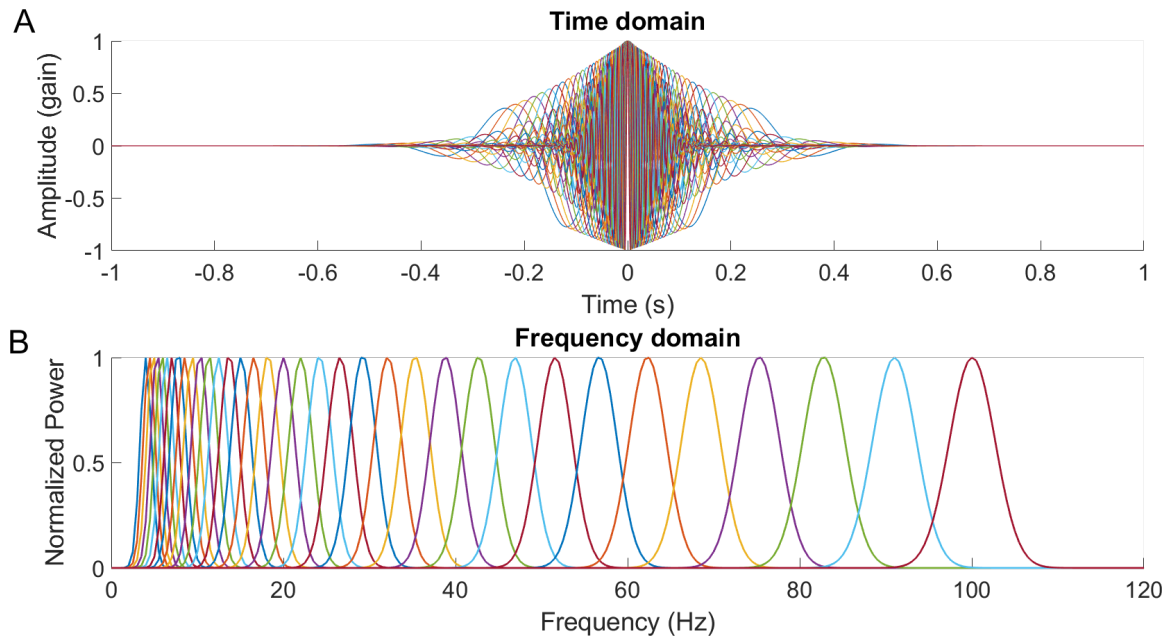


Figure 3.4. Set of 35 complex Morlet wavelets ranging in frequency from 4 to 100 Hz in 35 logarithmically spaced steps

A. The wavelets in the temporal domain must taper to 0 on each end so they can be convolved with the LFP signal to create the analytic signal containing power and phase. **B.** Wavelets in the frequency domain present as Gaussians with resolution decreasing as frequencies increase. This effect is a result of the width of the Gaussian window used in their creation.

In a further attempt to avoid edge artifacts, signals were reflected about their origin and termination prior to wavelet convolution (Figure 3.5). Wavelet convolution produces estimates based on the time point measurements occurring directly before and after in the original plot. Since the beginning and end of the recording have no time points before or after them, respectively, edge artifacts are introduced during convolution. Thus, reflecting the signal provides additional points for the convolution, permitting a smoother resulting estimate (Mike X Cohen, 2014).

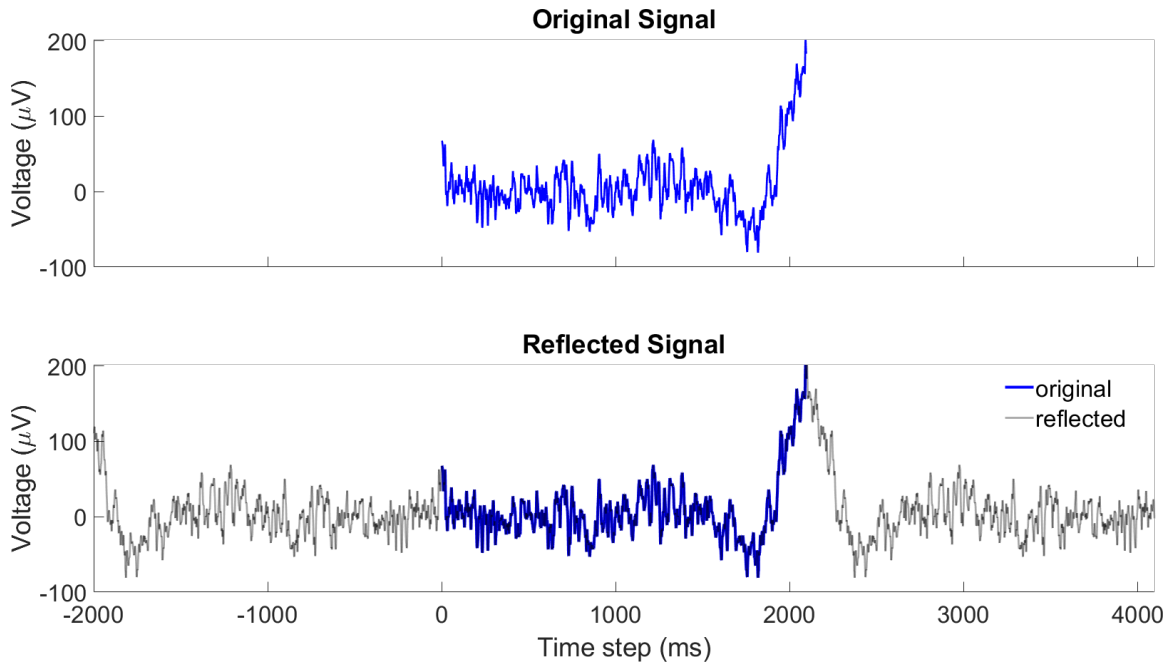


Figure 3.5. Example trial prior to convolution

The signal was reflected about the beginning and ending axes to provide more samples for the convolution step to minimize edge artifacts (Mike X Cohen, 2014).

Additionally, the beginning and end of each trial was cut off to minimize artifacts.

Instead of the trial beginning 504ms before cue onset, trials started at 400ms prior to cue onset. and ended 150ms after match onset, just prior to the monkey's response saccade.

The signal, prior to trimming, contained samples through 274ms after match onset, which included the monkey's response saccade artifact. The trimmed signal should have minimal, if any, artifacts related to edge or saccades.

3.2.5 Baseline Normalization

The time-frequency power spectrum was normalized using the decibel metric according to Equation 3.2:

$$dB_{tf} = 10 \log_{10} \frac{activity_{tf}}{baseline_f}$$

Equation 3.2. Time-frequency decibel baseline normalization

where *activity* is a vector comprised of raw power values for each time point within a single frequency component, *baseline* is a scalar representing the average raw power value over the entire baseline period within a single frequency component and *dB* is the decibel representation of power over time within a single frequency component.

A new baseline was computed for each day across conditions from 400ms to 100ms prior to stimulus onset. Averaging over conditions maximizes the number of baseline timepoints to produce a smoother baseline estimate. The baseline was applied to the trial average for each channel.

There are several advantages to normalizing the time-frequency power spectrum to baseline using the dB metric (Mike X Cohen, 2014). First, it enables comparison of the results with other studies from different animals with anatomical, experimental, and data quality differences. This is vital to validating the model, which was built using the results of other monkey studies. Second, it removes the 1/f dynamic which biases low frequencies with higher power and high frequencies with lower power, making them difficult to detect. Third, it enables the separation of activity directly related to the task from ongoing background activity. This permits the analysis of task-relevant spectral characteristics of visual working memory. Finally, baseline normalization yields power values that approximate a normal distribution, which is ideal for applying parametric statistical analyses. To test the hypotheses generated by the spectral visual working memory model, parametric statistics are applied to the data. Accordingly, the baseline normalization step enables compliance with the assumption of normality required by standard tests of parametric statistics.

3.2.6 Window Selection for T-test

The visual working memory spectral model yielded hypotheses for frequency bands defined as low (1-15Hz) during the delay in frontal and parietal regions, mid (12-35Hz) during the delay in frontal and parietal regions, and high (35Hz+) near the end of the delay in frontal regions. Thus, the timeframes to consider for the t-test are established. However, there are a couple issues with the frequency bands. First, each monkey has slightly different frequency band ranges. This can be addressed by establishing bounds unique to each monkey based on where the power is observed on an average spectrogram that is orthogonal to the condition being tested. It is important the average spectrogram is orthogonal to avoid double-dipping for the t-test. Second, the band boundaries must be sufficiently spaced to minimize leakage from neighboring frequencies introduced by the convolution step. The empirical FWHM can be used to ensure the bands are adequately distanced. To minimize outside contributions to a target frequency, the distance of the next component chosen should be about as much as the empirical FWHM of the target (Michael X Cohen, 2018).

The delay period of average spectrograms for each monkey was inspected across frontal and parietal regions and across correct and incorrect responses to determine what range would qualify as low, mid, and high when applying statistical tests (Figure 3.6 & Figure 3.7). This served as an appropriate orthogonal spectrogram for the t-test. Areas with distinct power increases or decreases largely within the band boundaries proposed by the spectral visual working memory model were used to establish band boundaries for each monkey. The borders of Monkey A's frequency bands were about 4Hz higher than the model, with the low band beginning around 8Hz and ending around 18Hz (Figure

3.6a). The FWHM is 4Hz (Figure 3.3b) at this frequency. Hence, the mid band starts at 22Hz and ends around 39Hz. The FWHM is 6Hz at this component. Accordingly, the high band starts around 46Hz and ends around 91Hz (Figure 3.6b). The average spectrogram across frontal and parietal channels was used for the low and mid band window selection to test hypotheses 1 and 2. These bands were sampled from 75ms after cue offset to 86ms prior to match onset, resulting in 650ms of band-limited activity. This comprises most of the delay period while avoiding the beginning and end to ensure edge artifacts related to epoch switches are not included. The average spectrogram across all frontal channels was used for the high band window selection testing hypothesis 3. The high band was sampled from 515ms after cue offset up to 86ms prior to match onset, resulting in 210ms of band-limited activity.

The borders of Monkey B's frequency bands fell within the original bounds established by the model. The low band begins around 5Hz and ends around 12Hz (Figure 3.7a) where the FWHM is 4Hz (Figure 3.3b). The mid band begins at 15Hz and ranges up to 32Hz where the FWHM is about 6Hz. So, the high band starts around 38Hz and ends around 91Hz (Figure 3.7b). The same time ranges identified for Monkey A above were selected for Monkey B.

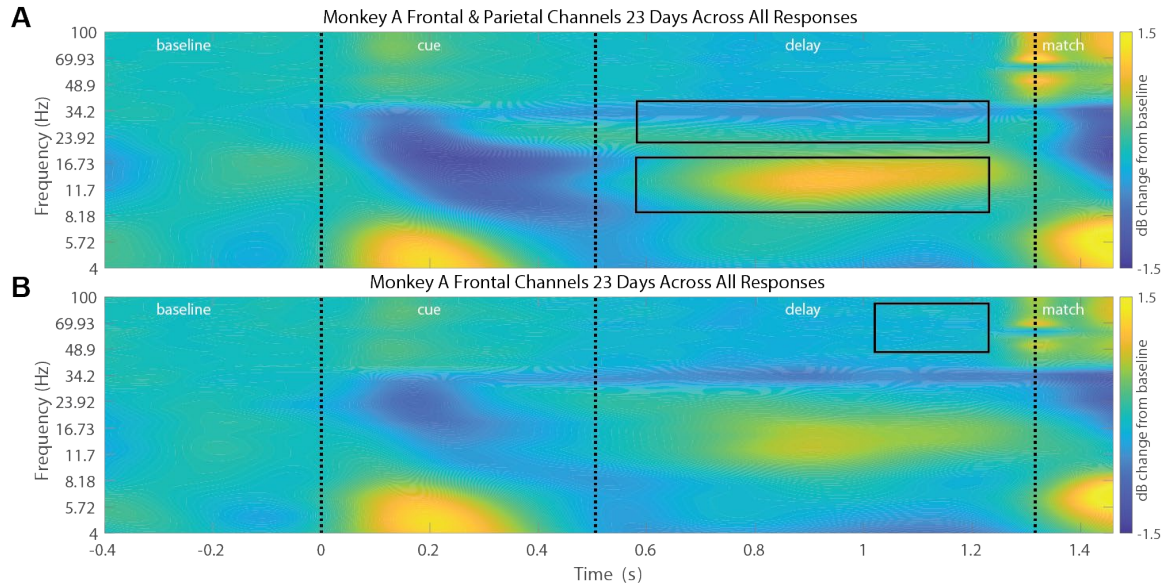


Figure 3.6. Monkey A Average Spectrograms Across All 23 Days & Across Correct & Incorrect Responses

A. Spectrogram averaged over all frontal and parietal channels. Rectangular windows of interest were drawn based on the timescales and frequencies identified in the visual working memory spectral model and visual observation of power emergence. The lower and upper windows represent the low band and mid band, respectively, for Monkey A. **B.** Spectrogram averaged over all frontal channels. A rectangular window of interest was drawn based on the timescales and frequencies identified in the visual working memory spectral model. The window represents the high band for Monkey A.

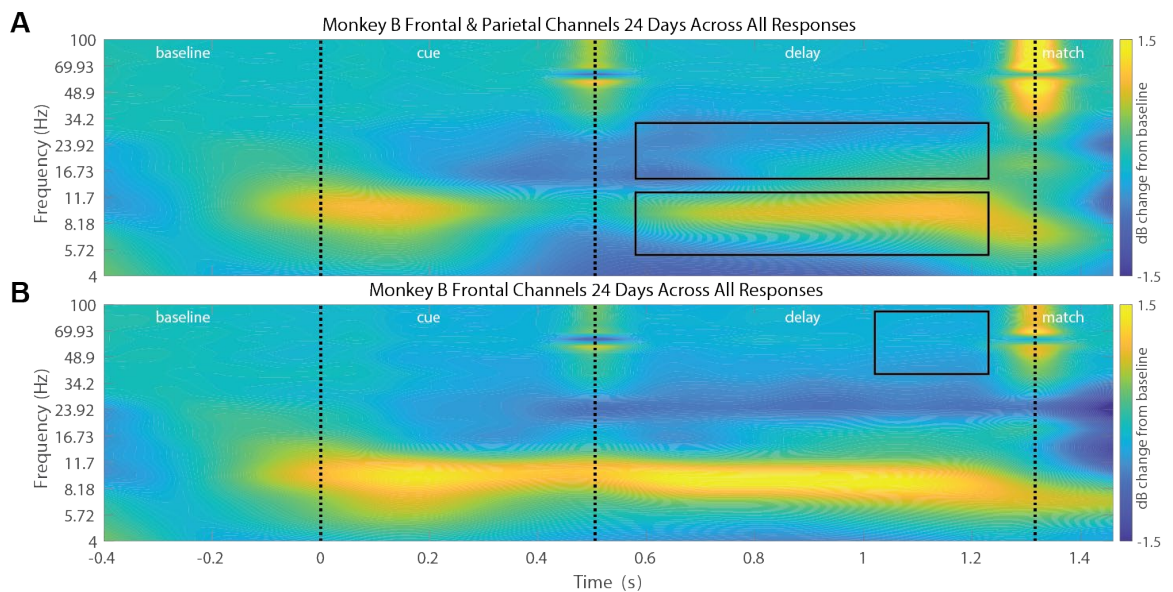


Figure 3.7. Monkey B Average Spectrograms Across All 24 Days & Across Correct & Incorrect Responses

A. Spectrogram averaged over all frontal and parietal channels. Rectangular windows of interest were drawn based on the timescales and frequencies identified in the visual working memory spectral model and visual observation of power emergence. The lower and upper windows represent the low band and mid

band, respectively, for Monkey B. **B.** Spectrogram averaged over all frontal channels. A rectangular window of interest was drawn based on the timescales and frequencies identified in the visual working memory spectral model. The window represents the high band for Monkey B.

3.2.7 One-way t-tests

A one-way single-sample t-test was used to test each hypothesis. Hypotheses 1 and 3 required a right-tailed t-test and hypothesis 2 required a left tailed t-test. Bonferroni correction was used to correct for the three tests at $p=0.05$, yielding an adjusted p-value of 0.0167.

First, all trials were averaged together for each channel, creating a single trial-averaged channel signal. Next, to address the issue of potential correlation between channels, all trial-averaged channels within each recording region were averaged together separately, yielding two regional signals per recording session: a frontal component and a parietal component. Thus, over 23 recording days, Monkey A produced 46 distinct regional components, treated as subjects for the t-test. Conversely, Monkey B produced 48 subjects for the t-test over its 24 recording days.

Finally, average power was calculated across time and frequencies within the rectangular window of interest for each regional component. The t-test was applied at the group level, testing the average of the regional components in order to generalize to neural populations in a single monkey. This process was completed for each monkey separately. The `ttest` function in MATLAB was used to run the test.

3.3 Results

Three Bonferroni-corrected single-sample one-way t-tests were conducted on each monkey to evaluate three hypotheses generated by the visual working memory spectral model (Figure 3.8 & Figure 3.9). The first test evaluated whether frontal and

parietal cortical regions presented with increased low band LFP power during the delay period of the experimental task. The test was significant in Monkeys A and B, $t(45) = 7.26$, $p = 2.12e-09$ and $t(47) = 2.80$, $p = 0.004$, respectively. Specifically, the area in Monkey A with strongest power appears to start at 0.72s and last until 1.2s with a beginning frequency of 11.33Hz and an ending frequency of 16.55Hz (Figure 3.8a). The area in Monkey B with strongest power appears to start slightly earlier at 0.69s and last until 1.22s with a beginning frequency around 8Hz and an ending frequency of 12.46Hz (Figure 3.9a). Surprisingly, the length of each monkey's low band delay-period activity is almost the same, just off by a few milliseconds. The low band is shifted up by about 3-4Hz in Monkey A.

The second test evaluated whether areas in frontal and parietal cortical regions presented with decreased mid band LFP power during the delay period of the task. This test was also significant in Monkeys A and B, $t(45) = -3.00$, $p = 0.002$ and $t(47) = -5.90$, $p = 1.87e-07$, respectively. The area in Monkey A showing the strongest delay-period power decrease appears to extend throughout the epoch beginning with frequency component 32.10Hz and ending around 37Hz (Figure 3.8a). There appears to be two areas in Monkey B showing strong delay-period power decreases. The first starts just after cue offset around 0.53s and is very brief, lasting only until 0.71s with beginning frequency at 13.69Hz and ending around 18Hz. The second starts shortly after cue offset around 0.59s and lasts until 1.2s beginning around frequency 26Hz and extending up around 33Hz (Figure 3.9a). Again, the boundary of the mid band is shifted up by about 4Hz in Monkey A relative to B. The second window of decreased power in Monkey B is similar in timescale to the decreased power window in Monkey A.

The third test evaluated whether frontal areas contained high band bursts of LFP power near the end of the delay period of the task. This test was not significant in either monkey, $t(22) = -3.62$, $p = 0.999$ for Monkey A and $t(23) = -14.17$, $p \sim 1$ for Monkey B. Indeed, there are no power increases visually observable in the high band near the end of the delay in Monkey A (Figure 3.8b) or Monkey B (Figure 3.9b). Instead, it appears slightly decreased during this time.

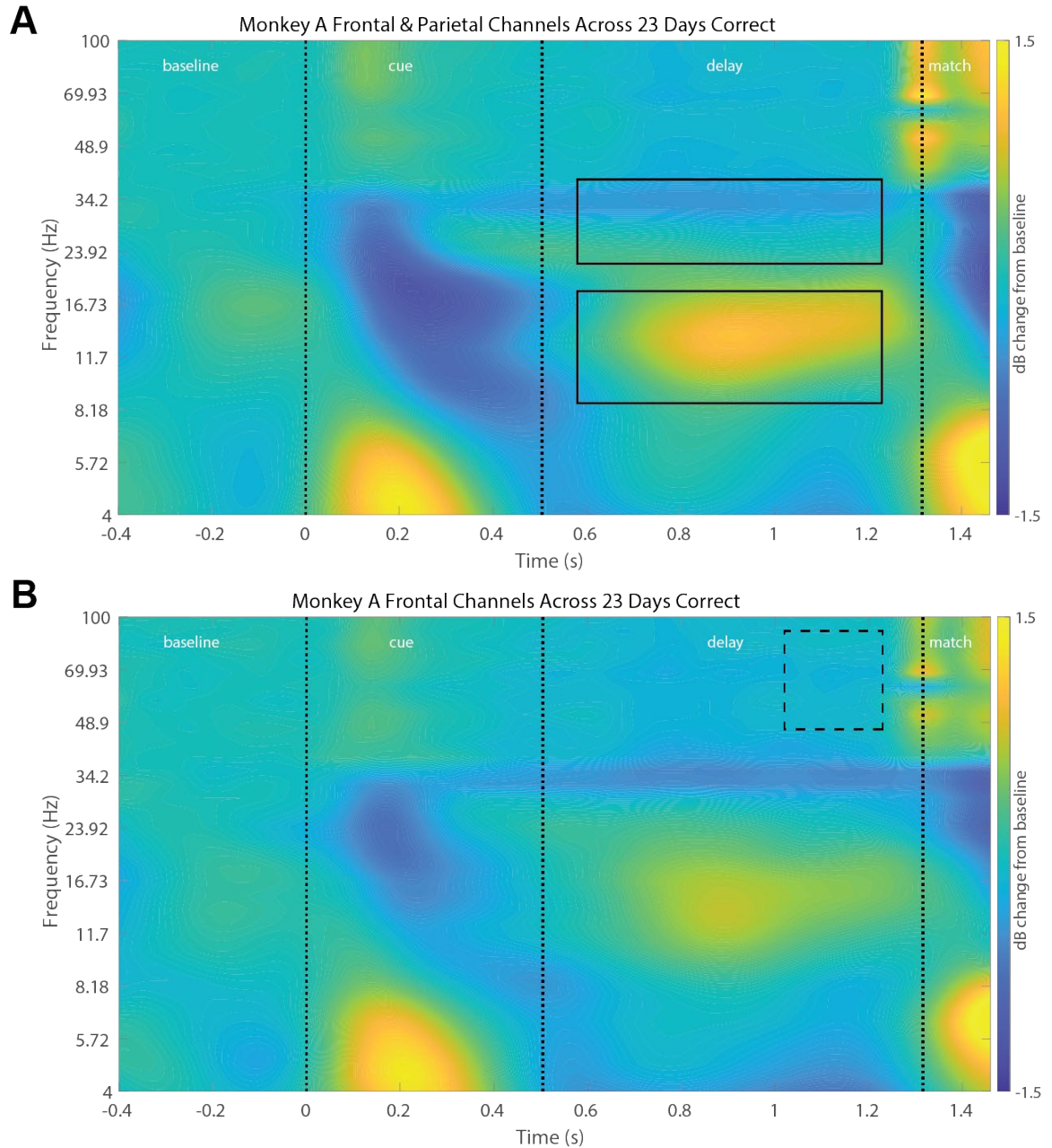


Figure 3.8. Monkey A time-frequency spectrograms showing dB baseline-normalized LFP power with rectangular windows of interest highlighted for each hypothesis generated by the visual working memory spectral model

A. The time-frequency spectrogram averaged across 143 total channels recorded over 23 days in frontal and parietal areas of Monkey A. The lower rectangle represents the window of interest for hypothesis 1. It ranges from time 0.58s to 1.23s and frequency 8.53Hz to 18.19Hz during the delay period. The upper rectangle represents the window of interest for hypothesis 2. It ranges from time 0.58s to 1.23s and frequency 21.99Hz to 38.80Hz during the delay period. Both lower and upper windows were significant $t(45) = 7.26$, $p = 2.12e-09$ and $t(45) = -3.00$, $p = 0.002$, respectively. **B.** The time-frequency spectrogram averaged across 69 frontal channels recorded over 23 days for Monkey A. The dashed rectangle represents the window of interest for hypothesis 3. It ranges from time 1.02s to 1.23s and frequency 46.89Hz to

90.97Hz during the delay period. It was not significant $t(22) = -3.62$, $p = 0.999$. See Methods for additional details.

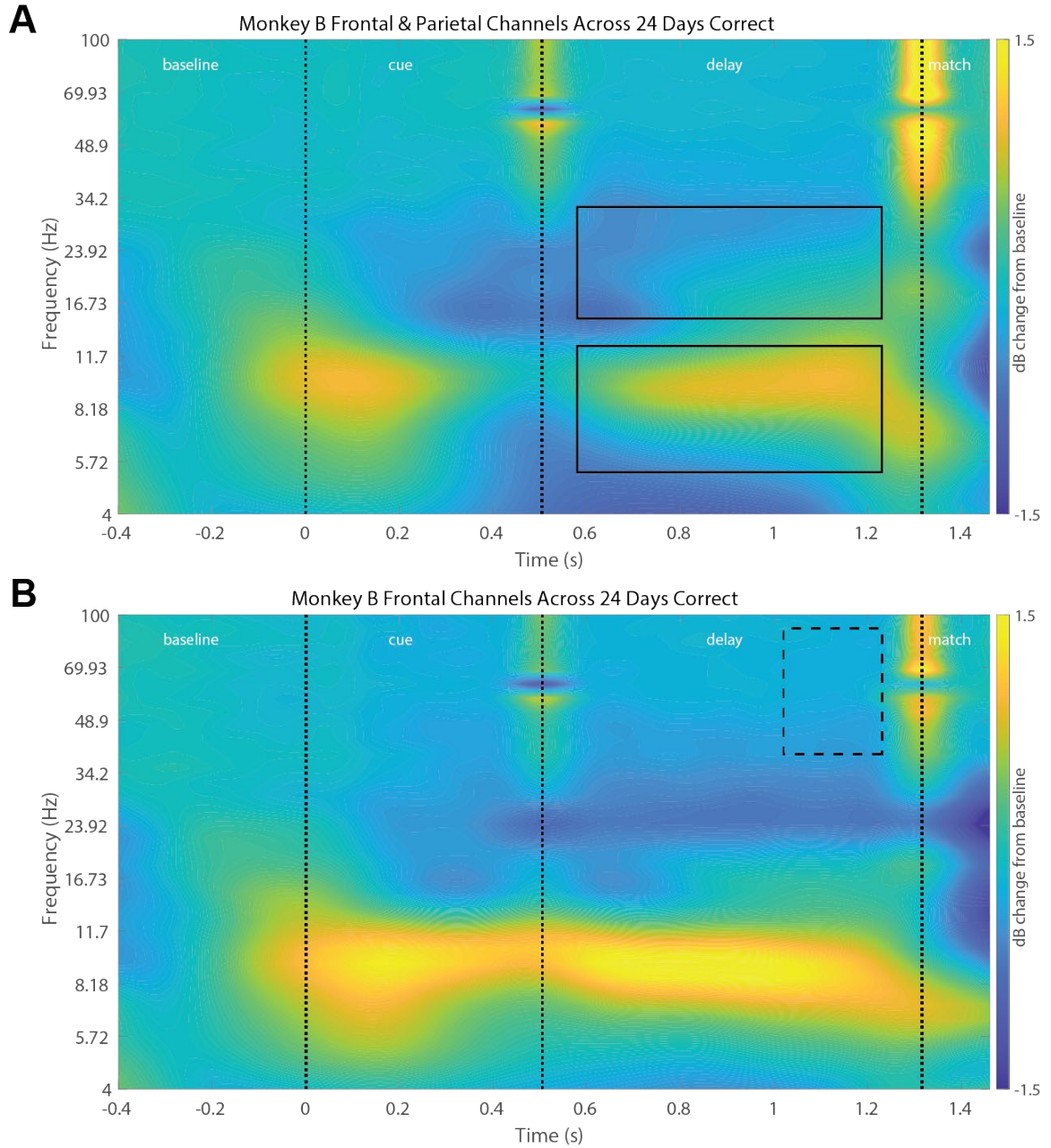


Figure 3.9. Monkey B time-frequency spectrograms showing dB baseline-normalized LFP power with rectangular windows of interest highlighted for each hypothesis generated by the visual working memory spectral model

A. The time-frequency spectrogram averaged across 318 total channels recorded over 24 days in frontal and parietal areas of Monkey B. The lower rectangle represents the window of interest for hypothesis 1. It ranges from time 0.58s to 1.23s and frequency 5.32Hz to 12.46 during the delay period. The upper rectangle represents the window of interest for hypothesis 2. It ranges from time 0.58s to 1.23s and frequency 15.06Hz to 32.11Hz during the delay period. Both lower and upper windows were significant $t(47) = 2.80$, $p = 0.004$ and $t(47) = -5.90$, $p = 1.87e-07$, respectively. **B.** The time-frequency spectrogram

averaged across 146 frontal channels recorded over 24 days for Monkey B. The dashed rectangle represents the window of interest for hypothesis 3. It ranges from time 1.02s to 1.23s and frequency 38.80Hz to 90.97Hz during the delay period. It was not significant $t(23) = -14.17$, $p \sim 1$. See Methods for additional details.

3.4 Conclusion

The monkey visual working memory spectral model generated three predictions relevant for the non-spatial visual working memory task analyzed in this study.

Hypothesis 1 stated that there should be an increase relative to baseline in the low band LFP power during the delay period across frontal and parietal cortical regions.

Hypothesis 2 stated that there should be a decrease relative to baseline in the mid band LFP power also during the delay period across frontal and parietal regions. Hypothesis 3 stated there would be high band power bursts observed in the LFP power near the end of the delay period in frontal cortical areas. Hypotheses 1 and 2 proved correct and hypothesis 3 was incorrect for both monkeys.

There are likely underlying recurring neural dynamics which give rise to the low and mid band oscillations reported here and elsewhere (Jacob et al., 2018; Lundqvist et al., 2018). It is to be expected that the band ranges differed per monkey. In fact, the very studies that went into the creation of the spectral model of visual working memory in the monkey were comprised of results with heterogeneous bands. For instance, in some studies the mid band was as narrow as 12-22Hz (Salazar et al., 2012) or 15-32Hz (Antzoulatos & Miller, 2016) or as wide as 15-50Hz (Kornblith et al., 2016). While the band ranges within monkeys may differ, the general theme of 3 different overall bands: a low, mid, and high is retained.

It was especially intriguing to see such similarity in the low and mid band timescales between monkeys. This lends support to the low band's role in visual attention

identified in the model and other studies (Fiebelkorn et al., 2018; Foster & Awh, 2019; Helfrich et al., 2018). Because it occurs during the delay, when the monkey is not presented with any external stimulus, the attention can be understood as internally focused, in service of the working memory process (Fuster, 2015). Moreover, the mid band's sustained decreased activity in both monkeys during the delay also supports a consistent functional role. The model proposes the mid band is maintaining the working memory content across the delay, which is vital for successful completion of the task.

The absence of power bursts near the end of the delay leaves open the explanation for how the working memory content is transferred within the frontal region, according to the model. There are two possibilities: either the bursts are there and were just not picked up by the current time-frequency analysis choice of decomposition method and group-level statistical test, or the model needs further studies to test the generalizability of LFP frontal high-frequency directed connectivity during non-spatial visual working memory tasks. Considering the first scenario, the complex Morlet wavelet convolution applied here is ideal for identifying lower frequencies found in the low and mid bands. It's possible higher frequencies could be better identified using the multi-taper method (Mitra & Bokil, 2009), which averages multiple higher frequency basis functions to yield a better representation of high frequency components. Furthermore, it is also possible that the power bursts occurred on a trial-by-trial basis in transient periods, much shorter than the kernel window. Because the trials were averaged to be used in a group-level statistical test, this activity may have been lost in the process. A within-subject test could be applied to test each channel grouped by the day of its recording. The second scenario simply

requires more studies to make further claims on whether the effect is a true spectral characteristic.

In addition to the hypotheses tested in this study, the visual working memory spectral model predicts a top-down low-band control signal from frontal to parietal areas both during and after the delay period. A future analysis can test this hypothesis using a directed functional connectivity measure such as phase-slope index (Nolte et al., 2008). Moreover, an overall exploratory directed functional connectivity analysis across all bands throughout the trial would be interesting. The results could further inform the model and motivate future studies.

In conclusion, the low and mid bands in the baseline normalized LFP power appear to have a role in support of non-spatial visual working memory in the monkey. This is predicted by the spectral monkey model of visual working memory. Further analysis and future studies have the potential to shed further light on the model's validity.

4 FUTURE DIRECTIONS AND OPPORTUNITIES IN MONKEY FRONTOPARIETAL NETWORK RESEARCH ON VISUAL WORKING MEMORY

This dissertation examined the spectral characteristics of the frontoparietal network supporting monkey visual working memory and the organization of the anatomical structure enabling it.

In chapter 1, studies reporting spectral characteristics of non-spatial, spatial, and visuospatial visual working memory in the monkey frontoparietal network were examined and synthesized into a new model. It highlighted how low, mid, and high frequency bands dynamically organize in support of spatial, non-spatial and visuospatial working memory tasks. The low band is responsible for attentional selection of the working memory content. The mid band maintains the content, protecting it from competing stimuli and distractors. Finally, the high band serves to transfer information within frontal and parietal regions related to the working memory content for successful completion of the task. Together, they enable the overall working memory process to transpire. The model is an important step in developing a better understanding of the spectral components underlying visual working memory.

In chapter 2, the organization of structural connectivity between areas of the monkey frontoparietal network was explored to better understand how it may be capable of supporting cognitive processes like visual working memory. A new binary association

matrix was proposed as a result of the collation of many tract-tracing studies. A graph theoretic analysis on the matrix found that the frontoparietal network's fundamental building block was the 3-node M9 dynamical relaying motif. This motif is optimally structured for the synchrony found in the spectral model and which was reported to support visual working memory (Antzoulatos & Miller, 2016; Buschman & Miller, 2007a; Salazar et al., 2012). Furthermore, the network was found to have a small-world architecture which provides both the integration and specialization of function required by visual working memory (Dotson et al., 2014). Finally, the degree of connectivity was diffused throughout the network, creating a reliable substrate for sustaining visual working memory dynamics.

In chapter 3, hypotheses generated by the spectral model of monkey visual working memory were tested on a real dataset from an experiment studying non-spatial visual working memory in two rhesus macaques. Two of the three hypotheses were supported by evidence. Specifically, there was an increase in the low band and decrease in the mid band LFP power relative to baseline during the delay period across frontal and parietal cortical regions. The third hypothesis that there would be high band power bursts near the end of the delay period responsible for transferring working memory content in the frontal region was not supported. This was due to the type of time-frequency decomposition method used, the amount of averaging imposed, or the low number of non-spatial visual working memory studies that went into the creation of the model.

Despite the efforts put forth to report on the structural organization and functional spectral characteristics of visual working memory in the monkey frontoparietal network,

much work remains to be done. Opportunities to expand on the topic of each chapter will be addressed in-turn below.

4.1 The Spectral Model of Visual Working Memory in the Monkey

Chapter 1 reviewed the literature reporting spectral characteristics of visual working memory in the monkey frontoparietal network. The results of 15 studies were aggregated and distilled to create a model comprising the spectral characteristics of spatial, non-spatial, and visuospatial working memory tasks. However, much remained to be explored with the model. First, the time-frequency decomposition method was not the same across studies. This can impact which frequency components are observed or deemed statistically significant as some methods bias lower frequencies while others bias higher frequencies (Mike X Cohen, 2014). As a result, each study may have reported only certain aspects of the data. It would be optimal if all visual working memory studies leveraged a standard, preferably open-source, analysis pipeline to identify spectral characteristics in a uniform and comprehensive manner. For instance, if they all applied complex Morlet wavelet convolution for frequencies under 60Hz and the multi-taper method for frequencies above 60Hz, that would provide a greater likelihood that all frequencies were represented by the optimal method. This would take much more computation time as there are two decompositions. Adding to the complexity, the results would need to be combined afterwards for visualizations on the same scale. There are further considerations at this point concerning what power or phase-based connectivity analyses to apply to the complex signal. These decisions would be made by the researchers, contingent on the question they are exploring. However, the main point is that they will have decomposed their simultaneously recorded electrophysiological visual

working memory data into the time-frequency domain using a standardized, open-source pipeline.

Second, the model was limited by the results of the 15 studies from which it was created. It is likely that the low, mid, and high bands interact in some manner to coordinate the visual working memory process. However, measures of cross-frequency coupling and other dynamic cross-band techniques were not tested. Simulations which identify the ways in which the bands could interact within the spatial constraints imposed by the monkey frontoparietal network would be illuminating. To avoid the significant temporal and financial restrictions imposed by empirical studies, software such as The Virtual Brain (Sanzleon et al., 2013) could be used to simulate activity in the low, mid, and high bands from separate neural mass models representing frontal and parietal regions. Much may be learned from simulated data testing aspects of the model.

4.2 The M9 Dynamical Relay Motif

In Chapter 2, the organization of areal connectivity in the monkey frontoparietal network was explored. This involved generation of a new connectivity matrix based on collated results of around 40 tract-tracing monkey studies. A graph theoretic analysis was applied to the connectivity matrix which found that the 3-node M9 dynamical relay motif was overrepresented. This means it occurred in the frontoparietal network to a statistically greater degree than was expected in a random or lattice-based network. The M9 motif is comprised of an apex node and two driven nodes. It is ideal for generating zero-lag and non-zero phase synchrony, which is an important aspect of the spectral model of visual working memory. Subsequently, questions were raised concerning how the areas were involved in the motif. Did some areas participate more than others as the

apex node, serving to drive two others? It would be beneficial to perform a follow-up analysis to better understand this question. The analysis could explore each node's M9 apex ratio (Sporns et al., 2007). An apex ratio is used to quantify the amount of time a node participates as the apex in any open triangle motif. Investigations building on the apex ratio have been performed elsewhere to better characterize networks (Gollo et al., 2015) and examine novel star-like structures (Harriger et al., 2012). It would be ideal to report the apex ratio and propose a new “driven-node” ratio to quantify the number of times a node participates in the M9 motif in a non-apical fashion. This will further characterize each node's role in the M9 motif in a quantifiable manner. As a follow-up, the closeness and betweenness centrality can be calculated for those nodes which have a high apex ratio. This is an effective method to identify if any nodes qualify as hubs, a point that was not addressed in Chapter 2 (Sporns et al., 2007).

4.3 Spatial vs Non-spatial Visual Working Memory Spectral Characteristics

Chapter 3 focused on an experiment where two monkeys had to perform an oculomotor delayed match-to-sample task which tested non-spatial visual working memory in some trials and spatial in others, depending on the rule currently in-play. Under the identity rule, the monkey was required to remember the identity of the object shown during the cue period over a delay. Under the location rule, the monkey had to remember where the object appeared during the cue period over a delay. It was assumed that visual non-spatial working memory was utilized under the identity rule and spatial under the location rule. A rule switch was not done until the monkey established proficiency under the current rule and had accumulated enough trials. The switch was not cued. Accordingly, there was a period where the monkey had to figure out which rule

was in play, prior to establishing proficiency. Further details can be found in the original manuscript (Salazar et al., 2012).

The spectral model (Chapter 1) was constructed from studies on visual non-spatial, spatial, and visuospatial working memory in monkeys. There was much overlap in the spectral characteristics for each type of visual working memory. However, there were also subtle differential spectral characteristics unique to the type of visual working memory employed by the monkey. Specifically, for spatial working memory, the spectral model generates several hypotheses regarding the roles of low (1-15Hz), mid (12-35Hz), and high (35Hz+) frequency band spiking and LFP activity both within and between frontal and parietal regions. First, frontal and parietal regions should show decreased low-band spiking power during the delay period. Additionally, there should be a top-down low-band control signal from frontal to parietal areas both during and after the delay period, prior to a response movement (Martínez-Vázquez & Gail, 2018). Second, frontal and parietal regions should each separately show increased power and synchrony within region during the cue and part of the delay period (Antzoulatos & Miller, 2016). Also, a bi-directional bottom-up signal during the delay (Martínez-Vázquez & Gail, 2018) and top-down signal during the cue and part of the delay (Antzoulatos & Miller, 2016) between frontal and parietal areas should be observed in the mid-band. The top-down signal was previously associated with spatial categorization and the bottom-up with a role in withholding movement, unrelated to working memory. Finally, parietal regions should show increased high-band LFP power during the delay period (Pesaran et al., 2002).

These five hypotheses can be tested using the dataset from Chapter 3 by focusing only on correct trials while the location rule was in play. The results of the analysis could

shed further light on the efficacy of the model and highlight areas of divergence. It would be valuable to compare the results with the non-spatial findings. It can be shown if and whether the model is better at predicting non-spatial or spatial characteristics.

There is debate as to whether the task during the location rule is really a test of spatial visual working memory. Instead of the monkey remembering the location of the cue over a delay period, the monkey may just be storing a motor plan of its intended saccade. The delay is short enough for this to be feasible. In this case, the monkey would be using a prospective motor working memory (Fuster, 2015). Other studies that were used in the creation of the spectral model also utilize this version of the task and consider it a test of spatial visual working memory. So, the spectral characteristics predicted by the model should still be valid hypotheses. It is just a matter of interpreting the results as characteristics of spatial visual or prospective motor working memory. One way to reduce the likelihood of a reliance on prospective motor working memory is to modify the task by adding nonmatch cues (Constantinidis & Steinmetz, 2001). This has the effect of increasing difficulty and raises the probability of spatial visual working memory usage.

4.4 Non-spatial Visual Working Memory Task Performance

Like chapter 3, most studies typically focus on analyzing the activity of correct trials to derive purported mechanisms of working memory (Jacob et al., 2018; Johnson et al., 2017; Kornblith et al., 2016; Salazar et al., 2012). However, this signal may contain temporally coincident confounds related to the task such as reward expectation and attentional motor set (Fuster, 2015). To obtain a signal with activity which more accurately depicts task relevant visual working memory, it may be important to contrast the correct trials with the incorrect, where working memory may have been impaired or

not utilized at all. Hence, to the extent that they populate the incorrect signal, the confounds are stripped away. The resulting signal should have a higher likelihood of containing elements that were relevant for correct performance of the task. Additionally, the experimental task should have already been established as a reliable test of visual working memory (Paule & Rodriguez, 2009). Consequently, the correct vs incorrect signal should have a higher likelihood than the correct signal of exhibiting characteristics useful for processing of task-relevant information resulting in correct visual working memory performance.

In Chapter 3, three hypotheses generated by the spectral visual working memory model on the role of the low, mid, and high frequency bands were tested for each monkey. While this analysis focused on time-frequency spectral characteristics, it remains to be established whether there is information in the time domain from the raw LFP signal related to task performance. The task performance signal could be tested using the same previously generated hypotheses for spatial and non-spatial visual working memory. The results of such an analysis would shed light on whether the model is effective at predicting spectral characteristics related to task performance.

4.4.1 Time Domain Task Performance Preliminary Analysis

It is necessary to first establish whether a task performance signal contains any useful information. This can be accomplished qualitatively by observing event-related potentials (ERP) in the time domain. ERPs are useful in identifying differences between two conditions, correct and incorrect trials in this case, with high temporal precision and accuracy (Mike X Cohen, 2014; Luck, 2014). A preliminary analysis was conducted with results below.

To calculate the event-related potential (ERP), the length of each epoch had to be the same across trials. Accordingly, timepoints -504ms through -1ms prior to sample onset were designated as the baseline period, while the monkey maintained fixation (504 samples). The stimulus was shown at time 0ms. The timepoints up to and including 504 ms after the stimulus was shown, just prior to it disappearing, make up the cue epoch (505 samples). Timepoints up to and including 810 ms after the sample was turned off comprise the delay epoch (811 samples). Finally, time points up to and including 200ms after the matching and distractor object were shown make up the match epoch (201 samples). So, the ERP was comprised of 2,021 samples or ms.

The task performance signal in the time domain is created by computing the difference between correct and incorrect trials at each time point of each trial. The raw LFP activity during the delay period of the resulting signal can be subsequently explored to discern whether meaningful non-spatial visual working memory activity related to task performance can be observed.

The average task performance signal was taken across all trials for each monkey, day, and channel combination to provide channel-level ERPs comparing correct vs incorrect responses. Next, the average across all trials and channels was calculated for each monkey and day to provide day-level ERPs comparing correct vs incorrect responses: 23 for Monkey A and 24 for Monkey B. Finally, the average across all trials, channels and days was calculated to provide overall monkey-level ERPs comparing correct vs incorrect responses (Figure 4.1). The correct and incorrect traces look similar for Monkey A. However, there appears to be a low frequency difference between correct

and incorrect trials in Monkey B during the delay period. This was explored further because it did not appear physiological in origin.

Suspicious days for Monkey B were identified by visual observation of the potentially non-physiological low frequency ($\sim 1\text{Hz}$) component during the delay period of correct trials. As a result, 7 recording sessions from days 17-22 and 24 were flagged as suspicious. The non-physiological component is easily observable in the suspicious day ERPs (Figure 4.2a). A new overall Monkey B ERP comparing correct and incorrect responses was re-calculated with recordings from the suspicious days removed (Figure 4.2b). There is still an observed difference between correct and incorrect signals during the delay period of correct trials. This means the task performance signal from Monkey B is more likely than A to exhibit characteristics useful for processing of task-relevant information resulting in correct visual working memory performance. Thus, to the extent that the model is appropriate for predicting spectral characteristics related to task performance, it may do so more successfully for Monkey B rather than Monkey A.

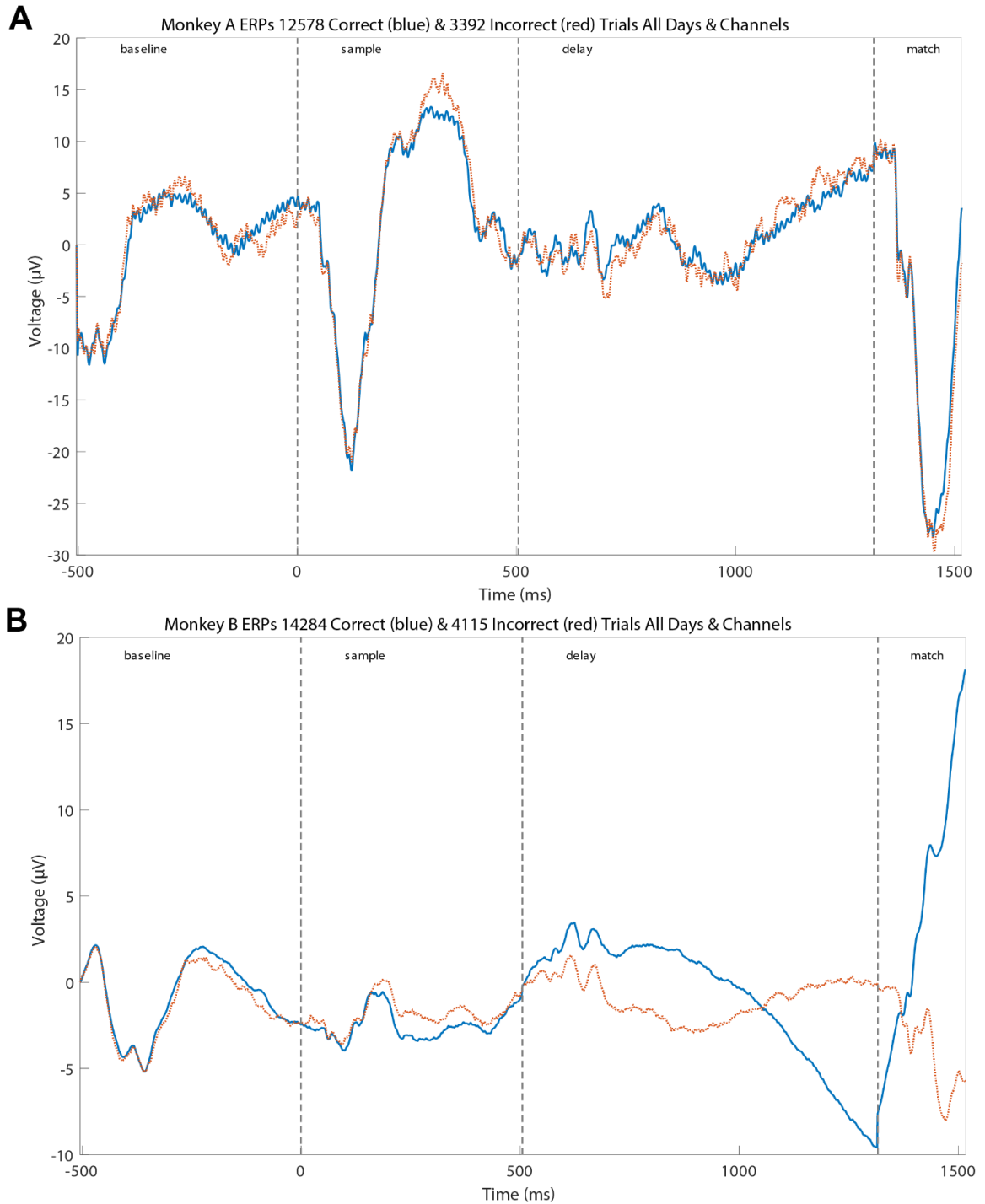


Figure 4.1. Event-related potentials (ERPs) for correct (blue solid) and incorrect (red dashed) trials across all recording days and channels

A. Monkey A ERPs calculated from the averages of 12,578 correct trials and 3,392 incorrect trials. Visually, there does not appear to be a difference. **B.** Monkey B ERPs calculated from the averages of 14,284 correct trials and 4,115 incorrect trials. There appears to be a large low frequency difference between correct and incorrect trials during the delay period for Monkey B.

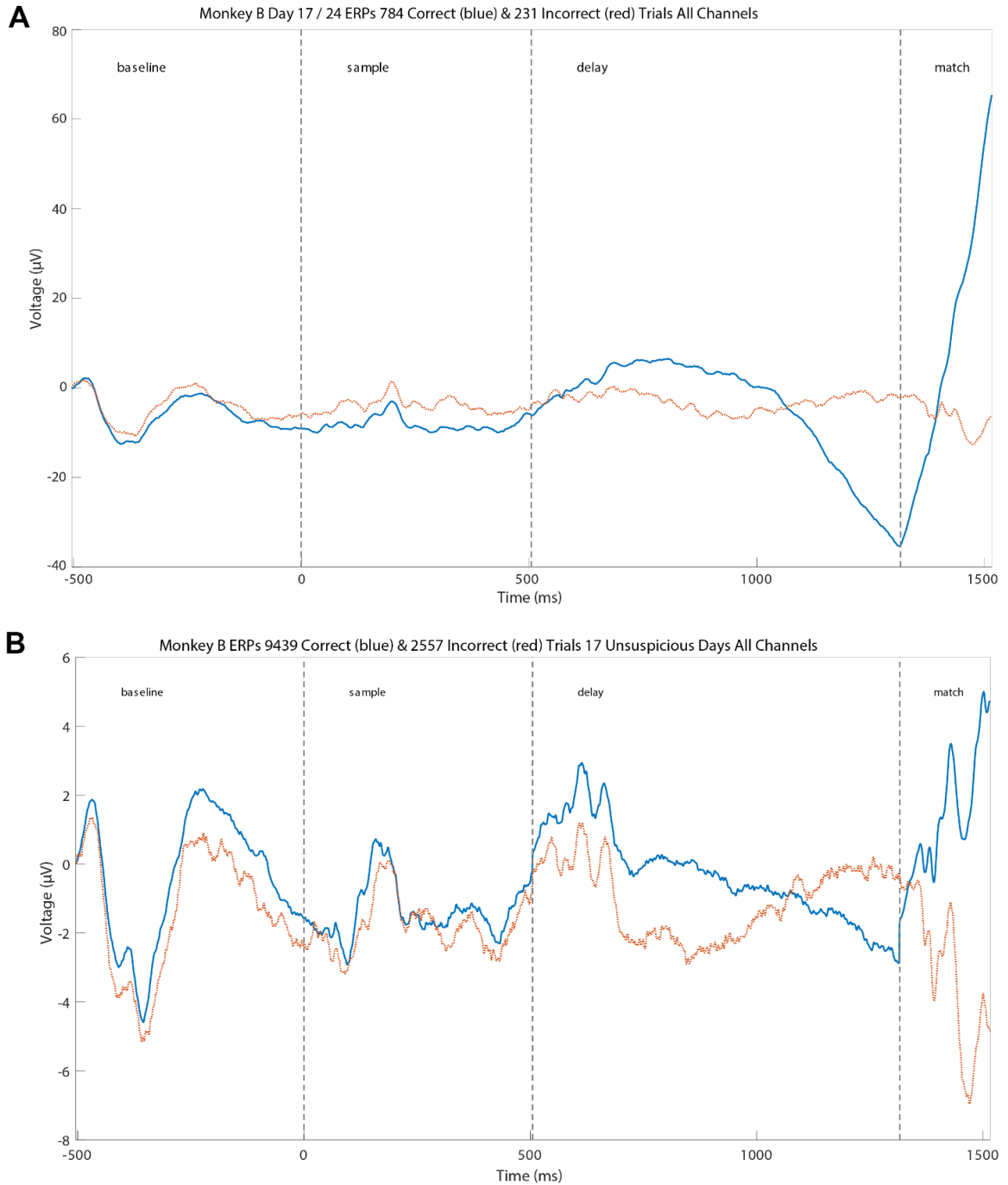


Figure 4.2. ERPs for correct (blue) and incorrect (red) trials from Monkey B
A. Example of a suspicious day distinguished by the potentially non-physiological ~ 1 Hz component observable during the delay period of correct trials. This represents the average over all channels for day 17, comprising 784 correct and 231 incorrect trials. **B.** The revised Monkey B overall ERP calculated from the averages of 9,439 correct and 2,557 incorrect trials across all channels from all days. There is still an observable difference between correct and incorrect signals during the delay period that no longer looks non-physiological in origin.

4.5 Spectral Model of Monkey Visual Working Memory

The spectral model is the first attempt, to this author's knowledge, at a qualitative description of the spectral characteristics associated with non-spatial, spatial, and visuospatial types of visual working memory. Contrary to the traditional EEG bands, it proposes new, more general, broad bands to functionally separate spectral activity. This establishes a more appropriate framework to report and interpret time-frequency analyses on electrophysiological visual working memory data. It also attempts to assign a role to each band, functionally linking them together in the overall visual working memory process, based on the literature. It can serve as a starting point for our understanding of how the monkey brain accomplishes visual working memory in the spectral domain. Future studies are expected to make the model more robust and generalizable through refinements and modifications.

It is important to point out that the model represents the synthesis of 15 different studies on spatial, nonspatial, and visuospatial visual working memory. Experiments on visual working memory typically use a task that falls into one of these three categories. Accordingly, to generate the most accurate task-appropriate predictions, the summary tables and corresponding interpretation that went into constructing the model should be referenced (Table 1.2 and Table 1.3). For instance, the model does not specify how low-band LFP power is differentially modulated within frontal and parietal regions according to whether the monkey is performing a spatial or non-spatial task. It merely illustrates a general role for the low band power in these regions. It also does not provide clear boundaries for each of the bands. Based on the data in the tables, they appear to differ slightly by monkey and potentially by the type of visual working memory tested.

Ultimately, the table and corresponding interpretation must be referenced to generate testable hypotheses on task-appropriate roles for the bands.

The solution may be to break the visual working memory model up into three separate models, one for each type: spatial, non-spatial and visuospatial. The new models could identify spectral characteristics reported for each type including boundaries and more specific roles for the bands. Examples may include explicitly stating the direction of power modulation and/or connectivity. The drawback is that instead of a model based on 15 studies, each model would be based on a handful. This does not engender confidence in their ability to successfully generalize. Therefore, more studies need to be conducted testing all three types of visual working memory in the monkey with reports of associated spectral characteristics. This would serve to further inform the current visual working memory model and motivate the move to break it up into three separate models once enough findings had accumulated.

4.6 Conclusion

Working memory is an important cognitive process central to higher level executive functions like cognitive control. It is best studied in the monkey, a mammal with a well-developed prefrontal cortex and the human's closest evolutionary relative which can serve as an experimental animal.

It should be clear from the ideas explored earlier that the spectral model has the potential for much further testing and expansion. It could even be broken up into three more focused models, given enough future studies on monkey visual working memory. In the long-term, it is this author's hope that the model evolves to accommodate future

results and eventually applies its predictions to humans in the pursuit of treatments for neurological disorders where visual working memory is impaired.

5 APPENDIX A

5.1 Supplementary Discussion for Chapter 2

The FPN's connection density is 45.86%. This qualifies it as a moderately dense network, with almost half of all possible interareal connections existing.

The binary directed adjacency matrix of the FPN provides both in and out-degree distributions which detail the number of incoming and outgoing connections to each area, respectively (Figure 5.1). Each distribution has an average degree of 13.3. Most of the nodes have an in-degree similar in quantity to their out-degree. However, 8 of the nodes have a large difference between incoming and outgoing connections, potentially signaling functional specialization. The ratios of in-to-out-degree and out-to-in-degree were calculated to identify those areas exhibiting a disparity greater than 1.5x. Frontal area 6DR and parietal areas PGop, IPd and PFop have in-to-out-degree ratios of 1.73, 1.88, 1.83 and 2.67, respectively. Frontal area 46v and parietal areas PEc, PEa and PE have out-to-in-degree ratios of 1.53, 1.71, 2.5 and 3.5, respectively.

A Pareto chart is used to quantify the portion each factor contributes to an overall distribution. When applied to a total degree distribution, the chart can identify the portion each area contributes to overall connectivity. In this way, a Pareto chart of the total degree distribution provides a qualitative assessment of whether specific areas contribute more to the overall connectivity, thereby suggesting these areas may qualify as hubs (Figure 5.2). In the FPN, the 80th percentile of total connectivity is not reached until 20 of

the 30 nodes of the network are accounted for, or 67.7% of the total network. In a network with hubs, the 80th percentile would generally be reached much earlier in the chart, indicating that a small number of nodes account for a large percentage of the connectivity in the network. These are the nodes which would qualify as potential hubs. Therefore, there do not appear to be any hubs in the FPN according to this qualitative assessment.

Areas 45, 47/12 and PGm were found to participate in the M9 motif with a significantly greater frequency in the empirical FPN than in random ($p = 0, 0$ and $0, z = 5.189, 8.358$ and 8.060) and lattice ($p = 0.046, 0.014$ and $0.029, z = 1.878, 2.440$ and 2.109) networks (Table 5.3). Interestingly, the structural connectivity profile of these areas form the M9 motif as well, with area 45 serving as the apex node and areas 47/12 and PGm serving as the outer nodes (see Figure 2.5 for M9 example).

5.1.1 Areal Specialization

Areas which have a great disparity between their total number of incoming and outgoing connections may have developed this topology through functional specialization. Specifically, nodes which have a high in-to-out-degree ratio suggest the node may be an information aggregator and distiller, acting as a filter for the nodes it sends projections to. Frontal area 6DR likely would be aggregating and disseminating information related to ocular motor movements to its target areas (Luppino & Rizzolatti, 2000).

Nodes which have a high out-to-in-degree ratio suggest the node may be an information source for the nodes it sends projections to. Frontal area 46v has been

reported to provide information to its target areas supporting a range of cognitive functions including visuospatial working memory (Goldman-Rakic, 2011).

The parietal areas identified may provide visual, visuospatial and sequential processing of somatosensory information in support of cognition such as visual and visuospatial working memory (Cavada & Goldman-Rakic, 1989; Cavada & Goldman-Rakic, 1989; Goldman-Rakic, 2011; D. N. Pandya & Seltzer, 1982; Rozzi et al., 2006). Parietal areas PGop, IPd and PFop may compile and filter the information while areas PEa, PEc and PE may act as information sources, thereby providing functional specialization in service of cognition. It is worth pointing out that 6 of the 8 areas which had a high difference between their incoming and outgoing connections were in the parietal region. This region may be under-explored as a result of not having enough tract-tracing studies with injections in the parietal areas of Pandya & Seltzer (1982). As a result, additional projections simply may not have been discovered yet.

5.1.2 Connectivity

There did not appear to be any areas serving as hubs in the FPN according to the Pareto chart. Hub areas would have produced a Pareto chart which reached the 80th percentile much earlier, while only a small percentage of the network was accounted for. For instance, the 50th percentile of the degree distribution of the incoming hyperlinks in the Web is reached after just 1.1% of the nodes in the network are accounted for. These nodes are considered hubs in the Web network (Newman, 2018). A more quantitative analysis was needed to properly classify the degree distributions of the FPN, which would yield insight into the likelihood of hubs (Alstott et al., 2014; Clauset et al., 2009).

5.1.3 Motifs

Synchrony in the FPN may originate from the over-represented frontal areas 45 and 47/12 and parietal area PGm. If all three areas were inactivated, it could be speculated that performance on cognitive tasks requiring synchrony in the FPN would be impaired. This would serve as an interesting follow-up experiment.

The M13 motif was very close to being significantly overrepresented. This motif differs from M9 through the addition of a reciprocal connection between its driven nodes. This serves to encourage non-zero lag synchrony and fails to promote zero lag synchrony due to frustration (Gollo et al., 2014). If the M13 motif had been significant, it would be interpreted as providing the FPN further topological flexibility to establish the kind of synchrony necessary for cognition.

5.1.4 Small World

This work focused on an established neural network observed in isolation from the rest of the brain. When whole-brain connectomes are analyzed at the macroscale, they generally present with hub nodes and power-law scaling of their degree distributions (Oh et al., 2014; Watts & Strogatz, 1998). This is likely because the heterogeneity of connectivity is much greater at the level of the whole brain. When analyzed in this way, there are a smaller number of highly connected nodes compared with a larger number of nodes with few connections.

5.2 Supplementary Figures for Chapter 2

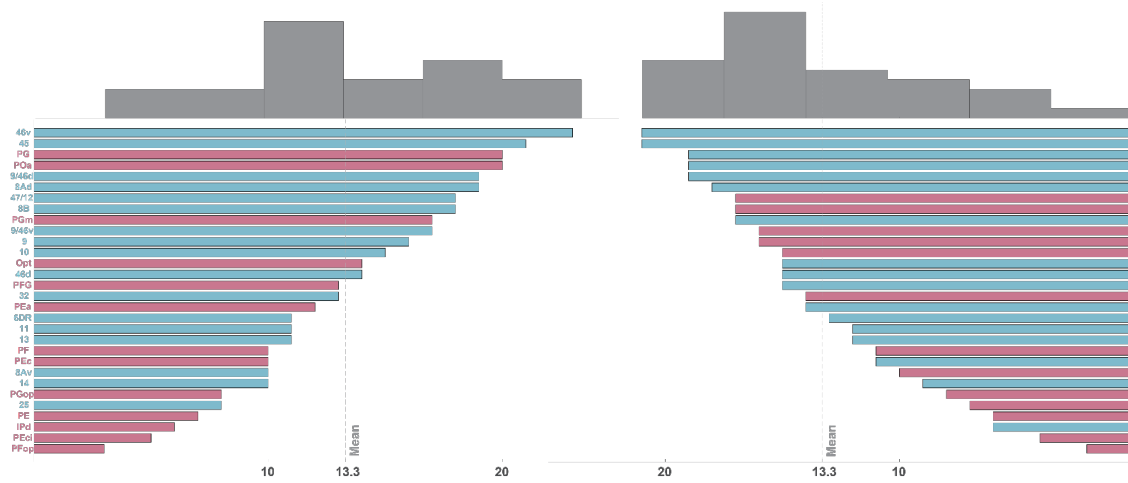


Figure 5.1. The degree distributions for the frontoparietal network. Out-degree is on the left and in-degree is on the right. The average degree for both distributions is 13.3. Frontal areas are colored blue and parietal areas are pink.

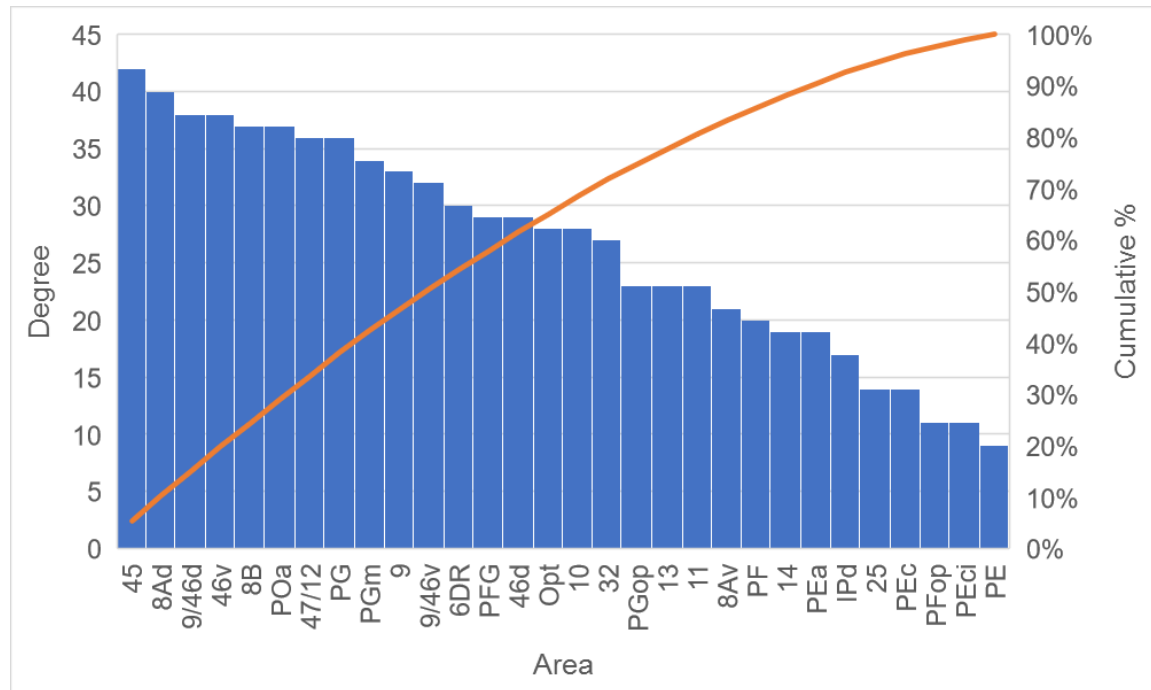


Figure 5.2. Pareto chart of the total degree for each node in the frontoparietal network. Totalling the degree counts for 20 of the 30 areas, up to area 11, accounts for 80% of overall connectivity in the network. This represents a traversal of about 67% of the network before reaching 80% total connectivity, which means it is unlikely that there are any hub nodes.

	Frontal																
	10	9	32	14	25	8B	8Ad	9/46d	46d	46v	9/46v	8Av	45	47/12	13	11	6DR
Frontal	10	1-4	1,2,4-6	1,2,4,5	4	2-4	4,6,7	3,7	1,3,4	4			4,8,9	1,4-6,9,10	4,5,10	1,4-6	4
	9	2,4,5	1,2,4-6	2,4,5	4	2-4	1,3,4,11	3,4,7	3,4	4			8,9	4-6,9,10	4,10	4-6	2,4,12
	32	1,2,4,5,13	1-4,13	1,2,4,5,13	1,4,13	2-4		3	1,3,4,13	1,4			9	1,4-6,9,10,13	1,4,5,10,13	4-6,13	4
	14	2,5	2,3	1,2,5,6		2,3		3	3				9	5,6,9,10	5,10	5,6	
	25	2,5	2	1,2,5,6	2,5	2								10	5,10	6	
	8B	2	2,3,14	6,14	2		3,6,7,11,14	3,7	3,14,15	14	6	3	8,9	3,6,10,14	10	14	3,12,14,16,17
	8Ad	2,14	1-3,14	6		1,2,14,18		1,3,7,14,18,19	1,3,14,15,18	1	1,6,18	1,3,14,18	1,9,14,18	1,6,14			1,12,14,16-21
	9/46d		2,3,14			3,14	3,6,7,11,14,19		3,14	14	6	14	8,9,14	6,14	10		3,12,14,16,17,21
	46d	2	2,3	1,2,6	2	2,3	3,6,7,11	3,7				3	8,9	6,9			12
	46v	2	1-3	2,6	2	1-3	3,6,11	1,3	3,15		6	1,3	1,8,9	1,6,9,10	1,10	6	1,17
	9/46v					14	3,6,11	14		14,15		14,19	8,9,14	6,9,10,14	10,14	6,14	14
	8Av					14	3,6,7,14				6,19		9,14,19	6,9,19			21
	45	8	8	6		3,8	3,6,7,11	3,8	3,8,15	8	6,8	3,19		5,6,8,9	5,8	5,6,8	12,16,20,21
	47/12	1,2,5	1-3	1,2,5,6	1	1-3	3,6	3	1,3	1,15	6,9	3,19	1,8,9		1,5,10	1,5,6	
	13	1,2,5	1-3	1,2,5,6	1	2,3		3			9		1,8,9	1,5,6,9,10		1,5,6	
	11	2,4,5	2,3	1,2,5,6	2,4,5			3	3	4,15	4,9		4,8,9	4-6,9,10	4,5,10		
	6DR		2,3,12	6		2,3,12	1,3,6,7,11,12,19,20	1,3,12			6,22		9,20				
Parietal	PE						23										
	PEcl						6										3
	PEc							23									3,23
	PEa						3,11,23										3,17
	PF										9,23-25	23,26	26	6,9,26			
	PFop																
	PFG						25,27			24	9,23-25,27		8,24,27	6,24,27			27
	IPd						6,11										
	POa		23			3,23	3,6,11,19,23,26-29	22,23,27-29	23	23,27,30	6,9,22,23,27,30	3,23,26,27,29,30	8,9,23,27	6,27,30			27
	PG					3,26	6,11,23,25,26,29,31	3,25,26,29	15,26	15,23,24	6,24-26	3,25,29	9,25,26			6,26	3,25
	PGm		27,32	6		3,27,32	6,23,27,32	3,27,32	3,27,32				27				3,17,23,27,33

	Frontal																
	10	9	32	14	25	8B	8Ad	9/46d	46d	46v	9/46v	8Av	45	47/12	13	11	6DR
PGop							3,23			23							
Opt	27	27				3,24,27	3,24,27	24	3,15,27	15,24,27	24		8,24,27				24

		Parietal												
		PE	PEci	PEc	PEa	PF	PFop	PFG	IPd	POa	PG	PGm	PGop	Opt
Frontal	10													27
	9											27,32		27
	32													
	14													
	25													
	8B										26	14,27		24,27
	8Ad							27	14,34	14,19,27–29,34	14,26,29,31,35,36	14,27,32	37	14,24,27
	9/46d		14	14					14,34	14,27–29	14,26,29,31,36	14,27,32	14	24
	46d										26,31,35,36	27,32		27
	46v					35	37	24	34	27	24,31,35,36		37	24,27
	9/46v					14,24,35		14,24,27		27,30	14,24,26,36	27	37	24
	8Av					26			14,34	14,27,29,30,34,35	29			
	45					26	37	8,24,27		8,27	26,36	27		8,24,27
	47/12					26		24,27		27,30				
	13													
11														
6DR							27		27		27		24,27	
Parietal	PE		38		28,38,39		38	40				40	37	
	PEci							40			24	40		
	PEc	38	38		38,39			40	39		24,38	32,38,40	38	
	PEa		38	38		24	37	24,40	34	34,40	24,26	32,40	38	
	PF				24		37,38	24,38,40	24	24,28,30,38,39			24	
	PFop							40		40			37	
	PFG				24,28	24	37		24,34,39	24,30,39,40	24		24,37	
	IPd					24		24		28,34,40		40	37	
	POa				30,40	24	37,40	24,40	28,34		24,26,28,36,40	40	37,40	24,40
	PG		24	24	24,26		37	24,40	39	24,26,28,30,40		26,32,33,40	24,37	24,40
	PGm	32	40	40	28,39,40				39,40	28,40	26,32,33,40		40	24,40
	PGop					24		24,40		40	24	40		24
	Opt									24,40	24,36,40	24,40	24	

Table 5.1. Association matrix for the frontoparietal network

The matrix uses the Petrides & Pandya (2007) parcellation scheme. The fields are populated with the references where a connection was identified. References related only to this table directly follow. Empty fields signify the absence of any reports of connectivity. However, this does not imply that there is no connection between those areas.

Supplementary Table References

1. Barbas, H. & Pandya, D. N. Architecture and intrinsic connections of the prefrontal cortex in the rhesus monkey. *J. Comp. Neurol.* **286**, 353–375 (1989).
2. Barbas, H., Ghashghaei, H. & Dombrowski, S. M. Medial Prefrontal Cortices Are Unified by Common Connections With Superior Temporal Cortices and Distinguished by Input From Memory-Related Areas in the Rhesus Monkey. **367**, 343–367 (1999).
3. Petrides, M. & Pandya, D. N. Dorsolateral prefrontal cortex: comparative cytoarchitectonic analysis in the human and the macaque brain and corticocortical connection patterns. *Eur. J. Neurosci.* **11**, 1011–1036 (1999).
4. Petrides, M. & Pandya, D. N. Efferent Association Pathways from the Rostral Prefrontal Cortex in the Macaque Monkey. *J. Neurosci.* **27**, 11573–11586 (2007).
5. Price, J. L., Carmichael, S. T. & Price, J. L. Connectional networks within the orbital and medial prefrontal cortex of macaque monkeys. *J. Comp. Neurol.* **371**, 179–207 (1996).
6. Barbas, H. Anatomic organization of basoventral and mediodorsal visual recipient prefrontal regions in the rhesus monkey. *J. Comp. Neurol.* **276**, 313–342 (1988).
7. Hackett, T. A., Stepniewska, I. & Kaas, J. H. Prefrontal connections of the parabelt auditory cortex in macaque monkeys. *Brain Res.* **817**, 45–58 (1999).
8. Gerbella, M. *et al.* Cortical connections of the macaque caudal ventrolateral prefrontal areas 45A and 45B. *Cereb. Cortex* **20**, 141–168 (2010).
9. Petrides, M. & Pandya, N. Comparative cytoarchitectonic analysis of human and macaque ventrolateral pfc and corticocortical cnxn patterns in monkey. *Eur. J. Neurosci.* **16**, 291–310 (2001).
10. Barbas, H. Organization of cortical afferent input to orbitofrontal areas in the rhesus monkey. *Neuroscience* **56**, 841–864 (1993).
11. Barbas, H. & Mesulam, M. M. -M M. Organization of afferent input to subdivisions of area 8 in the rhesus monkey. *J. Comp. Neurol.* **200**, 407–431 (1981).
12. Barbas, H. & Pandya, D. N. Architecture and frontal cortical connections of the premotor cortex (area 6) in the rhesus monkey. *J. Comp. Neurol.* **256**, 211–228 (1987).
13. Pandya, D. N., Van Hoesen, G. W. & Mesulam, M. M. Efferent connections of the cingulate gyrus in the rhesus monkey. *Exp. Brain Res.* **42**, 319–330 (1981).
14. Petrides, M. & Pandya, D. N. N. Efferent association pathways originating in the caudal prefrontal cortex in the macaque monkey. *J. Comp. Neurol.* **498**, 227–251 (2006).
15. Jacobson, S. & Trojanowski, J. Q. Prefrontal granular cortex of the rhesus monkey. I. Intrahemispheric cortical afferents. *Brain Res.* **132**, 209–233 (1977).
16. Luppino, G. *et al.* Prefrontal and agranular cingulate projections to the dorsal premotor areas F2 and F7 in the macaque monkey. *Eur. J. Neurosci.* **17**, 559–578 (2003).
17. Ghosh, S. & Gattera, R. A comparison of the ipsilateral cortical projections to the dorsal and ventral subdivisions of the macaque premotor cortex. *Somatosens. Mot. Res.* **12**, 359–378 (1995).
18. Stanton, G. B., Bruce, C. J. & Goldberg, M. E. Topography of projections to the frontal lobe from the macaque frontal eye fields. *J. Comp. Neurol.* **330**, 286–301 (1993).
19. Huerta, M. F., Krubitzer, L. A. & Kaas, J. H. O. N. H. Frontal eye field as defined by intracortical microstimulation in squirrel monkeys, owl monkeys, and macaque monkeys II. cortical connections. *J. Comp. Neurol.* **265**, 332–361 (1987).
20. Arikuni, T. O. M., Watanabe, K. & Kubota, K. Connections of area 8 with area 6 in the brain of the macaque monkey. *J. Comp. Neurol.* **277**, 21–40 (1988).
21. Luppino, G., Matelli, M. & Rizzolatti, G. Cortico-cortical connections of two electrophysiologically identified

- arm representations in the mesial agranular frontal cortex. *Exp. Brain Res.* **82**, 214–218 (1990).
22. Barbas, H. & Mesulam, M.-M. M. Cortical afferent input to the principals region of the rhesus monkey. *Neuroscience* **15**, 619–637 (1985).
 23. Petrides, M. & Pandya, D. N. Projections to the frontal cortex from the posterior parietal region in the rhesus monkey. *J. Comp. Neurol.* **228**, 105–116 (1984).
 24. Rozzi, S. *et al.* Cortical connections of the inferior parietal cortical convexity of the macaque monkey. *Cereb. Cortex* **16**, 1389–1417 (2006).
 25. Petrides, M. & Pandya, D. N. Distinct parietal and temporal pathways to the homologues of Broca’s area in the monkey. *PLoS Biol.* **7**, (2009).
 26. Andersen, R. A., Asanuma, C., Essick, G. & Siegel, R. M. Corticocortical connections of anatomically and physiologically defined subdivisions within the inferior parietal lobule. *J. Comp. Neurol.* **296**, 65–113 (1990).
 27. Cavada, C. & Goldman-Rakic, P. S. Posterior parietal cortex in rhesus monkey: II. Evidence for segregated corticocortical networks linking sensory and limbic areas with the frontal lobe. *J. Comp. Neurol.* **287**, 422–445 (1989).
 28. Blatt, G. J., Andersen, R. A. & Stoner, G. R. Visual receptive field organization and cortico-cortical connections of the lateral intraparietal area (area LIP) in the macaque. *J. Comp. Neurol.* **299**, 421–445 (1990).
 29. Medalla, M. & Barbas, H. Diversity of laminar connections linking periarculate and lateral intraparietal areas depends on cortical structure. *Eur. J. Neurosci.* **23**, 161–179 (2006).
 30. Borra, E. *et al.* Cortical Connections of the Macaque Anterior Intraparietal (AIP) Area. *Cereb. Cortex* **18**, 1094–1111 (2008).
 31. Maioli, M. G., Squatrito, S., Samolsky-dekel, B. G. & Riva Sanseverino, E. Corticocortical connections between frontal periarculate regions and visual areas of the superior temporal sulcus and the adjoining inferior parietal lobule in the macaque monkey. *Brain Res.* **789**, 118–125 (1998).
 32. Parvizi, J. *et al.* Neural connections of the posteromedial cortex in the macaque. *Proc. Natl. Acad. Sci.* **103**, 1563–1568 (2006).
 33. Luppino, G. & Rizzolatti, G. The Organization of the Frontal Motor Cortex. *News Physiol. Sci.* **15**, 219–224 (2000).
 34. Lewis, J. W. & Van Essen, D. C. Corticocortical connections of visual, sensorimotor, and multimodal processing areas in the parietal lobe of the macaque monkey. *J. Comp. Neurol.* **428**, 112–137 (2000).
 35. Neal, J. W., Pearson, R. C. A. & Powell, T. P. S. The ipsilateral corticocortical connections of area 7 with the frontal lobe in the monkey. *Brain Res.* **509**, 31–40 (1990).
 36. Andersen, R. A., Asanuma, C. & Cowan, W. M. Callosal and prefrontal associational projecting cell populations in area 7A of the macaque monkey: A study using retrogradely transported fluorescent dyes. *J. Comp. Neurol.* **232**, 443–455 (1985).
 37. Cipolloni, P. B. & Pandya, D. N. Cortical connections of the frontoparietal opercular areas in the Rhesus monkey. *J. Comp. Neurol.* **403**, 431–458 (1999).
 38. Pandya, D. N. & Seltzer, B. Intrinsic connections and architectonics of posterior parietal cortex in the rhesus monkey. *J. Comp. Neurol.* **204**, 196–210 (1982).
 39. Seltzer, B. & Pandya, D. N. Posterior parietal projections to the intraparietal sulcus of the rhesus monkey. *Exp. Brain Res.* **62**, 459–469 (1986).
 40. Cavada, C. & Goldman-Rakic, P. S. Posterior parietal cortex in rhesus monkey: I. Parcellation of areas based on distinctive limbic and sensory corticocortical connections. *J. Comp. Neurol.* **287**, 393–421 (1989).

	Motif Class ID												
	1	2	3	4	5	6	7	8	9	10	11	12	13
p-val rand	1.000	1.000	1.000	1.000	1.000	1.000	1.000	1.000	0.000	1.000	1.000	1.000	0.000
p-val latt	0.528	0.659	0.029	0.994	0.016	1.000	0.073	1.000	0.049	0.710	0.683	0.794	0.054
z-score rand	-8.269	-10.687	-8.087	-5.993	-5.830	-6.106	-5.375	-8.149	12.032	-10.516	-7.755	-7.863	19.122
z-score latt	-0.155	-0.516	1.864	-2.504	2.280	-4.169	-0.267	-3.401	1.612	-0.660	-0.589	-0.825	1.611

Table 5.2. Permutation test results by motif class

Results from a permutation test comparing the frequency of occurrence of motif classes in the empirical FPN with their frequency in 100,000 random and lattice networks. Motif class ID 9 (bolded) was found to be significantly overrepresented in the empirical FPN in comparison to both random ($p = 0$, $z = 12.032$) and lattice null networks ($p = 0.049$, $z = 1.612$).

		Area																														
		10	9	32	14	25	8B	8Ad	9/46d	46d	46v	9/46v	8Av	45	47/12	13	11	6DR	PE	PEci	PEc	PEa	PF	PFop	PFG	IPd	POa	PG	PGm	PGop	Opt	
Motif Class ID	1	0.997	1.000	1.000	1.000	1.000	0.999	0.999	0.840	0.994	0.374	0.987	0.991	0.965	1.000	1.000	1.000	0.851	1.000	0.977	1.000	0.996	1.000	0.490	1.000	0.901	0.995	0.978	1.000	0.859	1.000	
		0.307	0.860	0.862	0.623	0.624	0.745	0.861	0.235	0.397	0.139	0.304	0.232	0.623	0.863	0.861	0.625	0.023	0.142	0.232	0.139	0.045	0.622	0.062	0.862	0.139	0.626	0.398	0.863	0.062	0.860	
	2	1.000	1.000	1.000	1.000	1.000	1.000	0.997	0.659	1.000	1.000	1.000	1.000	0.998	1.000	1.000	1.000	1.000	1.000	1.000	1.000	1.000	1.000	1.000	1.000	1.000	1.000	1.000	1.000	1.000	1.000	
		0.409	0.905	0.122	0.172	0.409	0.783	0.312	0.001	0.409	0.907	0.787	0.170	0.526	0.907	0.905	0.086	0.524	0.236	0.124	0.523	0.526	0.906	0.522	0.786	0.171	0.787	0.906	0.788	0.232	0.905	
	3	1.000	1.000	1.000	0.996	1.000	1.000	0.966	0.930	0.997	0.608	1.000	0.998	0.997	1.000	0.997	1.000	0.485	0.797	0.974	0.916	0.924	0.999	0.995	1.000	0.973	1.000	0.945	1.000	1.000	1.000	
		0.845	0.844	0.844	0.227	0.845	0.844	0.550	0.310	0.308	0.001	0.845	0.161	0.844	0.846	0.163	0.420	0.007	0.227	0.046	0.165	0.086	0.312	0.007	0.845	0.004	0.846	0.165	0.845	0.119	0.846	
	4	0.988	0.999	0.855	0.602	1.000	1.000	0.068	0.784	0.994	0.908	0.875	0.994	0.999	1.000	1.000	0.936	0.171	0.889	0.161	0.994	0.974	0.998	0.989	0.543	0.938	0.566	0.973	0.886	0.845	0.984	
		0.823	0.847	0.546	0.329	0.953	0.825	0.005	0.298	0.848	0.848	0.551	0.870	0.734	0.963	0.977	0.702	0.080	0.216	0.330	0.394	0.547	0.887	0.978	0.268	0.866	0.328	0.770	0.472	0.733	0.798	
	5	1.000	1.000	1.000	0.999	0.999	0.999	0.981	0.992	0.994	1.000	1.000	0.972	0.998	0.999	1.000	1.000	1.000	0.354	0.547	0.975	0.959	0.998	0.956	0.996	0.986	1.000	1.000	1.000	0.996	1.000	
		0.626	0.624	0.627	0.626	0.628	0.626	0.131	0.232	0.132	0.038	0.624	0.038	0.629	0.627	0.626	0.629	0.038	0.001	0.004	0.019	0.004	0.388	0.070	0.134	0.038	0.629	0.630	0.627	0.009	0.625	
	6	0.999	0.986	0.908	1.000	1.000	0.972	0.993	0.329	0.851	0.136	0.815	0.573	0.990	1.000	0.998	0.874	0.941	0.966	0.998	0.978	0.996	0.974	0.395	0.997	0.849	0.942	0.803	0.867	0.931	0.990	
		0.918	0.798	0.666	0.939	0.992	0.724	0.821	0.218	0.601	0.038	0.510	0.384	0.722	0.891	0.875	0.606	0.800	0.979	0.841	0.941	0.918	0.753	0.106	0.892	0.354	0.511	0.355	0.573	0.603	0.840	
	7	0.994	0.994	0.995	0.991	0.974	0.990	0.981	0.988	0.995	0.936	0.993	0.993	0.975	0.991	0.993	0.994	0.973	0.776	0.951	0.929	0.981	0.992	0.889	0.994	0.975	0.986	0.985	0.993	0.978	0.995	
		0.007	0.007	0.008	0.008	0.008	0.008	0.008	0.007	0.008	0.007	0.008	0.008	0.007	0.008	0.008	0.008	0.008	0.008	0.008	0.008	0.008	0.008	0.007	0.008	0.008	0.008	0.007	0.008	0.008	0.008	
	8	0.999	1.000	1.000	0.771	0.981	1.000	0.999	0.999	0.998	0.980	1.000	0.999	1.000	1.000	0.999	0.998	1.000	0.690	0.378	0.987	0.975	0.990	0.535	0.938	0.841	0.997	1.000	1.000	0.969	1.000	
		0.791	0.705	0.890	0.327	0.790	0.504	0.253	0.505	0.506	0.506	0.792	0.791	0.702	0.891	0.790	0.707	0.408	0.411	0.611	0.611	0.502	0.702	0.790	0.137	0.607	0.608	0.891	0.793	0.409	0.889	
9	0.000	0.000	0.009	0.279	0.001	0.001	0.000	0.021	0.001	0.004	0.000	0.000	0.000	0.000	0.000	0.021	0.000	0.132	0.130	0.003	0.007	0.000	0.141	0.000	0.005	0.000	0.000	0.000	0.000	0.000		
	0.379	0.198	0.596	0.936	0.594	0.241	0.125	0.465	0.396	0.464	0.092	0.382	0.046	0.014	0.318	0.681	0.431	0.995	0.968	0.783	0.700	0.232	0.987	0.062	0.716	0.188	0.078	0.029	0.448	0.097		
10	1.000	1.000	1.000	0.998	1.000	1.000	1.000	1.000	1.000	1.000	1.000	1.000	1.000	1.000	1.000	1.000	1.000	0.917	0.966	0.998	1.000	1.000	0.902	1.000	1.000	1.000	1.000	1.000	1.000	1.000		
	0.770	0.769	0.450	0.160	0.607	0.162	0.449	0.048	0.233	0.160	0.769	0.452	0.608	0.770	0.769	0.162	0.328	0.607	0.327	0.607	0.452	0.608	0.326	0.606	0.446	0.447	0.232	0.605	0.159	0.767		
11	0.996	1.000	0.994	0.973	0.964	1.000	1.000	0.814	0.990	1.000	1.000	0.969	0.999	1.000	1.000	0.932	0.937	0.620	0.668	0.002	0.408	0.995	0.748	1.000	0.818	1.000	0.929	1.000	0.998	1.000		
	0.340	0.852	0.433	0.539	0.746	0.647	0.745	0.015	0.339	0.103	0.743	0.432	0.540	0.853	0.852	0.267	0.105	0.854	0.540	0.104	0.147	0.649	0.261	0.854	0.147	0.749	0.010	0.744	0.539	0.853		
12	0.998	1.000	0.912	0.034	0.379	1.000	1.000	0.997	0.742	0.949	1.000	0.247	1.000	1.000	0.973	0.422	0.418	0.059	0.010	0.277	0.256	0.939	0.002	1.000	0.020	0.999	1.000	1.000	0.471	1.000		
	0.583	0.557	0.386	0.507	0.928	0.234	0.315	0.036	0.178	0.007	0.559	0.507	0.405	0.702	0.775	0.434	0.075	0.986	0.914	0.928	0.670	0.879	0.891	0.730	0.639	0.076	0.317	0.252	0.478	0.892		
13	0.000	0.000	0.000	0.000	0.000	0.000	0.000	0.000	0.000	0.000	0.000	0.000	0.000	0.000	0.000	0.000	0.000	0.047	0.055	0.001	0.010	0.000	0.018	0.000	0.007	0.000	0.000	0.000	0.000	0.000		
	0.334	0.082	0.449	0.765	0.787	0.027	0.009	0.140	0.422	0.160	0.189	0.720	0.000	0.035	0.526	0.643	0.527	0.996	0.962	0.923	0.869	0.752	0.961	0.514	0.873	0.127	0.226	0.371	0.748	0.188		

Table 5.3. Permutation test results by area

Results from a permutation test comparing the frequency of participation of areas in motif classes in the empirical FPN with their frequency in 100,000 random and lattice networks. Random network p-values are represented in plain font and lattice network p-values are represented in italics. Bolded text highlights areas 45, 47/12 and PGm which were found to participate in motif class 9 with a significantly greater frequency in the FPN than in random ($p = 0.0$, $z = 5.189$, 8.358 and 8.060) and lattice networks ($p = 0.046$, 0.014 and 0.029 , $z = 1.878$, 2.440 and 2.109).

6 APPENDIX B

Permission to reprint from F. A. W. Wilson et al. (1993)

THE AMERICAN ASSOCIATION FOR THE ADVANCEMENT OF SCIENCE LICENSE TERMS AND CONDITIONS

Oct 21, 2020

This Agreement between Bryan Conklin ("You") and The American Association for the Advancement of Science ("The American Association for the Advancement of Science") consists of your license details and the terms and conditions provided by The American Association for the Advancement of Science and Copyright Clearance Center.

License Number	4904281302667
License date	Sep 08, 2020
Licensed Content Publisher	The American Association for the Advancement of Science
Licensed Content Publication	Science
Licensed Content Title	Dissociation of object and spatial processing domains in primate prefrontal cortex
Licensed Content Author	FA Wilson, SP Scalaide, PS Goldman-Rakic
Licensed Content Date	Jun 25, 1993
Licensed Content Volume	260
Licensed Content Issue	5116
Volume number	260
Issue number	5116
Type of Use	Thesis / Dissertation
Requestor type	Scientist/individual at a research institution
Format	Electronic
Portion	Text Excerpt
Number of pages requested	1
Title	Spectral Characteristics of Visuospatial Working Memory in the Monkey
Institution name	Florida Atlantic University
Expected presentation date	Nov 2020
Portions	Figure 3. If I was provided a better quality version (vector) that would be ideal. Otherwise I can reproduce.
Requestor Location	Bryan Conklin 610 Clematis St Apt 218 WEST PALM BEACH, FL 33401 United States Attn: Bryan Conklin
Total	0.00 USD

Terms and Conditions

American Association for the Advancement of Science TERMS AND CONDITIONS

Regarding your request, we are pleased to grant you non-exclusive, non-transferable permission, to republish the AAAS material identified above in your work identified above, subject to the terms and conditions herein. We must be contacted for permission for any uses other than those specifically identified in your request above.

The following credit line must be printed along with the AAAS material: "From [Full Reference Citation]. Reprinted with permission from AAAS."

All required credit lines and notices must be visible any time a user accesses any part of the AAAS material and must appear on any printed copies and authorized user might make.

This permission does not apply to figures / photos / artwork or any other content or materials included in your work that are credited to non-AAAS sources. If the requested material is sourced to or references non-AAAS sources, you must obtain authorization from that source as well before using that material. You agree to hold harmless and indemnify AAAS against any claims arising from your use of any content in your work that is credited to non-AAAS sources.

If the AAAS material covered by this permission was published in Science during the years 1974 - 1994, you must also obtain permission from the author, who may grant or withhold permission, and who may or may not charge a fee if permission is granted. See original article for author's address. This condition does not apply to news articles.

The AAAS material may not be modified or altered except that figures and tables may be modified with permission from the author. Author permission for any such changes must be secured prior to your use.

Whenever possible, we ask that electronic uses of the AAAS material permitted herein include a hyperlink to the original work on AAAS's website (hyperlink may be embedded in the reference citation).

AAAS material reproduced in your work identified herein must not account for more than 30% of the total contents of that work.

AAAS must publish the full paper prior to use of any text.

AAAS material must not imply any endorsement by the American Association for the Advancement of Science.

This permission is not valid for the use of the AAAS and/or Science logos.

AAAS makes no representations or warranties as to the accuracy of any information contained in the AAAS material covered by this permission, including any warranties of merchantability or fitness for a particular purpose.

If permission fees for this use are waived, please note that AAAS reserves the right to charge for reproduction of this material in the future.

Permission is not valid unless payment is received within sixty (60) days of the issuance of this permission. If payment is not received within this time period then all rights granted herein shall be revoked and this permission will be considered null and void.

In the event of breach of any of the terms and conditions herein or any of CCC's Billing and Payment terms and conditions, all rights granted herein shall be revoked and this permission will be considered null and void.

AAAS reserves the right to terminate this permission and all rights granted herein at its discretion, for any purpose, at any time. In the event that AAAS elects to terminate this permission, you will have no further right to publish, publicly perform, publicly display, distribute or otherwise use any matter in which the AAAS content had been included, and all fees paid hereunder shall be fully refunded to you. Notification of termination will be sent to the contact information as supplied by you during the request process and termination shall be immediate upon sending the notice. Neither AAAS nor CCC shall be liable for any costs, expenses, or damages you may incur as a result of the termination of this permission, beyond the refund noted above.

This Permission may not be amended except by written document signed by both parties.

The terms above are applicable to all permissions granted for the use of AAAS material. Below you will find additional conditions that apply to your particular type of use.

FOR A THESIS OR DISSERTATION

If you are using figure(s)/table(s), permission is granted for use in print and electronic versions of your dissertation or thesis. A full text article may be used in print versions only of a dissertation or thesis.

Permission covers the distribution of your dissertation or thesis on demand by ProQuest / UMI, provided the AAAS material covered by this permission remains in situ.

If you are an Original Author on the AAAS article being reproduced, please refer to your License to Publish for rules on reproducing your paper in a dissertation or thesis.

FOR JOURNALS:

Permission covers both print and electronic versions of your journal article, however the AAAS material may not be used in any manner other than within the context of your article.

FOR BOOKS/TEXTBOOKS:

If this license is to reuse figures/tables, then permission is granted for non-exclusive world rights in all languages in both print and electronic formats (electronic formats are defined below).

If this license is to reuse a text excerpt or a full text article, then permission is granted for non-exclusive world rights in English only. You have the option of securing either print or electronic rights or both, but electronic rights are not automatically granted and do garner additional fees. Permission for translations of text excerpts or full text articles into other languages must be obtained separately.

Licenses granted for use of AAAS material in electronic format books/textbooks are valid only in cases where the electronic version is equivalent to or substitutes for the print version of the book/textbook. The AAAS material reproduced as permitted herein must remain in situ and must not be exploited separately (for example, if permission covers the use of a full text article, the article may not be offered for access or for purchase as a stand-alone unit), except in the case of permitted textbook companions as noted below.

You must include the following notice in any electronic versions, either adjacent to the reprinted AAAS material or in the terms and conditions for use of your electronic products:

"Readers may view, browse, and/or download material for temporary copying purposes only, provided these uses are for noncommercial personal purposes. Except as provided by law, this material may not be further reproduced, distributed, transmitted, modified, adapted, performed, displayed, published, or sold in whole or in part, without prior written permission from the publisher."

If your book is an academic textbook, permission covers the following companions to your textbook, provided such companions are distributed only in conjunction with your textbook at no additional cost to the user:

- Password-protected website
- Instructor's image CD/DVD and/or PowerPoint resource
- Student CD/DVD

All companions must contain instructions to users that the AAAS material may be used for non-commercial, classroom purposes only. Any other uses require the prior written permission from AAAS.

If your license is for the use of AAAS Figures/Tables, then the electronic rights granted herein permit use of the Licensed Material in any Custom Databases that you distribute the electronic versions of your textbook through, so long as the Licensed Material remains within the context of a chapter of the title identified in your request and cannot be downloaded by a user as an independent image file.

Rights also extend to copies/files of your Work (as described above) that you are required to provide for use by the visually and/or print disabled in compliance with state and federal laws.

This permission only covers a single edition of your work as identified in your request.

FOR NEWSLETTERS:

Permission covers print and/or electronic versions, provided the AAAS material reproduced as permitted herein remains in situ and is not exploited separately (for example, if permission covers the use of a full text article, the article may not be offered for access or for purchase as a stand-alone unit)

FOR ANNUAL REPORTS:

Permission covers print and electronic versions provided the AAAS material reproduced as permitted herein remains in situ and is not exploited separately (for example, if permission covers the use of a full text article, the article may not be offered for access or for purchase as a stand-alone unit)

FOR PROMOTIONAL/MARKETING USES:

Permission covers the use of AAAS material in promotional or marketing pieces such as information packets, media kits, product slide kits, brochures, or flyers limited to a single print run. The AAAS Material may not be used in any manner which implies endorsement or promotion by the American Association for the Advancement of Science (AAAS) or Science of any product or service. AAAS does not permit the reproduction of its name, logo or text on promotional literature.

If permission to use a full text article is permitted, The Science article covered by this permission must not be altered in any way. No additional printing may be set onto an article copy other than the copyright credit line required above. Any alterations must be approved in advance and in writing by AAAS. This includes, but is not limited to, the placement of sponsorship identifiers, trademarks, logos, rubber stamping or self-adhesive stickers onto the article copies.

Additionally, article copies must be a freestanding part of any information package (i.e. media kit) into which they are inserted. They may not be physically attached to anything, such as an advertising insert, or have anything attached to them, such as a sample product. Article copies must be easily removable from any kits or informational packages in which they are used. The only exception is that article copies may be inserted into three-ring binders.

FOR CORPORATE INTERNAL USE:

The AAAS material covered by this permission may not be altered in any way. No additional printing may be set onto an article copy other than the required credit line. Any alterations must be approved in advance and in writing by AAAS. This includes, but is not limited to the placement of sponsorship identifiers, trademarks, logos, rubber stamping or self-adhesive stickers onto article copies.

If you are making article copies, copies are restricted to the number indicated in your request and must be distributed only to internal employees for internal use.

If you are using AAAS Material in Presentation Slides, the required credit line must be visible on the slide where the AAAS material will be reprinted

If you are using AAAS Material on a CD, DVD, Flash Drive, or the World Wide Web, you must include the following notice in any electronic versions, either adjacent to the reprinted AAAS material or in the terms and conditions for use of your electronic products: "Readers may view, browse, and/or download material for temporary copying purposes only, provided these uses are for noncommercial personal purposes. Except as provided by law, this material may not be further reproduced, distributed, transmitted, modified, adapted, performed, displayed, published, or sold in whole or in part, without prior written permission from the publisher." Access to any such CD, DVD, Flash Drive or Web page must be restricted to your organization's employees only.

FOR CME COURSE and SCIENTIFIC SOCIETY MEETINGS:

Permission is restricted to the particular Course, Seminar, Conference, or Meeting indicated in your request. If this license covers a text excerpt or a Full Text Article, access to the reprinted AAAS material must be restricted to attendees of your event only (if you have been granted electronic rights for use of a full text article on your website, your website must be password protected, or access restricted so that only attendees can access the content on your site).

If you are using AAAS Material on a CD, DVD, Flash Drive, or the World Wide Web, you must include the following notice in any electronic versions, either adjacent to the reprinted AAAS material or in the terms and conditions for use of your electronic products: "Readers may view, browse, and/or download material for temporary copying purposes only, provided these uses are for noncommercial personal purposes. Except as provided by law, this material may not be further reproduced, distributed, transmitted, modified, adapted, performed, displayed, published, or sold in whole or in part, without prior written permission from the publisher."

FOR POLICY REPORTS:

These rights are granted only to non-profit organizations and/or government agencies. Permission covers print and electronic versions of a report, provided the required credit line appears in both versions and provided the AAAS material reproduced as permitted herein remains in situ and is not exploited separately.

FOR CLASSROOM PHOTOCOPIES:

Permission covers distribution in print copy format only. Article copies must be freestanding and not part of a course pack. They may not be physically attached to anything or have anything attached to them.

FOR COURSEPACKS OR COURSE WEBSITES:

These rights cover use of the AAAS material in one class at one institution. Permission is valid only for a single semester after which the AAAS material must be removed from the Electronic Course website, unless new permission is obtained for an additional semester. If the material is to be distributed online, access must be restricted to students and instructors enrolled in that particular course by some means of password or access control.

FOR WEBSITES:

You must include the following notice in any electronic versions, either adjacent to the reprinted AAAS material or in the terms and conditions for use of your electronic products:

"Readers may view, browse, and/or download material for temporary copying purposes only, provided these uses are for noncommercial personal purposes. Except as provided by law, this material may not be further reproduced, distributed, transmitted, modified, adapted, performed, displayed, published, or sold in whole or in part, without prior written permission from the publisher."

Permissions for the use of Full Text articles on third party websites are granted on a case by case basis and only in cases where access to the AAAS Material is restricted by some means of password or access control. Alternately, an E-Print may be purchased through our reprints department (brocheleau@rockwaterinc.com).

REGARDING FULL TEXT ARTICLE USE ON THE WORLD WIDE WEB IF YOU ARE AN 'ORIGINAL AUTHOR' OF A SCIENCE PAPER

If you chose "Original Author" as the Requestor Type, you are warranting that you are one of authors listed on the License Agreement as a "Licensed content author" or that you are acting on that author's behalf to use the Licensed content in a new work that one of the authors listed on the License Agreement as a "Licensed content author" has written. Original Authors may post the 'Accepted Version' of their full text article on their personal or on their University website and not on any other website. The 'Accepted Version' is the version of the paper accepted for publication by AAAS including changes resulting from peer review but prior to AAAS's copy editing and production (in other words not the AAAS published version).

FOR MOVIES / FILM / TELEVISION:

Permission is granted to use, record, film, photograph, and/or tape the AAAS material in connection with your program/film and in any medium your program/film may be shown or heard, including but not limited to broadcast and cable television, radio, print, world wide web, and videocassette.

The required credit line should run in the program/film's end credits.

FOR MUSEUM EXHIBITIONS:

Permission is granted to use the AAAS material as part of a single exhibition for the duration of that exhibit. Permission for use of the material in promotional materials for the exhibit must be cleared separately with AAAS (please contact us at permissions@aaas.org).

FOR TRANSLATIONS:

Translation rights apply only to the language identified in your request summary above.

The following disclaimer must appear with your translation, on the first page of the article, after the credit line: "This translation is not an official translation by AAAS staff, nor is it endorsed by AAAS as accurate. In crucial matters, please refer to the official English-language version originally published by AAAS."

FOR USE ON A COVER:

Permission is granted to use the AAAS material on the cover of a journal issue, newsletter issue, book, textbook, or annual report in print and electronic formats provided the AAAS material reproduced as permitted herein remains in situ and is not exploited separately.

By using the AAAS Material identified in your request, you agree to abide by all the terms and conditions herein.

Questions about these terms can be directed to the AAAS Permissions department permissions@aaas.org.

Other Terms and Conditions:

v 2

Questions? customercare@copyright.com or +1-855-239-3415 (toll free in the US) or +1-978-646-2777.

Permission to reprint from Petrides & Pandya (2007)



Bryan Conklin <bconkli4@fau.edu>

Vector file request

The Journal of Neuroscience <jn@sfn.org>
To: Bryan Conklin <bconkli4@my.fau.edu>

Wed, Sep 11, 2019 at 9:26 AM

Hello Bryan,

Permission to use figure 2 in the article listed below in print and online is granted at no cost.

Efferent Association Pathways from the Rostral Prefrontal Cortex in the Macaque Monkey

Michael Petrides and Deepak N. Pandya

Journal of Neuroscience 24 October 2007, 27 (43) 11573-11586; DOI: <https://doi.org/10.1523/JNEUROSCI.2419-07.2007>

A full journal reference and link to the version of record, where appropriate, must be included.

For content published before 2010, a copyright statement ("Copyright [year] Society for Neuroscience") should be included.

Also, we are unable to provide a vector file.

Best,

Vince Carmona

Central Office

Journal of Neuroscience

[Quoted text hidden]

7 REFERENCES

- Albert, R., & Barabási, A. L. (2002). Statistical mechanics of complex networks. *Reviews of Modern Physics*, 74(1), 47–97. <https://doi.org/10.1103/RevModPhys.74.47>
- Albert, R., Jeong, H., & Barabási, A. L. (2000). Error and attack tolerance of complex networks. *Nature*, 406(6794), 378–382. <https://doi.org/10.1038/35019019>
- Alstott, J., Bullmore, E., & Plenz, D. (2014). Powerlaw: A python package for analysis of heavy-tailed distributions. *PLoS ONE*, 9(1). <https://doi.org/10.1371/journal.pone.0085777>
- Amaral, L. A. N., Scala, A., Barthélémy, M., Stanley, H. E., Barthelemy, M., & Stanley, H. E. (2000). Classes of small-world networks. *Proceedings of the National Academy of Sciences of the United States of America*, 97(21), 11149–11152. <https://doi.org/10.1073/pnas.200327197>
- Anderson, J. S., Druzgal, T. J., Froehlich, A., Dubray, M. B., Lange, N., Alexander, A. L., Abildskov, T., Nielsen, J. A., Cariello, A. N., Cooperrider, J. R., Bigler, E. D., & Lainhart, J. E. (2011). Decreased interhemispheric functional connectivity in autism. *Cerebral Cortex*, 21(5), 1134–1146. <https://doi.org/10.1093/cercor/bhq190>
- Antzoulatos, E. G., & Miller, E. K. (2016). Synchronous beta rhythms of frontoparietal networks support only behaviorally relevant representations. *ELife*, 5(NOVEMBER2016), 1–22. <https://doi.org/10.7554/eLife.17822>
- Ardestani, A., Shen, W., Darvas, F., Toga, A. W., & Fuster, J. M. (2016). Modulation of Frontoparietal Neurovascular Dynamics in Working Memory. *Journal of Cognitive Neuroscience*, 28(3), 379–401. https://doi.org/10.1162/jocn_a_00903
- Asaad, W. F., & Eskandar, E. N. (2008). A flexible software tool for temporally-precise behavioral control in Matlab. *Journal of Neuroscience Methods*, 174(2), 245–258. <https://doi.org/10.1016/j.jneumeth.2008.07.014>
- Asmussen, S. (2003). *Applied probability and queues. Second*. Springer-Verlag.
- Atkinson, R. C., & Shiffrin, R. M. (1968). Human Memory: A Proposed System and its Control Processes. *Psychology of Learning and Motivation - Advances in Research and Theory*, 2(C), 89–195. [https://doi.org/10.1016/S0079-7421\(08\)60422-3](https://doi.org/10.1016/S0079-7421(08)60422-3)

- Baddeley, A. D. (2012). Working Memory: Theories, models, and controversies. ,. *Annual Review of Psychology*, 63(1), 1–29. <https://doi.org/10.1146/annurev-psych-120710-100422>
- Baddeley, A. D., Eysenck, M. W., & Anderson, M. C. (2015). *Memory* (2nd ed.). Psychology Press.
- Baddeley, A. D., & Hitch, G. (1974). Working Memory. In *Psychology of learning and motivation* (Vol. 8, pp. 47–89). Academic Press. [https://doi.org/10.1016/S0079-7421\(08\)60452-1](https://doi.org/10.1016/S0079-7421(08)60452-1)
- Baddeley, A. D., Papagno, C., & Vallar, G. (1988). When long-term learning depends on short-term storage. *Journal of Memory and Language*, 27(5), 586–595. [https://doi.org/10.1016/0749-596X\(88\)90028-9](https://doi.org/10.1016/0749-596X(88)90028-9)
- Bakker, R., Wachtler, T., & Diesmann, M. (2012). CoCoMac 2.0 and the future of tract-tracing databases. *Frontiers in Neuroinformatics*, 6(DEC). <https://doi.org/10.3389/fninf.2012.00030>
- Barabási, A., & Albert, R. (1999). Emergence of Scaling in Random Networks. *Science*, 286(5439), 509–512. <https://doi.org/10.1126/science.286.5439.509>
- Barbosa, J., Stein, H., Martinez, R. L., Galan-Gadea, A., Li, S., Dalmau, J., Adam, K. C. S., Valls-Solé, J., Constantinidis, C., & Compte, A. (2020). Interplay between persistent activity and activity-silent dynamics in the prefrontal cortex underlies serial biases in working memory. *Nature Neuroscience*, 16–18. <https://doi.org/10.1038/s41593-020-0644-4>
- Bassett, D. S., & Bullmore, E. T. (2017). Small-World Brain Networks Revisited. In *Neuroscientist* (Vol. 23, Issue 5, pp. 499–516). SAGE Publications Inc. <https://doi.org/10.1177/1073858416667720>
- Bassett, D. S., & Sporns, O. (2017). Network neuroscience. *Nature Neuroscience*, 20(3), 353–364. <https://doi.org/10.1038/nn.4502>
- Bastian, M., Heymann, S., & Jacomy, M. (2009). Gephi: An Open Source Software for Exploring and Manipulating Networks. *Third International AAAI Conference on Weblogs and Social Media*, 361–362. <https://doi.org/10.1136/qshc.2004.010033>
- Bastos, André M., Loonis, R., Kornblith, S., Lundqvist, M., & Miller, E. K. (2018). Laminar recordings in frontal cortex suggest distinct layers for maintenance and control of working memory. *Proceedings of the National Academy of Sciences of the United States of America*, 115(5), 1117–1122. <https://doi.org/10.1073/pnas.1710323115>

- Bastos, André M., Vezoli, J., Bosman, C. A., Schoffelen, J.-M., Oostenveld, R., Dowdall, J. R., De Weerd, P., Kennedy, H., & Fries, P. (2015). Visual Areas Exert Feedforward and Feedback Influences through Distinct Frequency Channels. *Neuron*, 85(2), 390–401. <https://doi.org/10.1016/j.neuron.2014.12.018>
- Bastos, Andre M., Vezoli, J., & Fries, P. (2015). Communication through coherence with inter-areal delays. In *Current Opinion in Neurobiology* (Vol. 31). <https://doi.org/10.1016/j.conb.2014.11.001>
- Ben Bashat, D., Kronfeld-Duenias, V., Zachor, D. A., Ekstein, P. M., Hendler, T., Tarrasch, R., Even, A., Levy, Y., & Ben Sira, L. (2007). Accelerated maturation of white matter in young children with autism: A high b value DWI study. *NeuroImage*, 37(1), 40–47. <https://doi.org/10.1016/j.neuroimage.2007.04.060>
- Bonin, G. Von, & Bailey, P. (1947). The neocortex of Macaca Mulatta. In *University of Illinois Press*.
- Braver, T. S. (2012). The variable nature of cognitive control: A dual mechanisms framework. *Trends in Cognitive Sciences*, 16(2), 106–113. <https://doi.org/10.1016/j.tics.2011.12.010>
- Bressler, S. L., & Menon, V. (2010). Large-scale brain networks in cognition: emerging methods and principles. *Trends in Cognitive Sciences*, 14(6), 277–290. <https://doi.org/10.1016/j.tics.2010.04.004>
- Brodmann, K. (1909). *Vergleichende Lokalisationslehre der Grosshirnrinde in ihren Prinzipien dargestellt auf Grund des Zellenbaues*.
- Bruyer, R., & Scailquin, J. C. (1998). The visuospatial sketchpad for mental images: Testing the multicomponent model of working memory. *Acta Psychologica*, 98(1), 17–36. [https://doi.org/10.1016/S0001-6918\(97\)00053-X](https://doi.org/10.1016/S0001-6918(97)00053-X)
- Bullmore, E., & Sporns, O. (2009). Complex brain networks: Graph theoretical analysis of structural and functional systems. In *Nature Reviews Neuroscience*. <https://doi.org/10.1038/nrn2575>
- Buschman, T. J., & Miller, E. K. (2007a). Top-down versus bottom-up control of attention in the prefrontal and posterior parietal cortices. *Science*, 315(5820), 1860–1864. <https://doi.org/10.1126/science.1138071>
- Buschman, T. J., & Miller, E. K. (2007b). Top-Down Versus Bottom-Up Control of Attention in the Prefrontal and Posterior Parietal Cortices. *Science*, 315(5820), 1860–1862. <https://doi.org/10.1126/science.1138071>
- Buzsáki, G. (2010). Neural Syntax: Cell Assemblies, Synapsembles, and Readers. *Neuron*, 68(3), 362–385. <https://doi.org/10.1016/j.neuron.2010.09.023>

- Buzsáki, G., & Draguhn, A. (2004). Neuronal oscillations in cortical networks. *Science (New York, N.Y.)*, 304(5679), 1926–1929. <https://doi.org/10.1126/science.1099745>
- Campo, A. T., Martinez-Garcia, M., Nácher, V., Luna, R., Romo, R., & Deco, G. (2015). Task-driven intra- and interarea communications in primate cerebral cortex. *Proceedings of the National Academy of Sciences of the United States of America*, 112(15), 4761–4766. <https://doi.org/10.1073/pnas.1503937112>
- Cavada, C., & Goldman-Rakic, P. S. (1989). Posterior parietal cortex in rhesus monkey: II. Evidence for segregated corticocortical networks linking sensory and limbic areas with the frontal lobe. *Journal of Comparative Neurology*, 287(4), 422–445. <https://access.uke.de/+CSCO+0075676763663A2F2F62617976617279766F656E656C2E6A7679726C2E70627A++/doi/pdf/10.1002/cne.902870403>
- Cavada, C., & Goldman-Rakic, P. S. (1989). Posterior parietal cortex in rhesus monkey: I. Parcellation of areas based on distinctive limbic and sensory corticocortical connections. *Journal of Comparative Neurology*, 287(4), 393–421. <https://doi.org/10.1002/cne.902870402>
- Cawthon, L. K. (2005a). *Primate Factsheets: Owl monkey (Aotus) Taxonomy, Morphology, & Ecology*. Primate Info Net. http://pin.primate.wisc.edu/factsheets/entry/owl_monkey
- Cawthon, L. K. (2005b). *Primate Factsheets: Pigtail macaque (Macaca nemestrina) Taxonomy, Morphology, & Ecology*. Primate Info Net. http://pin.primate.wisc.edu/factsheets/entry/pigtail_macaque/taxon
- Cawthon, L. K. (2005c). *Primate Factsheets: Rhesus macaque (Macaca mulatta) Taxonomy, Morphology, & Ecology*. Primate Info Net. http://pin.primate.wisc.edu/factsheets/entry/rhesus_macaque
- Cawthon, L. K. (2006a). *Primate Factsheets: Long-tailed macaque (Macaca fascicularis) Taxonomy, Morphology, & Ecology*. Primate Info Net. http://pin.primate.wisc.edu/factsheets/entry/long-tailed_macaque
- Cawthon, L. K. (2006b). *Primate Factsheets: Squirrel monkey (Saimiri) Taxonomy, Morphology, & Ecology*. Primate Info Net. http://pin.primate.wisc.edu/factsheets/entry/squirrel_monkey
- Cherven, K. (2015). *Mastering Gephi Network Visualization*. Pakt Publishing. https://books.google.com/books?hl=en&lr=&id=RnJuBgAAQBAJ&oi=fnd&pg=PP1&dq=gephi&ots=fM89DC_viv&sig=SfIX8G5KSN9CQcyK80hCTiGAO9c
- Clauset, A., Shalizi, C. R., & Newman, M. E. J. (2009). Power-Law Distributions in Empirical Data. *SIAM Review*, 51(4), 661–703. <https://doi.org/10.1137/070710111>

- Cohen, Michael X. (2018). *A better way to define and describe Morlet wavelets for time-frequency analysis*.
- Cohen, Mike X. (2014). *Analyzing Neural Time Series Data*. The MIT Press.
<https://doi.org/10.7551/mitpress/9609.001.0001>
- Compte, A., Constantinidis, C., Tegnér, J., Raghavachari, S., Chafee, M. V., Goldman-Rakic, P. S., & Wang, X. J. (2003). Temporally Irregular Mnemonic Persistent Activity in Prefrontal Neurons of Monkeys during a Delayed Response Task. *Journal of Neurophysiology*, 90(5), 3441–3454.
<https://doi.org/10.1152/jn.00949.2002>
- Constantinidis, C., & Steinmetz, M. A. (2001). Neuronal responses in area 7a to multiple stimulus displays: II. Responses are suppressed at the cued location. *Cerebral Cortex*, 11(7), 592–597. <https://doi.org/10.1093/cercor/11.7.592>
- Contreras, D., Destexhe, A., Sejnowski, T. J., & Steriade, M. (1996). Control of spatiotemporal coherence of a thalamic oscillation by corticothalamic feedback. *Science*, 274(5288), 771–774. <https://doi.org/10.1126/science.274.5288.771>
- Conway, A. R. A., Kane, M. J., Bunting, M. F., Hambrick, D. Z., Wilhelm, O., & Engle, R. W. (2005). Working memory span tasks: A methodological review and user's guide. *Psychonomic Bulletin & Review*, 12(5), 769–786.
<https://doi.org/10.3758/BF03196772>
- Corbetta, M. (1998). Frontoparietal cortical networks for directing attention and the eye to visual locations: Identical, independent, or overlapping neural systems? *Proceedings of the National Academy of Sciences of the United States of America*, 95(3), 831–838. <https://doi.org/10.1073/pnas.95.3.831>
- Cowan, W. M., Gottlieb, D. I., Hendrickson, A. E., Price, J. L., & Woolsey, T. A. (1972). The autoradiographic demonstration of axonal connections in the central nervous system. *Brain Research*, 37(1), 21–51. [https://doi.org/10.1016/0006-8993\(72\)90344-7](https://doi.org/10.1016/0006-8993(72)90344-7)
- D'Esposito, M. (2007). From cognitive to neural models of working memory. *Philosophical Transactions of the Royal Society B: Biological Sciences*, 362(1481), 761–772. <https://doi.org/10.1098/rstb.2007.2086>
- Dijkstra, E. W. (1959). A note on two problems in connexion with graphs. *Numerische Mathematik*, 1(1), 269–271. <https://doi.org/10.1007/BF01386390>
- Dotson, N. M., Goodell, B., Salazar, R. F., Hoffman, S. J., & Gray, C. M. (2015). Methods, caveats and the future of large-scale microelectrode recordings in the non-human primate. *Frontiers in Systems Neuroscience*, 9(November), 1–8.
<https://doi.org/10.3389/fnsys.2015.00149>

- Dotson, N. M., Hoffman, S. J., Goodell, B., & Gray, C. M. (2017). A Large-Scale Semi-Chronic Microdrive Recording System for Non-Human Primates. *Neuron*, 96(4), 769-782.e2. <https://doi.org/10.1016/j.neuron.2017.09.050>
- Dotson, N. M., Salazar, R. F., & Gray, C. M. (2014). Frontoparietal Correlation Dynamics Reveal Interplay between Integration and Segregation during Visual Working Memory. *Journal of Neuroscience*. <https://doi.org/10.1523/JNEUROSCI.1961-14.2014>
- Downing, P., & Kanwisher, N. (2001). A cortical area specialized for visual processing of the human body. *Journal of Vision*, 1(3), 2470–2474. <https://doi.org/10.1167/1.3.341>
- Economo, C. von, & Koskinas, G. (1925). *Die cytoarchitektonik der hirnrinde des erwachsenen menschen*.
- Eguíluz, V. M., Chialvo, D. R., Cecchi, G. A., Baliki, M., & Apkarian, A. V. (2005). Scale-free brain functional networks. *Physical Review Letters*, 94(1). <https://doi.org/10.1103/PhysRevLett.94.018102>
- Engel, A. K., & Fries, P. (2010). Beta-band oscillations-signalling the status quo? *Current Opinion in Neurobiology*, 20(2), 156–165. <https://doi.org/10.1016/j.conb.2010.02.015>
- Engle, R. W., & Kane, M. J. (2003). Executive Attention, Working Memory Capacity, and a Two-Factor Theory of Cognitive Control. In *Psychology of Learning and Motivation - Advances in Research and Theory* (Vol. 44, pp. 145–199). [https://doi.org/10.1016/S0079-7421\(03\)44005-X](https://doi.org/10.1016/S0079-7421(03)44005-X)
- Felleman, D. J., & Van Essen, D. C. (1991). Distributed hierarchical processing in the primate cerebral cortex. *Cerebral Cortex*, 1(1), 1–47. <https://academic.oup.com/cercor/article-lookup/doi/10.1093/cercor/1.1.1-a>
- Fiebelkorn, I. C., & Kastner, S. (2019). A rhythmic theory of attention. *Trends in Cognitive Sciences*, 23(2), 1–36. <https://doi.org/10.1016/j.tics.2018.11.009>
- Fiebelkorn, I. C., Pinsk, M. A., & Kastner, S. (2018). A Dynamic Interplay within the Frontoparietal Network Underlies Rhythmic Spatial Attention. *Neuron*, 99(4), 842-853.e8. <https://doi.org/10.1016/j.neuron.2018.07.038>
- Fiebelkorn, I. C., Pinsk, M. A., & Kastner, S. (2019). The mediodorsal pulvinar coordinates the macaque fronto-parietal network during rhythmic spatial attention. *Nature Communications*, 10(1). <https://doi.org/10.1038/s41467-018-08151-4>

- Fornito, A., Zalesky, A., Pantelis, C., & Bullmore, E. T. (2012). Schizophrenia, neuroimaging and connectomics. In *NeuroImage* (Vol. 62, Issue 4, pp. 2296–2314). <https://doi.org/10.1016/j.neuroimage.2011.12.090>
- Foster, J. J., & Awh, E. (2019). The role of alpha oscillations in spatial attention: limited evidence for a suppression account. *Current Opinion in Psychology*, 29, 34–40. <https://doi.org/10.1016/j.copsyc.2018.11.001>
- Fries, P., Roelfsema, P. R., Engel, A. K., König, P., & Singer, W. (1997). Synchronization of oscillatory responses in visual cortex correlates with perception in interocular rivalry. *Proceedings of the National Academy of Sciences of the United States of America*, 94(23), 12699–12704. <https://doi.org/10.1073/pnas.94.23.12699>
- Fries, P., Womelsdorf, T., Oostenveld, R., & Desimone, R. (2008). The effects of visual stimulation and selective visual attention on rhythmic neuronal synchronization in macaque area V4. *Journal of Neuroscience*, 28(18), 4823–4835. <https://doi.org/10.1523/JNEUROSCI.4499-07.2008>
- Funahashi, S. (2006). Prefrontal cortex and working memory processes. *Neuroscience*, 139(1), 251–261. <https://doi.org/10.1016/j.neuroscience.2005.07.003>
- Funahashi, S., Bruce, C. J., & Goldman-Rakic, P. S. (1989). Mnemonic coding of visual space in the monkey's dorsolateral prefrontal cortex. *Journal of Neurophysiology*, 61(2), 331–349. <https://doi.org/10.1152/jn.1989.61.2.331>
- Funahashi, S., Bruce, C. J., & Goldman-Rakic, P. S. (1990). Visuospatial coding in primate prefrontal neurons revealed by oculomotor paradigms. *Journal of Neurophysiology*, 63(4), 814–831. <https://doi.org/10.1152/jn.1990.63.4.814>
- Funahashi, S., Bruce, C. J., & Goldman-Rakic, P. S. (1991). Neuronal activity related to saccadic eye movements in the monkey's dorsolateral prefrontal cortex. *Journal of Neurophysiology*, 65(6), 1464–1483. <https://doi.org/10.1152/jn.1991.65.6.1464>
- Fuster, J. M. (1973). Unit activity in prefrontal cortex during delayed-response performance: neuronal correlates of transient memory. *Journal of Neurophysiology*, 36(1), 61–78. <https://doi.org/10.1152/jn.1973.36.1.61>
- Fuster, J. M. (1995). Memory in the cortex of the primate. *Biological Research*.
- Fuster, J. M. (2000). The prefrontal cortex of the primate: A synopsis. *Psychobiology*, 28(2), 125–131. <https://doi.org/10.3758/BF03331972>
- Fuster, J. M. (2015). *The Prefrontal Cortex* (5th ed.). Academic Press.

- Fuster, J. M., & Alexander, G. E. (1971). Neuron Activity Related to Short-Term Memory. *Science*, 173(3997), 652–654. <https://doi.org/10.1126/science.173.3997.652>
- Fuster, J. M., Bauer, R. H., & Jervey, J. P. (1982). Cellular discharge in the dorsolateral prefrontal cortex of the monkey in cognitive tasks. *Experimental Neurology*, 77(3), 679–694. [https://doi.org/10.1016/0014-4886\(82\)90238-2](https://doi.org/10.1016/0014-4886(82)90238-2)
- Galvan, A., Stauffer, W. R., Acker, L., El-Shamayleh, Y., Inoue, K. I., Ohayon, S., & Schmid, M. C. (2017). Nonhuman primate optogenetics: Recent advances and future directions. *Journal of Neuroscience*, 37(45), 10894–10903. <https://doi.org/10.1523/JNEUROSCI.1839-17.2017>
- Goldman-Rakic, P. S. (1995). Cellular basis of working memory. *Neuron*, 14(3), 477–485. [https://doi.org/10.1016/0896-6273\(95\)90304-6](https://doi.org/10.1016/0896-6273(95)90304-6)
- Goldman-Rakic, P. S. (1996a). The prefrontal landscape: implications of functional architecture for understanding human mentation and the central executive. *Philosophical Transactions of the Royal Society of London. Series B: Biological Sciences*, 351(1346), 1445–1453. <https://doi.org/10.1098/rstb.1996.0129>
- Goldman-Rakic, P. S. (1996b). Regional and cellular fractionation of working memory. *Proceedings of the National Academy of Sciences*, 93(24), 13473–13480. <https://doi.org/10.1073/pnas.93.24.13473>
- Goldman-Rakic, P. S. (2011). Circuitry of Primate Prefrontal Cortex and Regulation of Behavior by Representational Memory. In *Comprehensive Physiology*. John Wiley & Sons, Inc. <https://doi.org/10.1002/cphy.cp010509>
- Goldman, P. S., & Rosvold, H. E. (1970). Localization of function within the dorsolateral prefrontal cortex of the rhesus monkey. *Experimental Neurology*, 27(2), 291–304. [https://doi.org/10.1016/0014-4886\(70\)90222-0](https://doi.org/10.1016/0014-4886(70)90222-0)
- Gollo, L. L., Mirasso, C. R., Atienza, M., Crespo-Garcia, M., & Cantero, J. L. (2011). Theta band zero-lag long-range cortical synchronization via hippocampal dynamical relaying. *PLoS ONE*, 6(3). <https://doi.org/10.1371/journal.pone.0017756>
- Gollo, L. L., Mirasso, C., Sporns, O., & Breakspear, M. (2014). Mechanisms of Zero-Lag Synchronization in Cortical Motifs. *PLoS Computational Biology*, 10(4). <https://doi.org/10.1371/journal.pcbi.1003548>
- Gollo, L. L., Zalesky, A., Matthew Hutchison, R., Van Den Heuvel, M., & Breakspear, M. (2015). Dwelling quietly in the rich club: Brain network determinants of slow cortical fluctuations. *Philosophical Transactions of the Royal Society B: Biological Sciences*, 370(1668). <https://doi.org/10.1098/rstb.2014.0165>

- Gray, C. M., Goodell, B., & Lear, A. (2007). Multichannel micromanipulator and chamber system for recording multineuronal activity in alert, non-human primates. *Journal of Neurophysiology*, 98(1), 527–536. <https://doi.org/10.1152/jn.00259.2007>
- Harriger, L., van den Heuvel, M. P., & Sporns, O. (2012). Rich Club Organization of Macaque Cerebral Cortex and Its Role in Network Communication. *PLoS ONE*, 7(9). <https://doi.org/10.1371/journal.pone.0046497>
- Helfrich, R. F., Fiebelkorn, I. C., Szczepanski, S. M., Lin, J. J., Parvizi, J., Knight, R. T., & Kastner, S. (2018). Neural Mechanisms of Sustained Attention Are Rhythmic. *Neuron*, 99(4), 854-865.e5. <https://doi.org/10.1016/j.neuron.2018.07.032>
- Helfrich, R. F., & Knight, R. T. (2016). Oscillatory Dynamics of Prefrontal Cognitive Control. *Trends in Cognitive Sciences*, xx(12), 1–15. <https://doi.org/10.1016/j.tics.2016.09.007>
- Honey, C. J., Kötter, R., Breakspear, M., & Sporns, O. (2007). Network structure of cerebral cortex shapes functional connectivity on multiple time scales. *Proceedings of the National Academy of Sciences*, 104(24), 10240–10245. <https://doi.org/10.1073/PNAS.0701519104>
- Hong, G., & Lieber, C. M. (2019). Novel electrode technologies for neural recordings. *Nature Reviews Neuroscience*, 20(6), 330–345. <https://doi.org/10.1038/s41583-019-0140-6>
- Hsueh, J. J., Chen, T. S., Chen, J. J., & Shaw, F. Z. (2016). Neurofeedback training of EEG alpha rhythm enhances episodic and working memory. *Human Brain Mapping*, 37(7), 2662–2675. <https://doi.org/10.1002/hbm.23201>
- Humphries, M. ., Gurney, K., & Prescott, T. . (2006). The brainstem reticular formation is a small-world, not scale-free, network. *Proceedings of the Royal Society B: Biological Sciences*, 273(1585), 503–511. <https://doi.org/10.1098/rspb.2005.3354>
- Hunter, W. S. (1913). The delayed reaction in animals and children. *Behavior Monographs*, 2, 1–85.
- Jacob, S. N., & Daniel, H. (2018). *Structuring of Abstract Working Memory Content by Fronto-parietal Synchrony in Primate Cortex* Article Structuring of Abstract Working Memory Content by Fronto-parietal Synchrony in Primate Cortex. 588–597. <https://doi.org/10.1016/j.neuron.2018.07.025>
- Jacob, S. N., Hähnke, D., & Nieder, A. (2018). Structuring of Abstract Working Memory Content by Fronto-parietal Synchrony in Primate Cortex. *Neuron*, 99(3), 588-597.e5. <https://doi.org/10.1016/j.neuron.2018.07.025>

- Jacobs, J. (1887). Experiments on “prehension.” *Mind*, *os-12*(45), 75–79.
<https://doi.org/10.1093/mind/os-12.45.75>
- Jacobsen, C. F., & Nissen, H. W. (1936). Studies of cerebral function in primates. *Johns Hopkins Press*, *13*(1), 101–112. <https://doi.org/10.1037/h0056632>
- Jaeggi, S. M., Buschkuhl, M., Perrig, W. J., & Meier, B. (2010). The concurrent validity of the N-back task as a working memory measure. *Memory*, *18*(4), 394–412.
<https://doi.org/10.1080/09658211003702171>
- Joelving, F. C., Compte, A., & Constantinidis, C. (2007). Temporal properties of posterior parietal neuron discharges during working memory and passive viewing. *Journal of Neurophysiology*, *97*(3), 2254–2266.
<https://doi.org/10.1152/jn.00977.2006>
- Johnson, E. L., Dewar, C. D., Solbakk, A.-K. K., Endestad, T., Meling, T. R., Knight, R. T., Johnson, E. L., Dewar, C. D., Solbakk, A.-K. K., Endestad, T., & Meling, T. R. (2017). Bidirectional Frontoparietal Oscillatory Systems Support Working Memory. *Current Biology*, *27*(12), 1829–1835.e4. <https://doi.org/10.1016/j.cub.2017.05.046>
- Judge, S. J., Richmond, B. J., & Chu, F. C. (1980). Implantation of magnetic search coils for measurement of eye position: An improved method. *Vision Research*, *20*(6), 535–538. [https://doi.org/10.1016/0042-6989\(80\)90128-5](https://doi.org/10.1016/0042-6989(80)90128-5)
- Kanwisher, N., McDermott, J., & Chun, M. M. (1997). The Fusiform Face Area: A Module in Human Extrastriate Cortex Specialized for Face Perception. *The Journal of Neuroscience*, *17*(11), 4302–4311. <https://doi.org/10.1523/JNEUROSCI.17-11-04302.1997>
- Katsuki, F., & Constantinidis, C. (2013). Time course of functional connectivity in primate dorsolateral prefrontal and posterior parietal cortex during working memory. *PLoS ONE*, *8*(11). <https://doi.org/10.1371/journal.pone.0081601>
- Kleinbart, J. E., Orsborn, A. L., Choi, J. S., Wang, C., Qiao, S., Viventi, J., & Pesaran, B. (2018). A Modular Implant System for Multimodal Recording and Manipulation of the Primate Brain. *2018 40th Annual International Conference of the IEEE Engineering in Medicine and Biology Society (EMBC), 2018-July*, 3362–3365.
<https://doi.org/10.1109/EMBC.2018.8512993>
- König, P., Engel, A. K., & Singer, W. (1995). Relation between oscillatory activity and long-range synchronization in cat visual cortex. *Proceedings of the National Academy of Sciences of the United States of America*, *92*(1), 290–294.
<https://doi.org/10.1073/pnas.92.1.290>

- Kornblith, S., Buschman, T. J., & Miller, E. K. (2016). Stimulus load and oscillatory activity in higher cortex. *Cerebral Cortex*, 26(9), 3772–3784. <https://doi.org/10.1093/cercor/bhv182>
- Kubota, K., Iwamoto, T., & Suzuki, H. (1974). Visuokinetic activities of primate prefrontal neurons during delayed response performance. *Journal of Neurophysiology*, 37(6), 1197–1212. <https://doi.org/10.1152/jn.1974.37.6.1197>
- Lago-Fernández, L. F., Huerta, R., Corbacho, F., & Sigüenza, J. A. (2000). Fast response and temporal coherent oscillations in small-world networks. *Physical Review Letters*, 84(12), 2758–2761. <https://doi.org/10.1103/PhysRevLett.84.2758>
- Lara, A. H., & Wallis, J. D. (2014). Executive control processes underlying multi-item working memory. *Nature Neuroscience*, 17(6), 876–883. <https://doi.org/10.1038/nn.3702>
- Lavail, J. H., & Lavail, M. M. (1972). Retrograde Axonal Transport in the Central Nervous System. *Science*, 176(4042), 1416–1417. <https://doi.org/10.1126/science.176.4042.1416>
- Logie, R. H., Cocchini, G., Della Sala, S., & Baddeley, A. D. (2004). Is there a specific executive capacity for dual task coordination? Evidence from Alzheimer’s disease. *Neuropsychology*, 18(3), 504–513. <https://doi.org/10.1037/0894-4105.18.3.504>
- Luck, S. J. (2014). *An Introduction to the Second Edition Event-Related Potential Technique* (2nd ed.). The MIT Press. <https://doi.org/10.1073/pnas.0703993104>
- Lundqvist, M., Herman, P., Warden, M. R., Brincat, S. L., & Miller, E. K. (2018). Gamma and beta bursts during working memory readout suggest roles in its volitional control. *Nature Communications*, 9(1), 1–12. <https://doi.org/10.1038/s41467-017-02791-8>
- Lundqvist, M., Rose, J., Herman, P., Brincat, S. L. L., Buschman, T. J., & Miller, E. K. (2016). Gamma and Beta Bursts Underlie Working Memory. *Neuron*, 90(1), 152–164. <https://doi.org/10.1016/j.neuron.2016.02.028>
- Luppino, G., & Rizzolatti, G. (2000). The Organization of the Frontal Motor Cortex. *News in Physiological Sciences : An International Journal of Physiology Produced Jointly by the International Union of Physiological Sciences and the American Physiological Society*, 15(August 2015), 219–224. <https://doi.org/10.1152/physiologyonline.2000.15.5.219>
- Luria, A. R. (1962). The Role of Speech in the Regulation of Normal and Abnormal Behaviour. *Proceedings of the Royal Society of Medicine*, 55(3), 243. <https://doi.org/10.1097/00005053-196207000-00014>

- Marek, S., & Dosenbach, N. U. F. (2018). The frontoparietal network: function, electrophysiology, and importance of individual precision mapping. *Dialogues in Clinical Neuroscience*, 20(2), 133–140. <http://www.ncbi.nlm.nih.gov/pubmed/30250390>
- Markov, N. T., Ercsey-Ravasz, M. M., Ribeiro Gomes, A. R., Lamy, C., Magrou, L., Vezoli, J., Misery, P., Falchier, A., Quilodran, R., Gariel, M. A., Sallet, J., Gamanut, R., Huissoud, C., Clavagnier, S., Giroud, P., Sappey-Marinier, D., Barone, P., Dehay, C., Toroczkai, Z., ... Kennedy, H. (2014). A weighted and directed interareal connectivity matrix for macaque cerebral cortex. *Cerebral Cortex*, 24(1), 17–36. <https://doi.org/10.1093/cercor/bhs270>
- Markowitz, D. A., Curtis, C. E., & Pesaran, B. (2015). Multiple component networks support working memory in prefrontal cortex. *Proceedings of the National Academy of Sciences of the United States of America*, 112(35), 11084–11089. <https://doi.org/10.1073/pnas.1504172112>
- Martínez-Vázquez, P., & Gail, A. (2018). Directed interaction between monkey premotor and posterior parietal cortex during motor-goal retrieval from working memory. *Cerebral Cortex*, 28(5), 1866–1881. <https://doi.org/10.1093/cercor/bhy035>
- Maslov, S., & Sneppen, K. (2002). Specificity and stability in topology of protein networks. *Science*, 296(5569), 910–913. <https://doi.org/10.1126/science.1065103>
- Masuda, N., & Aihara, K. (2004). Global and local synchrony of coupled neurons in small-world networks. *Biological Cybernetics*, 90(4), 302–309. <https://doi.org/10.1007/s00422-004-0471-9>
- Mathworks®. (2019). Curve Fitting Toolbox™: User's Guide (R2019b). In *MATLAB Manual*. https://www.mathworks.com/help/pdf_doc/curvefit/curvefit.pdf
- Medalla, M., & Barbas, H. (2006). Diversity of laminar connections linking periarculate and lateral intraparietal areas depends on cortical structure. *European Journal of Neuroscience*, 23(1), 161–179. <https://doi.org/10.1111/j.1460-9568.2005.04522.x>
- Mesulam, M. (1990). Large-scale neurocognitive networks and distributed processing for attention, language, and memory. *Annals of Neurology*, 28(5), 597–613. <https://doi.org/10.1002/ana.410280502>
- Miller, E. K. (2000). The prefrontal cortex and cognitive control. *Nature Reviews Neuroscience*, 1(1), 59–65. <https://doi.org/10.1038/35036228>
- Miller, E. K., & Cohen, J. (2001). An integrative theory of prefrontal cortex function. *Neuroscience*, 24(1), 167–202. <https://doi.org/10.1146/annurev.neuro.24.1.167>

- Miller, G. (1956). The magical number seven, plus or minus two: some limits on our capacity for processing information. *Psychological Review*, 101(2), 343–352. <https://doi.org/10.1037/h0043158>
- Milo, R. (2002). Network Motifs: Simple Building Blocks of Complex Networks. *Science*, 298(5594), 824–827. <https://doi.org/10.1126/science.298.5594.824>
- Milo, R., Kashtan, N., Itzkovitz, S., Newman, M. E. J., & Alon, U. (2003). *On the uniform generation of random graphs with prescribed degree sequences*. <http://arxiv.org/abs/cond-mat/0312028>
- Mishkin, M., & Manning, F. J. (1978). Non-spatial memory after selective prefrontal lesions in monkeys. *Brain Research*, 143(2), 313–323. [https://doi.org/10.1016/0006-8993\(78\)90571-1](https://doi.org/10.1016/0006-8993(78)90571-1)
- Mishkin, M., & Ungerleider, L. G. (1982). Contribution of striate inputs to the visuospatial functions of parieto-preoccipital cortex in monkeys. *Behavioural Brain Research*, 6(1), 57–77. [https://doi.org/10.1016/0166-4328\(82\)90081-X](https://doi.org/10.1016/0166-4328(82)90081-X)
- Mitra, P., & Bokil, H. (2009). Observed Brain Dynamics. In *Observed Brain Dynamics*. <https://doi.org/10.1093/acprof:oso/9780195178081.001.0001>
- Modha, D. S., & Singh, R. (2010). Network architecture of the long-distance pathways in the macaque brain. *Proceedings of the National Academy of Sciences*, 107(30), 13485–13490. <https://doi.org/10.1073/pnas.1008054107>
- Moreno, Y., Nekovee, M., & Vespignani, A. (2004). Efficiency and reliability of epidemic data dissemination in complex networks. *Physical Review E - Statistical Physics, Plasmas, Fluids, and Related Interdisciplinary Topics*, 69(5), 4. <https://doi.org/10.1103/PhysRevE.69.055101>
- Mottaghy, F. M. (2002). Segregation of Areas Related to Visual Working Memory in the Prefrontal Cortex Revealed by rTMS. *Cerebral Cortex*, 12(4), 369–375. <https://doi.org/10.1093/cercor/12.4.369>
- Müller, N. G., & Knight, R. T. (2006). The functional neuroanatomy of working memory: Contributions of human brain lesion studies. *Neuroscience*, 139(1), 51–58. <https://doi.org/10.1016/j.neuroscience.2005.09.018>
- Müller, Notger G., Machado, L., & Knight, R. T. (2002). Contributions of subregions of the prefrontal cortex to working memory: Evidence from brain lesions in humans. *Journal of Cognitive Neuroscience*, 14(5), 673–686. <https://doi.org/10.1162/08989290260138582>
- Nakagawa, T. T., Jirsa, V. K., Spiegler, A., McIntosh, A. R., & Deco, G. (2013). Bottom up modeling of the connectome: Linking structure and function in the resting brain

- and their changes in aging. *NeuroImage*, 80, 318–329.
<https://doi.org/10.1016/j.neuroimage.2013.04.055>
- Newman, M. (2018). *Networks*.
https://books.google.com/books?hl=en&lr=&id=YdZjDwAAQBAJ&oi=fnd&pg=PP1&dq=newman+networks&ots=V_MZ4Ml7sw&sig=RK73hoSKUgNzkCOVezTjEs2h0hM
- Nolte, G., Ziehe, A., Nikulin, V. V., Schlögl, A., Krämer, N., Brismar, T., & Müller, K. R. (2008). Robustly estimating the flow direction of information in complex physical systems. *Physical Review Letters*, 100(23), 1–4.
<https://doi.org/10.1103/PhysRevLett.100.234101>
- Norman, D. A., & Shallice, T. (1986). Attention to action: willed and automatic control of behavior. In *Consciousness and self-regulation: Advances in research and theory* (Vol. 4, pp. 1–18).
- Oh, S. W., Harris, J. A., Ng, L., Winslow, B., Cain, N., Mihalas, S., Wang, Q., Lau, C., Kuan, L., Henry, A. M., Mortrud, M. T., Ouellette, B., Nguyen, T. N., Sorensen, S. A., Slaughterbeck, C. R., Wakeman, W., Li, Y., Feng, D., Ho, A., ... Zeng, H. (2014). A mesoscale connectome of the mouse brain. *Nature*, 508(7495), 207–214.
<https://doi.org/10.1038/nature13186>
- Pandya, D. N., & Sanides, F. (1973). Architectonic parcellation of the temporal operculum in rhesus monkey and its projection pattern. *Zeitschrift Für Anatomie Und Entwicklungsgeschichte*, 139(2), 127–161. <https://doi.org/10.1007/BF00523634>
- Pandya, D. N., & Seltzer, B. (1982). Intrinsic connections and architectonics of posterior parietal cortex in the rhesus monkey. *Journal of Comparative Neurology*, 204(2), 196–210. <https://doi.org/10.1002/cne.902040208>
- Pandya, D. N., & Yeterian, E. H. (1985). *Architecture and Connections of Cortical Association Areas* (pp. 3–61). https://doi.org/10.1007/978-1-4757-9619-3_1
- Pandya, D., Seltzer, B., Petrides, M., & Cipolloni, P. B. (2015). *Cerebral Cortex: Architecture, Connections and the Dual Origin Concept*. Oxford University Press.
- Parker Jones, O., Alfaro-Almagro, F., & Jbabdi, S. (2018). An empirical, 21st century evaluation of phrenology. *Cortex*, 106, 26–35.
<https://doi.org/10.1016/j.cortex.2018.04.011>
- Passingham, R. (1975). Delayed matching after selective prefrontal lesions in monkeys (Macaca mulatta). *Brain Research*, 92(1), 89–102. [https://doi.org/10.1016/0006-8993\(75\)90529-6](https://doi.org/10.1016/0006-8993(75)90529-6)

- Passingham, R. E. (1985). Memory of monkeys (*Macaca mulatta*) with lesions in prefrontal cortex. *Behavioral Neuroscience*, 99(1), 3–21. <https://doi.org/10.1037/0735-7044.99.1.3>
- Paule, M., & Rodriguez, J. (2009). Working Memory Delayed Response Tasks in Monkeys. In J. Buccafusco (Ed.), *Methods of Behavior Analysis in Neuroscience* (2nd ed., pp. 247–265). CRC Press/Taylor & Francis. <https://doi.org/10.1201/NOE1420052343.ch12>
- Paxinos, G., Huang, X., & Toga, A. W. (1999). The Rhesus Monkey Brain in Stereotaxic Coordinates. In *Academic Press*.
- Pearson, D. G., Logie, R. H., & Gilhooly, K. J. (1999). Verbal Representations and Spatial Manipulation During Mental Synthesis. *European Journal of Cognitive Psychology*, 11(3), 295–314. <https://doi.org/10.1080/713752317>
- Persson, J., Nyberg, L., Lind, J., Larsson, A., Nilsson, L. G., Ingvar, M., & Buckner, R. L. (2006). Structure-function correlates of cognitive decline in aging. *Cerebral Cortex*, 16(7), 907–915. <https://doi.org/10.1093/cercor/bhj036>
- Pesaran, B., Pezaris, J. S., Sahani, M., Mitra, P. P., & Andersen, R. A. (2002). Temporal structure in neuronal activity during working memory in macaque parietal cortex. *Nature Neuroscience*, 5(8), 805–811. <https://doi.org/10.1038/nn890>
- Pesaran, B., Vinck, M., Einevoll, G. T., Sirota, A., Fries, P., Siegel, M., Truccolo, W., Schroeder, C. E., & Srinivasan, R. (2018). Investigating large-scale brain dynamics using field potential recordings: analysis and interpretation. *Nature Neuroscience*, 21(7), 903–919. <https://doi.org/10.1038/s41593-018-0171-8>
- Petrides, M. (2005). Lateral prefrontal cortex: architectonic and functional organization. *Philosophical Transactions of the Royal Society B: Biological Sciences*, 360(1456), 781–795. <https://doi.org/10.1098/rstb.2005.1631>
- Petrides, M., & Pandya, D. N. (1994). Comparative architectonic analysis of the human and the macaque frontal cortex. In *Handbook of neuropsychology*.
- Petrides, Michael, & Pandya, D. N. (2007). Efferent Association Pathways from the Rostral Prefrontal Cortex in the Macaque Monkey. *Journal of Neuroscience*, 27(43), 11573–11586. <https://doi.org/10.1523/jneurosci.2419-07.2007>
- Polanía, R., Nitsche, M. A., Korman, C., Batsikadze, G., & Paulus, W. (2012). The importance of timing in segregated theta phase-coupling for cognitive performance. *Current Biology*, 22(14), 1314–1318. <https://doi.org/10.1016/j.cub.2012.05.021>

- Qi, X.-L. (2010). Comparison of neural activity related to working memory in primate dorsolateral prefrontal and posterior parietal cortex. *Frontiers in Systems Neuroscience*, 4(May), 1–11. <https://doi.org/10.3389/fnsys.2010.00012>
- Qi, X. L., & Constantinidis, C. (2012). Correlated discharges in the primate prefrontal cortex before and after working memory training. *European Journal of Neuroscience*, 36(11), 3538–3548. <https://doi.org/10.1111/j.1460-9568.2012.08267.x>
- Quintana, J., & Fuster, J. M. (1992). Mnemonic and predictive functions of cortical neurons in a memory task. *NeuroReport*, 3(8), 721–724. <https://doi.org/10.1097/00001756-199208000-00018>
- Quintana, J., & Fuster, J. M. (1999). From perception to action: Temporal integrative functions of prefrontal and parietal neurons. *Cerebral Cortex*, 9(3), 213–221. <https://doi.org/10.1093/cercor/9.3.213>
- Rao, S. C., Rainer, G., & Miller, E. K. (1997). Integration of what and where in the primate prefrontal cortex. *Science*, 276(5313), 821–824. <https://doi.org/10.1126/science.276.5313.821>
- Reinhart, R. M. G., & Nguyen, J. A. (2019). Working memory revived in older adults by synchronizing rhythmic brain circuits. *Nature Neuroscience*, 22(5). <https://doi.org/10.1038/s41593-019-0371-x>
- Reis, J., Portugal, A. M., Fernandes, L., Afonso, N., Pereira, M., Sousa, N., & Dias, N. S. (2016). An alpha and theta intensive and short neurofeedback protocol for healthy aging working-memory training. *Frontiers in Aging Neuroscience*, 8(JUN), 1–11. <https://doi.org/10.3389/fnagi.2016.00157>
- Robbins, T. W., Anderson, E. J., Barker, D. R., Bradley, A. C., Fearnlyhough, C., Henson, R., Hudson, S. R., & Baddeley, A. D. (1996). Working memory in chess. *Memory and Cognition*, 24(1), 83–93. <https://doi.org/10.3758/BF03197274>
- Rosene, D. L., & Pandya, D. N. (1983). Architectonics and connections of the posterior parahippocampal gyrus in the rhesus monkey. *Soc Neurosci Abstr*, 9:222.
- Rozzi, S., Calzavara, R., Belmalih, A., Borra, E., Gregoriou, G. G., Matelli, M., Luppino, G., Neuroscienze, D., & Fisiologia, S. (2006). Cortical connections of the inferior parietal cortical convexity of the macaque monkey. *Cerebral Cortex*, 16(10), 1389–1417. <https://doi.org/10.1093/cercor/bhj076>
- Rubinov, M., & Sporns, O. (2010). Complex network measures of brain connectivity: Uses and interpretations. *NeuroImage*, 52(3), 1059–1069. <https://doi.org/10.1016/j.neuroimage.2009.10.003>

- Rubinov, M., Ypma, R. J. F., Watson, C., Bullmore, E. T., & Raichle, M. E. (2015). Wiring cost and topological participation of the mouse brain connectome. *Proceedings of the National Academy of Sciences of the United States of America*, 112(32), 10032–10037. <https://doi.org/10.1073/pnas.1420315112>
- Saalmann, Y. B., Pigarev, I. N., & Vidyasagar, T. R. (2007). Neural Mechanisms of Visual Attention: How Top-Down Feedback Highlights Relevant Locations. *Science*, 316(5831), 1612–1615. <https://doi.org/10.1126/science.1139140>
- Salazar, R. F., Dotson, N. M., Bressler, S. L., & Gray, C. M. (2012). Content-Specific Fronto-Parietal Synchronization During Visual Working Memory. *Science*, 338(6110), 1097–1100. <https://doi.org/10.1126/science.1224000>
- Sanzleon, P., Knock, S. A., Woodman, M. M., Domide, L., Mersmann, J., McIntosh, A. R., & Jirsa, V. (2013). The virtual brain: A simulator of primate brain network dynamics. *Frontiers in Neuroinformatics*, 7(MAY). <https://doi.org/10.3389/fninf.2013.00010>
- Sasaki, R., Anzai, A., Angelaki, D. E., & DeAngelis, G. C. (2020). Flexible coding of object motion in multiple reference frames by parietal cortex neurons. *Nature Neuroscience*, 23(August). <https://doi.org/10.1038/s41593-020-0656-0>
- Schuman, C. D., Potok, T. E., Patton, R. M., Birdwell, J. D., Dean, M. E., Rose, G. S., & Plank, J. S. (2017). *A Survey of Neuromorphic Computing and Neural Networks in Hardware*. 1–88. <http://arxiv.org/abs/1705.06963>
- Seltzer, B., & Pandya, D. N. (1978). Afferent cortical connections and architectonics of the superior temporal sulcus and surrounding cortex in the rhesus monkey. *Brain Research*, 149(1), 1–24. [https://doi.org/10.1016/0006-8993\(78\)90584-X](https://doi.org/10.1016/0006-8993(78)90584-X)
- Shafi, M., Zhou, Y., Quintana, J., Chow, C., Fuster, J., & Bodner, M. (2007). Variability in neuronal activity in primate cortex during working memory tasks. *Neuroscience*, 146(3), 1082–1108. <https://doi.org/10.1016/j.neuroscience.2006.12.072>
- Shallice, T., & Warrington, E. K. (1970). Independent functioning of verbal memory stores: a neuropsychological study. *The Quarterly Journal of Experimental Psychology*, 22(2), 261–273. <https://doi.org/10.1080/00335557043000203>
- Siegel, M., Buschman, T. J., & Miller, E. K. (2015). Cortical information flow during flexible sensorimotor decisions. *Science*, 348(6241), 1352–1355. <https://doi.org/10.1126/science.aab0551>
- Siegel, M., Donner, T. H., & Engel, A. K. (2012). Spectral fingerprints of large-scale neuronal interactions. *Nature Reviews Neuroscience*, 13(2), 121–134. <https://doi.org/10.1038/nrn3137>

- Siegel, M., Warden, M. R., & Miller, E. K. (2009). Phase-dependent neuronal coding of objects in short-term memory. *Proceedings of the National Academy of Sciences of the United States of America*, 106(50), 21341–21346. <https://doi.org/10.1073/pnas.0908193106>
- Singer, W. (1999). Neuronal Synchrony: A Versatile Code for the Definition of Relations? *Neuron*, 24(1), 49–65. [https://doi.org/10.1016/S0896-6273\(00\)80821-1](https://doi.org/10.1016/S0896-6273(00)80821-1)
- Singer, W., & Gray, C. M. (1995). Visual feature integration and the temporal correlation hypothesis. *Annual Review of Neuroscience*, 18, 555–586. <https://doi.org/10.1146/annurev.ne.18.030195.003011>
- Sporns, O., Chialvo, D. R., Kaiser, M., & Hilgetag, C. C. (2004). Organization, development and function of complex brain networks. *Trends in Cognitive Sciences*, 8(9), 418–425. <https://doi.org/10.1016/j.tics.2004.07.008>
- Sporns, O., Honey, C. J., & Kötter, R. (2007). Identification and Classification of Hubs in Brain Networks. *PLoS ONE*, 2(10). <https://doi.org/10.1371/journal.pone.0001049>
- Sporns, O., & Kötter, R. (2004). Motifs in Brain Networks. *PLoS Biology*, 2(11). <https://doi.org/10.1371/journal.pbio.0020369>
- Sporns, O., & Zwi, J. D. (2004). The small world of the cerebral cortex. In *Neuroinformatics* (Vol. 2, Issue 2, pp. 145–162). <https://doi.org/10.1385/NI:2:2:145>
- Squire, L. R. (1992). Declarative and nondeclarative memory: Multiple brain systems supporting learning and memory. *Journal of Cognitive Neuroscience*, 4, 232–243. <https://doi.org/10.1162/jocn.1992.4.3.232>
- Squire, L. R. (2009). The Legacy of Patient H.M. for Neuroscience. *Neuron*, 61(1), 6–9. <https://doi.org/10.1016/j.neuron.2008.12.023>
- Steinmetz, N. A., Koch, C., Harris, K. D., & Carandini, M. (2018). Challenges and opportunities for large-scale electrophysiology with Neuropixels probes. *Current Opinion in Neurobiology*, 50, 92–100. <https://doi.org/10.1016/j.conb.2018.01.009>
- Stephan, K. E., Kamper, L., Bozkurt, A., Burns, G. A. P. C., Young, M. P., & Kötter, R. (2001). Advanced database methodology for the Collation of Connectivity data on the Macaque brain (CoCoMac). *Philosophical Transactions of the Royal Society of London. Series B: Biological Sciences*, 356(1412), 1159–1186. <https://doi.org/10.1098/rstb.2001.0908>
- Stokes, M. G., Buschman, T. J., & Miller, E. K. (2017). *Dynamic Coding for Flexible Cognitive Control*. 221–241.

- Telesford, Q. K., Joyce, K. E., Hayasaka, S., Burdette, J. H., & Laurienti, P. J. (2011). The Ubiquity of Small-World Networks. *Brain Connectivity*, 1(5), 367–375. <https://doi.org/10.1089/brain.2011.0038>
- Tognoli, E., & Kelso, J. A. S. (2014). The Metastable Brain. *Neuron*, 81(1), 35–48. <https://doi.org/10.1016/j.neuron.2013.12.022>
- Tonegawa, S., Liu, X., Ramirez, S., & Redondo, R. (2015). Memory Engram Cells Have Come of Age. *Neuron*, 87(5), 918–931. <https://doi.org/10.1016/j.neuron.2015.08.002>
- Traub, R. D., Whittington, M. A., Stanford, I. M., & Jefferys, J. G. R. (1996). A mechanism for generation of long-range synchronous fast oscillations in the cortex. *Nature*, 383(6601), 621–224. <https://doi.org/10.1038/383621a0>
- van den Heuvel, M. P., Stam, C. J., Boersma, M., & Hulshoff Pol, H. E. (2008). Small-world and scale-free organization of voxel-based resting-state functional connectivity in the human brain. *NeuroImage*, 43(3), 528–539. <https://doi.org/10.1016/j.neuroimage.2008.08.010>
- Varela, F., Lachaux, J. P., Rodriguez, E., & Martinerie, J. (2001). The brainweb: Phase synchronization and large-scale integration. *Nature Reviews Neuroscience*, 2(4), 229–239. <https://doi.org/10.1038/35067550>
- Varshney, L. R., Chen, B. L., Paniagua, E., Hall, D. H., & Chklovskii, D. B. (2011). Structural properties of the *Caenorhabditis elegans* neuronal network. *PLoS Computational Biology*, 7(2). <https://doi.org/10.1371/journal.pcbi.1001066>
- Vicente, R., Gollo, L. L., Mirasso, C. R., Fischer, I., & Pipa, G. (2008). Dynamical relaying can yield zero time lag neuronal synchrony despite long conduction delays. *Proceedings of the National Academy of Sciences of the United States of America*, 105(44), 17157–17162. <https://doi.org/10.1073/pnas.0809353105>
- Vogt, C., & Vogt, O. (1919). Allgemeine Ergebnisse unserer Hirnforschung. *Journal of Psychology and Neurology*.
- Walker, A. E. (1940). A cytoarchitectural study of the prefrontal area of the macaque monkey. *Journal of Comparative Neurology*, 73(1), 59–86. <https://doi.org/10.1002/cne.900730106>
- Wang, X.-J. (2010). Neurophysiological and Computational Principles of Cortical Rhythms in Cognition. *Physiological Reviews*, 90(3), 1195–1268. <https://doi.org/10.1152/physrev.00035.2008>

- Wang, Z., Dai, Z., Gong, G., Zhou, C., & He, Y. (2015). Understanding structural-functional relationships in the human brain: A large-scale network perspective. *Neuroscientist*, 21(3), 290–305. <https://doi.org/10.1177/1073858414537560>
- Watson, C. E., & Chatterjee, A. (2012). A bilateral frontoparietal network underlies visuospatial analogical reasoning. *NeuroImage*, 59(3), 2831–2838. <https://doi.org/10.1016/j.neuroimage.2011.09.030>
- Watts, D. J., & Strogatz, S. H. (1998). Collective dynamics of ‘small-world’ networks. *Nature*, 393(6684), 440–442. <https://doi.org/10.1038/30918>
- Wilson, B. A., Baddeley, A. D., & Kapur, N. (1995). Dense amnesia in a professional musician following herpes simplex virus encephalitis. *Journal of Clinical and Experimental Neuropsychology*, 17(5), 668–681. <https://doi.org/10.1080/01688639508405157>
- Wilson, F. A. W., Scalaidhe, S. P. ., & Goldman-Rakic, P. S. (1993). Dissociation of object and spatial processing domains in primate prefrontal cortex. *Science*, 260(5116), 1955–1958. <https://doi.org/10.1126/science.8316836>
- Womelsdorf, T., Schoffelen, J. M., Oostenveld, R., Singer, W., Desimone, R., Engel, A. K., & Fries, P. (2007). Modulation of neuronal interactions through neuronal synchronization. *Science*, 316(5831), 1609–1612. <https://doi.org/10.1126/science.1139597>
- Yazdan-Shahmorad, A., Diaz-Botia, C., Hanson, T. L., Kharazia, V., Ledochowitsch, P., Maharbiz, M. M., & Sabes, P. N. (2016). A Large-Scale Interface for Optogenetic Stimulation and Recording in Nonhuman Primates. *Neuron*, 89(5), 927–939. <https://doi.org/10.1016/j.neuron.2016.01.013>
- Zalesky, A., Fornito, A., & Bullmore, E. T. (2016). Fundamentals of Brain Network Analysis. In *Fundamentals of Brain Network Analysis*. <https://doi.org/10.1016/C2012-0-06036-X>
- Zanto, T. P., & Gazzaley, A. (2013). Fronto-parietal network: flexible hub of cognitive control. *Trends in Cognitive Sciences*, 17(12), 602–603. <https://doi.org/10.1016/j.tics.2013.10.001>